



MONASH University

Design of Surface Acoustic Waves Field for Manipulation of Particles in Microfluidics

Armaghan Fakhfouri

Bachelor of Engineering (Mechanical) (Hons.)

A thesis submitted for the degree of (*Doctor of Philosophy*) at
Monash University in 2018

Department of Mechanical and Aerospace Engineering

© Copyright

by

Armaghan Fakhfouri

2018

To my parents,

Farzaneh Dehdashtian & Akbar Fakhfoori

For what you've been
&
what you've done

Design of Surface Acoustic Waves Field for Manipulation of Particles in Microfluidics

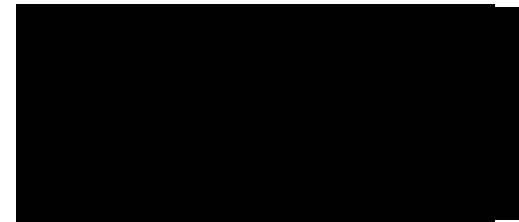
Copyright Notices

Notice 1

Under the Copyright Act 1968, this thesis must be used only under the normal conditions of scholarly fair dealing. In particular no results or conclusions should be extracted from it, nor should it be copied or closely paraphrased in whole or in part without written consent of the author. Proper written acknowledgement should be made for any assistance obtained from this thesis.

Notice 2

I certify that I have made all reasonable efforts to secure copyright permissions for third-party content included in this thesis and have not knowingly added copyright content to my work without the owner's permission.



Armaghan Fakhfouri
1st November 2018

Abstract

The manipulation of cells is fundamental to numerous medical diagnosis and biological processes. Hence, there is a significant demand for the development of highly precise and high-resolution manipulation techniques. Lab on a chip (LOC), as a powerful tool for chemical, biological and medical analysis has emerged as a promising platform to meet this demand. Built on the unique behaviour of liquids at the micrometre length scales enabling the use of different phenomena, LOC performs a much more precise analysis at a faster rate and by using considerably reduced sample and reagent than standard lab-based methods. However, the dominance of different physical phenomena at reduced dimensions give rise to the need for new techniques to fully capture the potential of such miniaturised systems. Amongst various on-chip manipulation approaches, acoustic forces have received considerable attention owing to their non-invasive, non-contact and biocompatible nature. The use of high-frequency surface acoustic waves (SAW), in particular, allows for an exciting range of promising techniques for a powerful, yet gentle manipulation of particles and cells. Despite increasing significance of SAW-driven technologies for on-chip manipulation, the physical phenomena underlying these systems are yet to be fully elucidated and a number of feasible benefits of SAW systems still remain unrealised. This dissertation presents an in-depth understanding of various phenomena underlying SAW-systems by challenging the common assumptions typically made in the present literature. Firstly, the influence of elevated frequencies in standing SAW systems is explored. In doing so, a novel membraneless filtration system is developed allowing for a high resolution, size-deterministic filtration of particles, the size of which approaches that of half a wavelength. Specifically, the filtration of 8 μm particles from 5 μm particles and 10.36 μm particles from 5 μm and 7 μm particles is achieved using a pair of opposing focused interdigital transducers (IDTs) operating at 258 MHz, 129.5 MHz, and 192.5 MHz respectively. Secondly, the influence of diffraction in travelling SAW (TSAW) systems is explored. In doing so, an operating condition has been identified under which patterning of particles into spatially stable locations takes place. Based on this new observation, the system is characterised experimentally and numerically revealing the existence of five distinct mechanisms in an individual TSAW system. In addition to the unidirectional migration typically reported in the literature, particle patterning in two orthogonal directions and particle swirling in two orthogonal planes are presented. Finally, the influence of size as a function of frequency and applied power in the outcome behaviour of particles in a TSAW driven system is explored. As a result, three regions of behaviour along with two transition regions are identified as drifting, patterning and swirling as the particle size reduces. The deeper understanding of SAW actuated devices acquired in this thesis can be a starting point for unlocking new application spaces that were previously not deemed possible.

List of Publications

Articles in peer-reviewed journals

1. Armaghan Fakhfouri, Citsabehsan Devendran, David J. Collins, Ye Ai, and Adrian Neild. Virtual membrane for filtration of particles using surface acoustic waves (SAW). *Lab on a Chip*, 16:3515-3523, 2016. [241]
2. Armaghan Fakhfouri, Citsabehsan Devendran, Thomas Albrecht, David John Collins, Andreas Winkler, Hagen Schmidt, and Adrian Neild. Surface acoustic wave diffraction driven mechanisms in microfluidic systems. *Lab on a Chip*, 18:2214-2224, 2018. [242]
3. Armaghan Fakhfouri, Citsabehsan Devendran, Asif Ahmed, Julio Soria, and Adrian Neild. The size dependant behaviour of particles driven by a travelling surface acoustic wave (TSAW). *Lab on a Chip*, 18:3926-3938, 2018. [1]

Conference proceedings

1. Armaghan Fakhfouri, Citsabehsan Devendran, David J. Collins, Ye Ai, and Adrian Neild. Virtual membrane for filtration of particles using surface acoustic waves (SAW). *Flow 17 for microfluidics, Paris, France*, 2017. Poster Presentation.

Thesis including published works declaration

I hereby declare that this thesis contains no material which has been accepted for the award of any other degree or diploma at any university or equivalent institution and that, to the best of my knowledge and belief, this thesis contains no material previously published or written by another person, except where due reference is made in the text of the thesis.

This thesis includes 2 original papers published in peer reviewed journals and 1 unpublished publications. The core theme of the thesis is particle manipulation within microfluidic systems using surface acoustic waves. The ideas, development and writing up of all the papers in the thesis were the principal responsibility of myself, the student, working within the Laboratory for Micro Systems (LMS), Department of Mechanical and Aerospace Engineering, Faculty of Engineering, under the supervision of Prof. Adrian Neild and Dr. Tuncay Alan.

The inclusion of co-authors reflects the fact that the work came from active collaboration between researchers and acknowledges input into team-based research.

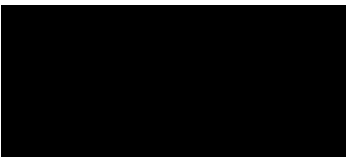
In the case of chapters 3 and 4 my contribution to the work involved the following:

Thesis chapter	Publication title	Status
3	Virtual membrane for filtration of particles using surface acoustic waves (SAW)	Published
4	Surface acoustic wave diffraction driven mechanisms in microfluidic systems	Published
5	The size dependant behaviour of particles driven by a travelling surface acoustic wave (TSAW)	Published

Nature and % of student contribution	Co-author name(s) Nature and % of Co-author's contribution *	Co-author(s), Monash student Y/N*
80 % Design, fabrication of devices, experimentation, numerical modelling, development, results analysis, interpretation and writing.	1)Citsabehsan Devendran (numerical modeling, review of drafts 5%), 2)David Collins (Component fabrication, review of drafts 5%), 3)Ye Ai (review of drafts 3%), 4)Adrian Neild (Contributions to theory, overall supervision and review of drafts 7%)	N, N, N, N
80 % Design and fabrication of devices, experimentation, development, results analysis, interpretation and writing.	1)Citsabehsan Devendran (numerical modeling, review of drafts 5%), 2)Thomas Albrecht (data analysis 2%), 3)David Collins (Contributions to theory 2%), 4)Andreas Winkler (data analysis 2%), 5)Hagen Schmidt (data analysis 2%), 6)Adrian Neild (Contributions to theory, overall supervision and review of drafts 7%)	N, N, N, N, N, N
85 % Design and fabrication of devices, experimentation, development, results analysis, interpretation and writing.	1)Citsabehsan Devendran (numerical modeling, review of drafts 5%), 2)Asif Ahmed (data analysis 1%), 3)Julio Soria (data analysis 2%), 4)Adrian Neild (Contributions to theory, overall supervision and review of drafts 7%)	N, Y, N, N

I have not renumbered sections of submitted or published papers in order to generate a consistent presentation within the thesis.

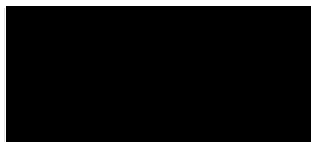
Student signature:



Candidates name: Armaghan Fakhfouri

Date: 1st November 2018

The undersigned hereby certify that the above declaration correctly reflects the nature and extent of the student's and co-authors' contributions to this work. In instances where I am not the responsible author I have consulted with the responsible author to agree on the respective contributions of the authors.



Main Supervisor signature:

Main Supervisor name: Prof. Adrian Neild

Date: 1st November 2018

Acknowledgements

First and formost, I would like to thank my main supervisor prof. Adrian Neild. It has been a huge privilege to be your student. Thank you for being a constant source of support, encouragement and guidance during my PhD. I cannot possibly count the number of times that a few words of encouragement from you motivated me to overcome a challenge, scientific and non-scientific. A great appreciation to Dr Tuncay Alan for taking the role of my co-supervisor and for always being supportive during this endeavour.

LMS lab have made a significant contribution to my learning and success during the PhD process. Citsabehsan (Saab) Devendran, you have been a great source of knowledge, support and fun, thanks kindly for that. A big thank you to Dr David Collins for his valuable collaboration to my project. Jason Brenker, Ninnuja Sivanantha, Muhsincan Sesen, Rui Habibi, Sara Gholam Nejad, Jia wei Ng and Yaqi Zhang thank you for the support and all the fun.

This project would not have been possible without the financial support received from the Faculty of Engineering Postgraduate Research Scholarship (ERLA). I would also like to thank the Department of Mechanical and Aerospace Engineering, the Faculty of Engineering and the Monash Institute of Graduate Research, for the technical and administrative support given throughout my candidature.

A huge thanks to our collaborators, in and out of the university, Dr Thomas Albrecht, Asif Ahmed, Dr Andreas Winkler and Dr Hagen Schmidt. In Particular, I am grateful to Prof. Julio Soria for giving me the honour of working with you, and to Mazyar Forouzandeh for your support, patience, valuable knowledge and contributions.

Mahdokht Shaibani, you are the best thing that happened to me at the beginning of this journey and I could not get to the end without you being constantly there for me. Thank you for always putting a smile on my face and countless overwhelming me with your unconditional support. Alireza Esmaeili, thank you for keeping me sane through the tough times, and creating countless enjoyable moments. Behrouz Bahrani, thank you for your kindness, genuine care and valuable friendship.

Huge thanks and love to my family for their immense support and encouragement: Azadeh Fakhfoori & Iman Fakhfoori, thanks for being the most supportive siblings. Azadeh, thank you for all that you have done for me, things would have been much difficult and much different without you. Iman, thank you for being my constant source of strength and support. Darya Hadad Solaymani, thank you for being so kind and lovely. Mehran Orangi, thank you for welcoming me to your home and thank you for all your support. Nikka Orangi, Sophia Orangi, Avin Fakhfoori, Radin Fakhfoori you are all my constant source of happiness.

Contents

List of Figures	xii
List of Tables	xvi
1 Introduction	1
1.1 Microfluidics	1
1.2 Thesis Overview	3
1.2.1 Chapter 2 : Background, Theory and Fabrication	4
1.2.2 Chapter 3 : Virtual Membrane for Filtration of Particle	4
1.2.3 Chapter 4 : Diffraction Driven Mechanisms	5
1.2.4 Chapter 5 : Size-dependant Behaviour of Particles	5
1.2.5 Chapter 6 : Conclusion & Future Work	5
2 Background, Theory & Fabrication	6
2.1 Lab on a Chip	6
2.1.1 Scaling Effects	8
2.1.2 Manipulation in Microfluidics	12
2.2 Actuation Methods	14
2.2.1 Passive Systems	14
2.2.2 Active Systems	16
2.3 Acoustofluidics	19
2.3.1 Acoustic Radiation Forces	20
2.3.2 Acoustic Streaming induced Drag Forces	24
2.3.3 Bjerknes Forces	26
2.4 Acoustic Excitation Methods	27
2.4.1 Bulk Acoustic Waves	27
2.4.2 Surface Acoustic Waves	28
2.5 Fabrication	34
2.5.1 SAW Device Fabrication	35
2.5.2 Chamber Fabrication	36
2.5.3 Device Assembly	38
3 Virtual Membrane for Filtration of Particles	39
3.1 Overview	39
3.2 Publication	40

4	Diffraction Driven Mechanisms	50
4.1	Overview	50
4.2	Publication	51
5	Size-dependant Behaviour of Particles	63
5.1	Overview	63
5.2	Publication	64
6	Conclusions & Future Work	78
6.1	Conclusions	78
6.2	Future Work	79
	Bibliography	81

List of Figures

1.1 The approximate number of publications on surface acoustic wave (SAW) for manipulation in microfluidics over the recent years based on Google Scholar's database (Keyword: surface acoustic waves for manipulation in microfluidics)	3
2.1 An example of a compact, stand alone lab on a chip (LOC) device that is capable of performing blood analysis without the need for any external connectors. Reproduced from [35] with permission from The Royal Society of Chemistry.	7
2.2 Reduced dimensions of microscale devices give rise to a range of phenomena of which a few examples are illustrated. (a) Fluid (here, fluorescein (green) fluid and rhodamine B (red) fluid) flow in laminar regime due to low Reynolds number, wherein mixing is minimised. Reproduced from [63] with permission from The Royal Society of Chemistry. (b) An example of a micromixer, where a specific device architecture is used to increase the diffusion rate and achieve mixing. Reproduced from [64] with permission from The Royal Society of Chemistry. (c-h) Shrinking the size highly increases the significance of surface forces. Benefiting from this, a range of droplet sizes in a precisely controllable manner can be generated. (c-e) Cell-laden hydrogel microcapsules in aqueous solution, Reproduced from [65] with permission from The Royal Society of Chemistry. (f) & (h) Various monodisperse multiple emulsions containing a controlled number of inner and middle droplets, W/O/W/O (W:water, O:oil) using a capillary microfluidic device. (f) Reproduced from [66] with permission from Wiley Online Library. (h) Reproduced from [67] with permission from The Royal Society of Chemistry. (g) Rapid mixing in moving plugs using a particular architecture of microfluidic channel. Reproduced from [68], with permission of API publishing.	12

- 2.3 Passive Manipulation techniques are shown here. (a) A pinched flow fractionation (PFF), Reprinted from [101] © 2010 Optical Society of America. (b) A semi-spiral passive system that benefits from the combination of long loops and sharp corners to isolate circulating tumor cells, Reprinted from [102] with permission from Elsevier. (c) A passive system using asymmetrically curved channels to focus the flow stream. Reprinted with permission from [93]. Copyright 2010, American Chemical Society. (d) A contraction-expansion structure applied to the pinched section of (e) a PFF device to better position particles to the desired streams. (d) & (e) Reprinted with permission from [99]. Copyright 2009, American Chemical Society. (f) SEM micrographs of pillar, and (i) weir structure, Reprinted from [103] with permission from Elsevier. (g) An schematic illustration of deterministic lateral displacement (DLD) system and (h) SEM micrographs representing the details of pillar structures. Reprinted with permission from [95]. Copyright 2006, National Academy of Sciences.

2.4 Schematic illustration of active systems. (a) Levitation of particles using magnetic forces. (ii) Particles are stably levitated in the absence of the magnetic field. (i) & (iii) Once the magnetic field is applied particles are attracted to the different positions depending on the orientation of the applied field shown with blue arrows. Reprinted from [140] Copyright 2005 National Academy of Sciences. (b) Optical tweezers make use of a highly focused light to manipulate particles. The intensity gradient in the light beam, attract small objects towards the focal point. In turn, the radiation pressure act to push them down along the optical axes. The dominance of gradient force tend to trap particles in the focal point. Reprinted by permission from Springer Nature. Nature [141] copyright 2003. (c) Manipulation by dielectrophoresis (DEP) force is illustrated. When neutral cells are placed in a nonuniform electrical field, they are polarized and attracted to either (i) low strength (away from the electrodes) or (ii) high strength part of the field (near the electrodes) depending on the field. Reprinted with permission from [142]. Copyright 2017, Elsevier. (C-iii) The schematic of a DEP cell-manipulator unit. Reproduced from [143] with permission from The Royal Society of Chemistry.

2.5 (a) Schematic illustrating the streaming arisen due to viscous effects at the limits of the fluid volume. Reproduced from [172] with permission from The Royal Society of Chemistry. (b) The cross-sectional view of the streaming within a microfluidic channel. Reproduced from [173] with permission from The Royal Society of Chemistry. (c) Streaming vortices formed in a bulk fluid by an oscillating cylinder in the centre. Reproduced from [172] with permission from The Royal Society of Chemistry. (d) Streaming within a microfluidic channel generated by surface acoustic waves (SAW), here is used for size-based sorting of particles. Scale bar is 200 μm . Reproduced from [174] with permission from The Royal Society of Chemistry.

List of Tables

2.1 Scaling laws of various physical quantities. [53]	9
---	---

Microfluidics is an emerging arena that integrates several scientific disciplines to facilitate the study and application of micro-scale physics for fluid handling in a finely controlled manner. This chapter provides a brief introduction to the microfluidic technologies with a focus on their potential for manipulation of cells and particles. This is followed by a brief overview of the upcoming chapters.

1

Introduction

1.1 Microfluidics

Microfluidics is a multidisciplinary field involving the physical study and engineered manipulation of a tiny volume of fluids in the range of microliters (μl) to femtoliters ($f\text{l}$). [2, 3] By benefiting from microfabrication technologies, this field makes use of microscale devices comprising fluid-filled channels with length scales of tens to hundreds of micrometres. As such, these devices are uniquely designed to exploit the scale-dependent effects to their benefit. For example, the reduced dimensions of microchannel cause the fluid flow to occur within the laminar regime, where fluid behaviour is highly predictable. Furthermore, by operating at such small scales the relative significance of surface forces (e.g. surface tensions) to volume forces (e.g. gravity) increases. [4] These features permit fundamentally new abilities in the precise manipulation of fluid and the solutes both spatially and temporally. Exploration of microscale phenomena for practical use is relatively new, though, nature has long been using microfluidics to its advantage. For example, transportation of fluid and essential components in plant's vascular system or human's cardiovascular system occurs through microchannels and is made possible by scale-dependant phenomena in particular capillary effects.

The study of fluid systems at the micron length scale dates back more than a hundred years, starting with capillary experiments. [5] Although, the birth of microfluidics as a distinct research field had to wait for the establishment of microfabrication technologies,

1. Introduction

developed by micro-electromechanical systems (MEMS) in the early 1980s. The quest for cheap, portable and highly sensitive analytical methods for, amongst others, biodefense and molecular biology expanded the research field to emerge as a platform for widespread use ranging from medicine to industry. [6] With the development of microfluidic functional elements including valves, pumps, actuators, sensors, mixers and filters, microfluidics has found applications in display technology, [7] ink jet printing technology, [8, 9] chemical threat detectors, [10] 3D bio printings of organs, [11] and tissue engineering, [12] and hold a tremendous promise to revolutionize global healthcare in the near future.

Integration of the microfluidic elements performing the functions and processes required for analysis, on a single microchip has led to the rise of lab on a chip (LOC); a platform with the aim to generate compact, efficient and portable systems for medical diagnostic and monitoring. [13] LOC systems have a tremendous potential to promote decentralization of biomedical testing from the developed-world laboratories to sophisticated point-of-care diagnostic devices; drastically reducing the cost and eliminating the need for highly trained operators, and in doing so allowing diagnosis and disease monitoring to take place in resource-poor settings and remote areas. [14]

Fundamental to applications in diagnosis, and numerous other functions in a microfluidic system is the on-demand manipulation of fluid and dispersed species (e.g. suspended particles, cells and biomolecules). The application of methodologies that drive manipulation in the full-scale laboratories, however, is not transferable to the micro-scales. Instead of using centrifugation, for example, externally applied force fields including magnetic, [15, 16] electrical, [17, 18] optical, [19, 20] and acoustics [21–23] are used to achieve controllable manipulation in microsystems. The use of acoustics, in particular surface acoustic waves (SAW) in microfluidics is relatively new compared to the other methods but has started to receive considerable attention over the past few years. Apart from being highly compatible with microfluidic devices, SAW provide sufficient force strength for a powerful, yet gentle and non-contact manipulation. Introducing SAW to the microfluidic field as a manipulation method occurred only about a decade ago (see Fig. 1.1). [24] As opposed to the primary acoustic technologies known as bulk acoustic wave (BAW) [184, 185] that considerably restrict

1. Introduction

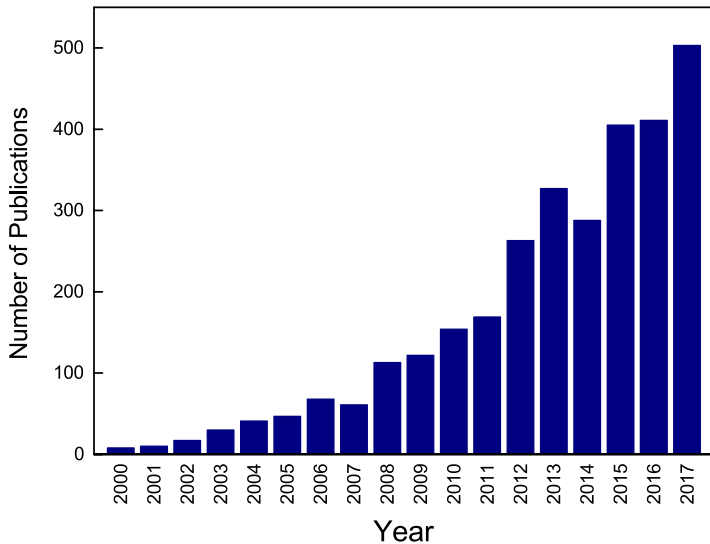


Figure 1.1: The approximate number of publications on surface acoustic wave (SAW) for manipulation in microfluidics over the recent years based on Google Scholar's database (Keyword: surface acoustic waves for manipulation in microfluidics).

the choice of excitation field, to that of the resonant modes of the fluid volume, SAW-driven microfluidics make use of surface-bound localised energy that can be concentrated on any section of the microfluidic system where they are required. [25] By retaining the benefit of being highly versatile and flexible, SAW is emerging as a powerful tool for manipulation in microfluidics. The newness of this technology, however, means that many advantages, made feasible by SAW, are still waiting for full realisation.

1.2 Thesis Overview

The scope of this thesis has been to explore the physical principles that underline SAW-driven systems with a focus on particle manipulation. In particular, the research in this thesis aims to seek more in-depth understanding of SAW systems by breaking down the common assumptions typically made in the present literature. The dissertation is presented in six chapters; a thorough literature review is provided in chapter 2. The research in (i) the effect of elevated frequencies in standing SAW systems (as opposed to the common assumption of $a \ll \lambda_{\text{SAW}}$), (ii) the influence of diffractive patterns in travelling SAW systems (as opposed to the common assumption that SAW propagate in a simple planar fashion), and (iii) the role of size in behaviour of particles driven by travelling SAW (while

1. Introduction

taking into account the diffractive effects in TSAW systems) is presented in three separate publications comprising chapters 3 to 5. The thesis concludes with a summary of the major findings and potential future works in chapter 6.

1.2.1 Chapter 2 : Background, Theory and Fabrication

In Chapter 2, a detailed literature review is presented summarising the relevant background theories, prospects and challenges of particle manipulation in microfluidics. Primarily, the principles and scaling effects of microfluidics in the context of lab on a chip is discussed. With a focus on particle manipulation performance, an overview of the LOC actuation methodologies is presented, concluding that amongst several alternatives, SAW is particularly appealing owing to the tremendous benefits it provides for manipulation in microfluidics. Following this a historic review to acoustically driven microfluidic devices, particularly SAW, along with underlying physics, applications and fabrication techniques are provided.

1.2.2 Chapter 3 : Virtual Membrane for Filtration of Particle

In Chapter 3 the influence of elevated frequencies in SAW-driven systems is explored. This effect is realised by reducing the SAW half-wavelength to the dimension of particles ($\lambda_{SAW} \sim 2D_{Particle}$), a capability that is hard, if at all possible, to exploit in bulk acoustic waves (BAW) systems. In particular, a pair of opposing focused IDTs are used to generate a highly localised standing field. In doing so, a tuneable and highly sensitive size-deterministic filtration technique has been developed that allow for sorting of particles with diameter differences of only 3 μm . Specifically, the filtration of 8 μm particles from 5 μm particles and 10.36 μm particles from 7 μm and 5 μm particles are achieved at operation frequencies of 258 MHz, 192.5 MHz, and 129.5 MHz respectively. The underlying mechanism of this deterministic particle filtration system was established via numerical simulations, followed by experimental validation.

1. Introduction

1.2.3 Chapter 4 : Diffraction Driven Mechanisms

Chapter 4 aims to seek an in-depth understanding of the effects which arise due to the incidence of a travelling SAW through a microfluidic channel, an excitation mode which cannot be realised with resonant BAW (which establish standing waves). In particular, this work explores the influence of diffractive effects in such systems. In a typical TSAW-driven system, SAW is often assumed to propagate in a simple planar fashion. However, the finite realm of a microsystem substantially increases the significance of the diffractive effects. By realising this, we have identified five distinct mechanisms within an individual system. These include periodic particle patterning in two distinct directions; (i) orthogonal and (ii) parallel to the TSAW propagation direction. The former results from diffractive effects on the substrate surface, while the latter arises due to diffractive effects at the substrate/fluid intersection. Furthermore, fluid swirling in two orthogonal planes driven by acoustic streaming; (iii) at the peripheral region of the SAW beam, here termed peripheral streaming, and (iv) within the extent of the beam, here termed lobe streaming. Finally, (v) particle migration away from the SAW emanating source, the only particle manipulation effect discussed widely in the literature.

1.2.4 Chapter 5 : Size-dependant Behaviour of Particles

Chapter 5 builds off the mechanisms elucidated in chapter 4, here the impact of size as a function of frequency and power on the outcome behaviour of particles in a travelling SAW system is examined. Three distinct behaviours of particles have been identified; (i) unidirectional migration away from the SAW emanating source, (ii) patterning in a spatially periodic manner and, (iii) continuous swirling. Whilst the mono-directional migration and acoustic streaming effects are widely discussed in the literature, patterning effects have only recently been reported. As such, this study explores the size-dependent nature of this effect and the influential factors involved.

1.2.5 Chapter 6 : Conclusion & Future Work

The final chapter summarizes the major contributions made to the SAW microfluidics by the research presented in this thesis. Finally, suggestions and ideas for future studies and possible applications are provided.

This chapter aims to summarise the background theories, prospects and challenges of manipulation in microfluidics. The concept of lab on a chip (LOC) is introduced, several techniques are discussed amongst which surface acoustic wave (SAW) is explored in its potential as a promising tool for a powerful manipulation.

2

Background, Theory & Fabrication

2.1 Lab on a Chip

The idea of shrinking the full laboratory set onto a small chip was proposed about two decades ago and has been the dream of microfluidic researchers ever since. [26] This intriguing concept entered the academic research following the development of “miniaturized total chemical analysis systems (μ TAS)” technologies in 1990, [27] and was termed lab on a chip (LOC). LOCs are highly compact devices with the goal to replicate the ability of a full-scale laboratory to perform analytical tasks on a significantly smaller scale platform. This is achieved by substituting each step in a macro-scale process with a miniaturized functional element that is far smaller than their room-size counterparts, all embodied on an integrated and automated device. A typical LOC consists of paths for the transportation of fluid (channels) and several functional elements including sensors, [28] valves, [29] mixers, [30,31] sorters, [32] and pumps. [33] Miniaturization and integration give rise to numerous benefits; firstly, reducing the size result in favourable improvement of the scaling dependent parameters that dictate fluid behaviour at the microscale. With a higher control over “molecular concentrations and interactions” [34] error rates are highly minimized, while the sensitivity of the system and accuracy of the results dramatically increases. By enabling parallelization and automation, LOC technology substantially reduces the time required to complete the analytical process. Furthermore, the low volume of sample and reagent requirements result in significantly reduced wastage and cost. Realisation of these benefits has motivated scientists

2. Background, Theory & Fabrication

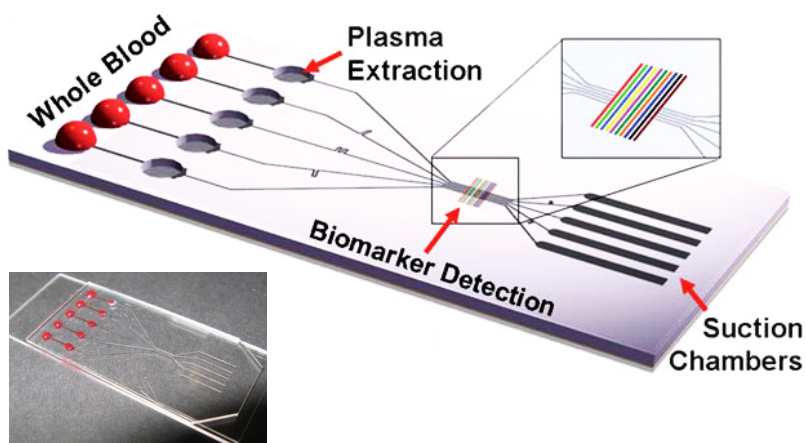


Figure 2.1: An example of a compact, stand alone lab on a chip (LOC) device that is capable of performing blood analysis without the need for any external connectors. Reproduced from [35] with permission from The Royal Society of Chemistry.

and researchers from a wide variety of fields including physics, chemistry, material, biomedical and engineering to bring the dream of LOC to a practical reality. In particular, LOC technologies retain tremendous potential to enhance biological diagnosis and detection for point of care applications, (an example is shown in Fig. 2.1) specifically for infrastructure and resource-poor areas. By developing a sophisticated technology that is portable, cheap and simple to use, the need for a sophisticated laboratory and highly trained staff is eliminated and diagnosis is possible anywhere in the world.

Ever since the modern inception of LOC, around 1990, the use of the technology has been rapidly expanded and a few devices have already been commercialized. For example, “Biosite Incorporated” was one of the first companies that commercialized a data-acquisition technology offering the ability to diagnose whether or not the patient had suffered a heart attack. [36] Furthermore, the new developments in employing LOC for analytical chemistry, [37–40] synthesizing new material, [41] cell culture, [42] genomic research, [13,43–45] pharmaceutical drug development, [46–48] and environmental monitoring [49–52] are only a few examples amongst many.

Manipulation of fluid and suspended objects is considered one of the fundamental tasks allocated to the LOC technologies. Over the past few years, numerous solutions have been provided by the researchers to enhance the performance of the on-chip manipulation. However,

2. Background, Theory & Fabrication

even the state-of-the-art methods require further improvements to more fully realise and exploit the benefits promised by the LOC technologies. In this section, the underlying concepts of LOC paradigm are discussed, with attention later on given to the actuation methods, particularly the surface acoustic wave that has the potential to tackle the issues preventing widespread use of the LOC technologies.

2.1.1 Scaling Effects

The greatest potential of microfluidics, in particular LOC, lies in the new opportunities being made possible by the use of fascinating physical phenomena that dominate fluid behaviour at the microscale. As a result of shrinking the system and working with small volumes (10^{-9} to 10^{-18} litres) of fluid; (i) the ratio of the surface area to volume increases by several orders of magnitude, [5] (ii) the influence of boundary effects become significant, [53] and (iii) the use of near-field forces (i.e. electrical, magnetic, optical and acoustics) become possible. This allows for the use of certain favourable effects and mechanisms that are not accessible to the macroscale platform. [54–56] Furthermore, the ability to operate on the length scales comparable to the analyte (i.e. cells and biomolecules) have made this field increasingly important for manipulation. [55, 56]

The primary goal of LOC, to replicate the capability of a full-scale laboratory, is only possible by realising the significance of the scaling effects. The physics that govern the macroscale world can no longer be considered suitable to predict the behaviour of fluid at the microscales. For example, the relative importance of gravitational forces at the microscales is greatly reduced, often considered negligible, compared to their dominance at the macroscales. The equilibria in microscales are instead dominated by surface forces such as capillary, adhesion and wetting. [53] Additionally, forces such as near-field electrical, [57] and optical [58] are sufficient to manipulate objects at small length scales, whereas the inherent attenuation in the far-field renders them impractical at macroscales.

To establish a fundamental understanding of the governing physics at the microscale, the idea of scaling laws was introduced by Galileo Galilei in 1638 [59] and further expanded by Thompson in 1942. [60] The scaling laws are basic statements indicating how dependant

2. Background, Theory & Fabrication

Physical Quantity	Scaling Law
Intermolecular Van der Waals Force	L^{-7}
Density of Van der Waals Forces between interfaces	L^{-3}
Time	L^0
Capillary Forces	L^1
Distance	L^1
Flow Velocity	L^1
Thermal power transferred by conduction	L^1
Electrostatic Force	L^2
Diffusion time	L^2
Volume	L^3
Mass	L^3
Gravitational Force	L^3
Electrical Motive Power	L^3
Magnetic force with an exterior field	L^3
Magnetic force without an exterior field	L^4
Centrifugal Force	L^4

Table 2.1: Scaling laws of various physical quantities. [53]

variables scale with the independent variables. By benefiting from the dimensional analysis, they determine the modification of physical quantities as the size of the system varies, typically defined based on a characteristic length (L). The use of scaling laws is beneficial in understanding, designing and analysing microfluidic devices. A range of scaling laws for various physical quantities are expressed in Table 2.1. [53] Particle manipulation in microfluidic systems often involves transfer of the particle to a specific location controlled by an externally applied force (e.g. magnetic, electrical, optical and acoustic). In a continuous flow system, for instance, the force typically controls particle transfer between the flow streams. By choosing the particle's diameter as the length scale, the scaling laws can determine the right choice for the appropriate force and the channel dimensions required for an efficient manipulation (further explanation is provided in section 2.2.2).

In a given microsystem, several different physical phenomena play a role. This necessitates the use of dimensionless numbers to express the relative importance of these phenomena and determine the essential fluid physics of the system. The development of a microfluidic system for precise manipulation requires designing the system in a way to exploit the desirable phenomena while minimizing the undesired ones. This often includes using a range of passive and active methods (as will be discussed in section 2.2) to achieve controllable

2. Background, Theory & Fabrication

manipulation. [61] The need for a variety of manipulation techniques arises by the difference in the length scale, L , whereby different forces are dominant for different L values as shown previously. Here, we look at a series of dimensionless numbers dictating the dominant phenomena at different characteristic length scales.

Reynolds number

The Reynold's number, Re , is considered one of the most fundamental dimensionless numbers in fluid physics that relates the inertial forces to viscous forces given by,

$$Re = \frac{\rho U L}{\eta} \quad (2.1)$$

where ρ , U and η are the fluid density, characteristic velocity, and the fluid viscosity respectively. As a result of reducing the length scale, L , fluid behaviour in microfluidic systems is significantly influenced by viscous forces rather than inertia. This effect results in a very low Re ($Re \sim 1$) permitting the fluid to flow predominantly within the laminar regime, whereby hydrodynamic instabilities are minimized and fluid behaviour is highly predictable. (Fig. 2.2 (a) & (b))

Weber number

In a multi-phase fluid flow, the Weber number, We , is used to characterise the interfacial effects. It essentially relates the inertial forces to the surface tension forces as given by,

$$We = \frac{\rho U^2 L}{\gamma} \quad (2.2)$$

where γ indicates the fluid surface tension of the interface. The value of Weber number retains a particular importance in the formation of droplets and emulsions (droplet within droplets). [62] (Fig. 2.2 (c) - (h))

2. Background, Theory & Fabrication

Péclet number

The Peclet number, Pe , reflects the relative importance of convection compared to diffusion given by,

$$Pe = \frac{UL}{D} \quad (2.3)$$

where D is the diffusion constant. In microfluidics, the laminar flow prevents transport of the solute by convective bulk flow such that mixing is mainly driven by diffusion (Fig. 2.2 (d) & (g)).

Capillary number

The Capillary number, Ca , is the most important surface tension phenomenon that relates viscous forces to the surface tension defined as,

$$Ca = \frac{\eta U}{\gamma} \quad (2.4)$$

where, η , U and γ indicate the fluid viscosity, characteristic velocity and the fluid surface tension respectively. Whilst the Capillary number is independent of the length scale, it becomes more significant as a system's size reduces. The value corresponding to Ca can be adjusted to precisely control the generation, break-up and coalescence of droplets. [5] (Fig. 2.2 (f) & (g))

The reduced dimensions along with the long-range nature of viscous flows in microfluidic systems tend to yield small Re and Pe numbers, preventing the mixing that inherently occurs by advection in turbulent flows (Fig. 2.2 (a)). This is desirable in most of the microsystems to retain the analytes spatially separated in the channel for practical interest. [69] However, the ability of microsystems to perform mixing highly relies on diffusion gradients to draw fluid dispersion (Fig. 2.2 (b) & (g)). Controllable laminar mixing in a temporal and spatial manner is broadly achieved by introducing a steady flow in a microchannel, where the increased surface area between layers of various fluid species enhance the diffusive transport of the species and promote rapid mixing. By using this concept, numerous techniques have been developed to overcome the large viscous forces and achieve mixing. [70, 71] A highly effective

2. Background, Theory & Fabrication

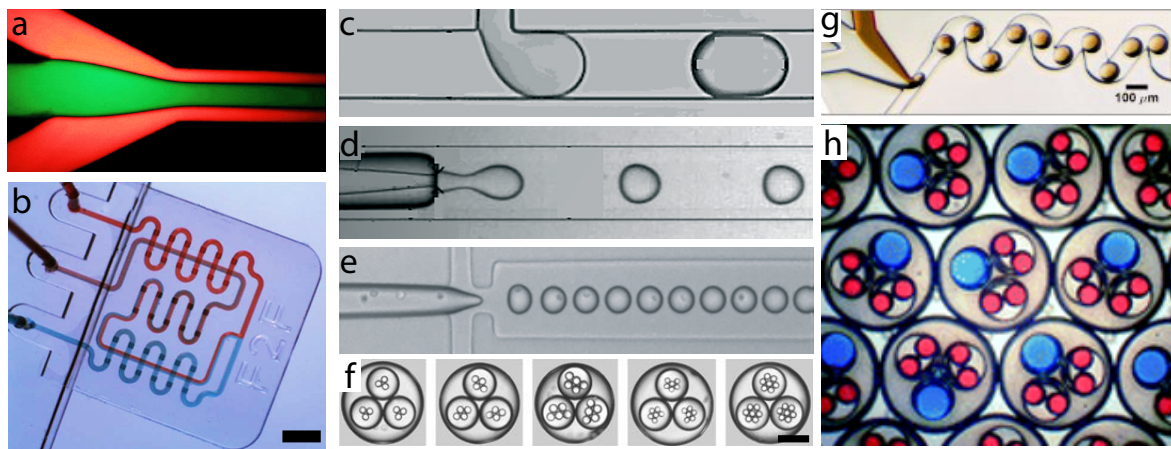


Figure 2.2: Reduced dimensions of microscale devices give rise to a range of phenomena of which a few examples are illustrated. (a) Fluid (here, fluorescein (green) fluid and rhodamine B (red) fluid) flow in laminar regime due to low Reynolds number, wherein mixing is minimised. Reproduced from [63] with permission from The Royal Society of Chemistry. (b) An example of a micromixer, where a specific device architecture is used to increase the diffusion rate and achieve mixing. Reproduced from [64] with permission from The Royal Society of Chemistry. (c-h) Shrinking the size highly increases the significance of surface forces. Benefiting from this, a range of droplet sizes in a precisely controllable manner can be generated. (c-e) Cell-laden hydrogel microcapsules in aqueous solution, Reproduced from [65] with permission from The Royal Society of Chemistry. (f) & (h) Various monodisperse multiple emulsions containing a controlled number of inner and middle droplets, W/O/W/O (W:water, O:oil) using a capillary microfluidic device. (f) Reproduced from [66] with permission from Wiley Online Library. (h) Reproduced from [67] with permission from The Royal Society of Chemistry. (g) Rapid mixing in moving plugs using a particular architecture of microfluidic channel. Reproduced from [68], with permission of API publishing.

method makes use of the acoustic streaming mechanism (section 2.3.2) to induce a localised powerful flow and effectively enhance the mixing abilities of the system. [72]

In microfluidics, the inherent large ratio of surface area to volume allows for the availability of more interfaces, thus more efficient transfer of mass and energy. [5] The dominance of interfacial forces along with the high energy coupling by the use of a locally applied external force, lead to a wide range of possibilities such as generation and handling of fluid droplets on the order of picoliter and femtoliter [73–75] (Fig. 2.2 (c) - (h)). By realising the benefits of microscale phenomena, manipulation can be achieved with an excellent precision and exceptionally high resolution that is impossible to achieve at the macroscales.

2.1.2 Manipulation in Microfluidics

Manipulation of particles and cells is fundamental to tasks such as sorting, concentration and patterning. The ability to concentrate cells of interest directly from their host medium, to sort

2. Background, Theory & Fabrication

cells into distinct populations and to pattern cells in defined spatially separated positions are all vital functions in a range of biomedical applications. Haematology diagnostic procedures, for example, often require concentration of blood cells from plasma. [76, 77] In a laboratory setting a centrifugal system performs this task, however, the use of a similar procedure in microsystems is not practical due to the dominance of different physical phenomena at microscales. A range of alternative methods are employed for use in microfluidics as will be discussed in section 2.2. The growing tendency towards on-chip manipulation, though, comes from a prospect that microsystem manipulators offer new opportunities for a substantially higher precision, sensitivity and resolution, relative to that achievable at the laboratory setting. In cancer screening, for instance, sorting of circulating tumour cells from the whole blood is a powerful tool for early diagnosis. [78] The rarity of cancer cells necessitates the use of a highly sensitive and high-resolution technique, where loss of even a single cell lead to considerable inaccuracies of the outcome results. [79] By retaining the ability to manipulate on the scale of the individual cell, microfluidics offer the best tool for such applications.

Trapping and patterning of cells within determined locations in microfluidics enables observation of single cell behaviour, [80] study of cell-cell interactions, [81] drug development, [82] and bioprinting. [83–85] Prolonged observation of heterogeneous cellular development and the analysis of their parameters at the level of the individual cell and in response to their local surrounding environment, is of great importance in biological and pharmaceutical researches. [86] In the field of neurology, for instance, the properties of cells (e.g. collection of proteins) differ from one another. The fact that these cells cannot be cultured clearly highlights the significance of the single-cell approach. [53]

In blood diagnosis procedures, high specificity in manipulation is a vital factor, where the difference in the intrinsic properties of healthy and diseased cells are often very small. Relative to the healthy red blood cell, cancerous cells are slightly stiffer and only a few microns larger, [78] the malaria-infected cells are slightly denser, more rigid and have higher permeability. [87, 88] This phenomenon is also applicable to infectious diseases, where the size of a virus is smaller than a cell by several order of magnitudes. [89]

2. Background, Theory & Fabrication

In microsystems, cells with different properties are acted upon differently by externally applied forces (e.g. acoustics, optical, magnetic, or electrical), channel conditions and physical features (e.g. pillars or weirs). As such different on-chip manipulation techniques have been developed depending on the nature of the intended application, as will be discussed subsequently.

2.2 Actuation Methods

The on-demand manipulation of particles, cells and droplets in LOC systems require the exploitation of the favourable characteristics of microscale phenomena by the use of specific microchannel physical features and externally applied force gradients. The key challenge is to overcome the substantial surface and viscous forces that resist fluid and suspended particles motion at microscales. To date, several techniques have been developed that are generally classified into passive (section 2.2.1) and active (section 2.2.2) methods based on the nature of the force employed for manipulation. With each technique providing certain benefits and limitations, there is a range of applications for which they are well suited. The key factors for an appropriate choice of the suitable technique include the force strength and localization ability, straightforward integration in the chip, system's versatility and tunability, biocompatibility, throughput requirements and economic aspects such as cost and disposability.

2.2.1 Passive Systems

Passive manipulation is enabled by specifically designing the channel geometries and structure to exploit hydrodynamic forces and manipulate particles based on their physical parameters (i.e. size, shape and deformability). Passive systems highly rely on laminar flow regime and the use of Dean flow to manipulate the steady-state equilibrium position of the particles. Several passive techniques have been developed to perform mixing, [90–92] concentration, [93, 94] and separation. [95, 96] Pinched flow fractionation (PFF) (Fig. 2.3 (a) & (e)), for instance, is a passive sorting system with a specific channel architecture consisting of two segments; (i) The pinched part yields a focused flow of particles, each following the streamline that passes through their centre of mass. (ii) The broadened part allows for the spreading of streamlines, where particle trajectories are directed towards various outlet branches. [69] The sorting efficiency of the conventional PFF systems can be highly enhanced by applying particular alterations

2. Background, Theory & Fabrication

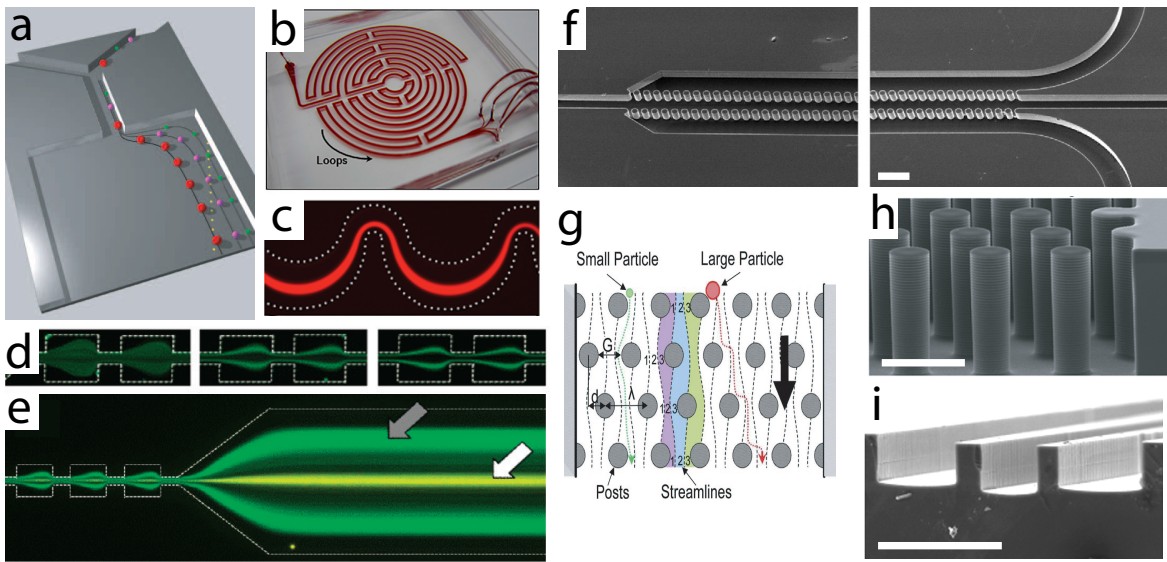


Figure 2.3: Passive Manipulation techniques are shown here. (a) A pinched flow fractionation (PFF), Reprinted from [101] © 2010 Optical Society of America. (b) A semi-spiral passive system that benefits from the combination of long loops and sharp corners to isolate circulating tumor cells, Reprinted from [102] with permission from Elsevier. (c) A passive system using asymmetrically curved channels to focus the flow stream. Reprinted with permission from [93]. Copyright 2010, American Chemical Society. (d) A contraction-expansion structure applied to the pinched section of (e) a PFF device to better position particles to the desired streams. (d) & (e) Reprinted with permission from [99]. Copyright 2009, American Chemical Society. (f) SEM micrographs of pillar, and (i) weir structure, Reprinted from [103] with permission from Elsevier. (g) An schematic illustration of deterministic lateral displacement (DLD) system and (h) SEM micrographs representing the details of pillar structures. Reprinted from [95]. Copyright 2006, National Academy of Sciences.

to the channel configuration; by breaking the symmetry of outlet branches (AsPFF), [97] making use of a curved broadened segment, [98] and adding contraction-expansion structure (Fig. 2.3 (c) & (d)) to the pinched microchannel. [99, 100]

In alternative approaches, passive sorting is achieved using field flow fractionation (FFF), [104] adhesion based methods, [105] hydrodynamic filtration, [106, 107] and spiral systems [108, 109] (Fig. 2.3 (b)). Introducing physical obstructions such as pillars, [110, 111] (Fig. 2.3 (f) & (g)) and weirs [103] (Fig. 2.3 (i)) assist with translating particles in the desired direction. Deterministic lateral displacement (DLD) (Fig. 2.3 (g)), for instance, is an efficient sorting technique that employs this concept, wherein a particular arrangement of cylindrical pillars throughout the channel facilitate particle separation based on size. [95, 112, 113] With a simple and cheap implementation, high throughput and biocompatibility passive systems are considered a popular choice. However, generation of a force gradient for efficient manipulation requires very small channel features close to the dimensions of micro-objects. This often

2. Background, Theory & Fabrication

results in blockage of the channel, thus failure of the system. Another major drawback of passive systems is their lack of flexibility, tunability and thus robustness.

2.2.2 Active Systems

In active systems, typically a force field relevant on the micro-scale is externally applied to manipulation particles on demand. These include magnetic, optical, electrical (an example of each is shown in Fig. 2.4) and acoustic force fields. Benefiting from the near-field effects, these forces are applicable to microsystems whilst in macro scales their magnitude drop across larger length scales due to the inherent attenuation of the force field. Active techniques are easily adaptable and offer relatively higher efficiency, power, tunability and throughput compared to passive systems.

Magnetic

The magnetic manipulation of particles and cells require a high gradient magnetic field generated by the use of a permanent magnet. The resultant magnetophoretic force affects the inherent or induced paramagnetic species enabling a highly sensitive and specific sorting technique. [114, 115] Magnetic sorting is mainly based on size and magnetic susceptibility, where the cells of interest have intrinsic magnetic properties in nature or tagged by magnetic labels. [116, 117] In breast cancer screening, for example, the separation of the cancer cells from the peripheral blood has been reported based on their intrinsic electrophysiological characteristics without any magnetic labelling. [118] In another example, the isolation of malaria-infected red blood cells from the blood sample is presented in the dialysis-like treatments. [119] On-chip magnetic actuation is a simple, inexpensive, sensitive and highly selective particle manipulation technique used for applications such as purification processes and immunoassays, [120–122] nucleic acid processing and detection, [123–125] catalysis, [126] and droplet handling [127] to name a few. The applications, however, are only limited to the magnetic species or when labelling is an acceptable cost.

2. Background, Theory & Fabrication

Dielectrophoresis

When electrically neutral particles are placed in a spatially non-homogeneous electric field, they become polarized and experience a lateral force, termed dielectrophoresis (DEP). [128, 129] As a result, particles are translated towards strong or weak regions of the field depending on the relative amplitude of particle and medium permittivities (Fig. 2.4 (c)). The use of alternating (AC) fields highly promotes the versatility of the DEF system. [17] By manipulating based on particle's intrinsic properties (i.e. size and dielectric), DEP actuated systems have been broadly used for electrically controlled trapping, [130, 131] concentration, [129, 132] fractionation, [133] and characterization [134] of particles and biological cells. The main drawback of DEP is the high voltage requirement that reduces operation efficiency of the system and leads to considerable local heating, proposing potential damage to the suspended cells and biological species.

Optical

Optical actuation, typically known as optical tweezers, makes use of an intense light (laser) beam for a non-contact manipulation of submicron particles ranging from 10s of nm to 10s of μm . [135] By operating at the immediate near-field, optical tweezers are potentially capable of manipulating individual bacteria, viruses, and molecules, [136] as such are considered a powerful tool in molecular biology, [137] biochemistry, [138] and biophysics. [139] Optical manipulation is made possible by creating a large gradient in light intensity (see Fig. 2.4 (b)) using a high-numerical aperture microscope objective. By adjusting the light wavelength and power, particles in suspension are attracted towards the position with the highest intensity (stable trapping positions) in the focused light beam. [20] Besides exceptionally high spatial resolution, optical tweezers offer high specificity, high speed and high responsiveness. However, the high intensity of the laser beam considerably damages the cells and causes photobleaching. Furthermore, the complicated and sensitive setup required for optical manipulation pose drawbacks that reduce the practicality of the method for microfluidic applications.

2. Background, Theory & Fabrication

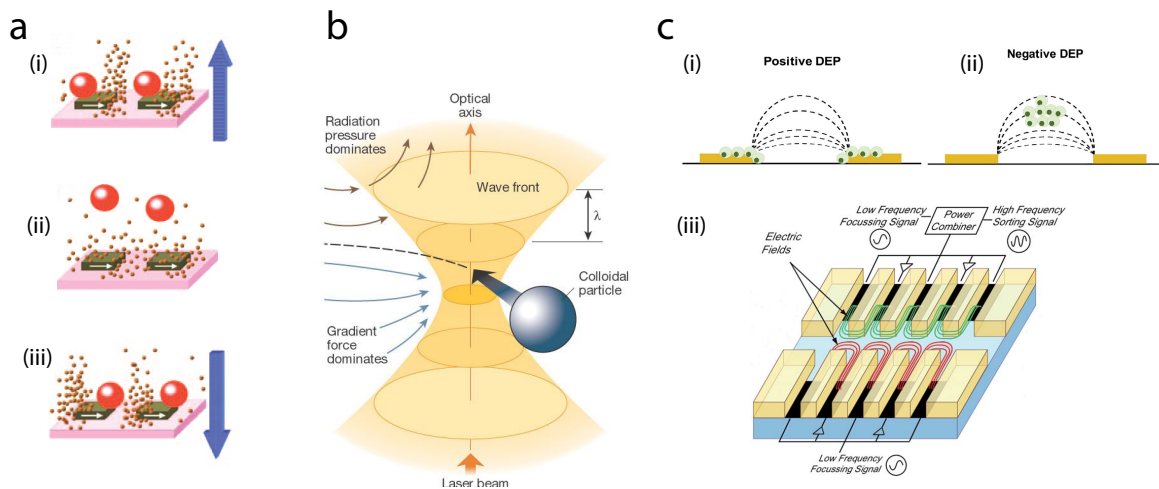


Figure 2.4: Schematic illustration of active systems. (a) Levitation of particles using magnetic forces. (ii) Particles are stably levitated in the absence of the magnetic field. (i) & (iii) Once the magnetic field is applied particles are attracted to the different positions depending on the orientation of the applied field shown with blue arrows. Reprinted from [140] Copyright 2005 National Academy of Sciences. (b) Optical tweezers make use of a highly focused light to manipulate particles. The intensity gradient in the light beam, attract small objects towards the focal point. In turn, the radiation pressure act to push them down along the optical axes. The dominance of gradient force tend to trap particles in the focal point. Reprinted by permission from Springer Nature. Nature [141] copyright 2003. (c) Manipulation by dielectrophoresis (DEP) force is illustrated. When neutral cells are placed in a nonuniform electrical field, they are polarized and attracted to either (i) low strength (away from the electrodes) or (ii) high strength part of the field (near the electrodes) depending on the field. Reprinted with permission from [142]. Copyright 2017, Elsevier. (C-iii) The schematic of a DEP cell-manipulator unit. Reproduced from [143] with permission from The Royal Society of Chemistry.

Acoustics

Acoustic actuation offers remarkable benefits for particle manipulation purposes and has been used as the preferred method in this thesis. A detailed literature review, along with the underlying principles and the use of acoustics is provided in the subsequent section.

The sensitivity and resolution of each technique depend on the response of particles to the applied force based on their properties. Furthermore, the type and scaling of the forces (that differs in each method) determine what type of species the method can be applied to. In passive systems, hydrodynamic forces scale with the particle's radius and density. [144] The magnetic and dielectrophoretic forces are proportional to the radius cubed, [17, 145] ($F \propto r^3$) whilst in the case of optical tweezers and acoustic forces, this relationship is either to the third power [146] ($F \propto r^3$ for standing wave field) or the sixth power [147, 148] ($F \propto r^6$ in case of travelling optical/acoustic wave force). Compared to the other force fields, magnetic forces are relatively weak, though non-contact and biocompatible to retain the

2. Background, Theory & Fabrication

viability of the cells over time. Optical tweezers are viable for very small microfluidic species (submicron/nano), however, can be damaging to biological samples. DEP forces are strong at the immediate vicinity of an electrode, though their strength drops off rapidly at the increasing distance from the electrode. Similar to optical tweezers, DEP actuated systems suffer from biocompatibility issues. By providing strong forces whilst being non-contact and bio-compatible, acoustic forces are an excellent alternative and have emerged as a powerful tool for manipulation, thus are the focus of this thesis. As opposed to the magnetic methods, where manipulation mainly relies on magnetic properties, acoustics retain the ability to manipulate particles purely based on their intrinsic mechanical properties (i.e. shape, size and density). Acoustically actuated microfluidic devices are studied in the field of acoustofluidics and are discussed with more details in section 2.3.

2.3 Acoustofluidics

The propagation of sound waves through a medium (e.g. fluid or gas), has found a unique place in modern research, for a powerful, yet gentle manipulation of fluid and the microfluidic species (e.g. particle, cell and droplets) in suspension. The non-contact, non-invasive, biocompatible, and straightforward microfluidic integration nature of the acoustic actuation have rendered them an attractive manipulation method, particularly for biologically oriented systems. [149,150] Sound waves are generally described as mechanical pressure waves propagating with a certain length (frequency) and amplitude (pressure level) in two main modes; transverse (shear) and longitudinal, whereby the motion of medium is orthogonal and parallel to the propagation direction, respectively. [151] Waves at the frequency range of (20 Hz to 20 kHz) are audible to humans, beyond this range acoustic waves are classified as ultrasonic (20 kHz to 10 MHz). For many decades, ultrasonics have been implemented in a variety of engineering applications including sound navigation systems (SONAR), [152] non-destructive testing, [153] ultrasonic cleaning, [154] medical instrumentation, [155] and sonography. [156]

The study of acoustic waves dates back to the 18th century. Most of the contemporary acoustic concepts stem from fundamental work performed many years ago, such as that on acoustic streaming by Rayleigh, [157] and vibration-induced surface waves observations by

2. Background, Theory & Fabrication

Faraday, [158, 159] both performed in the mid-19th Century. However, the widespread use of acoustic waves, particularly those at frequencies in the ultrasonic range, for applications spanning a diverse range of disciplines appeared at the close of the 20th century. [160] The overlap of acoustic and microfluidics occurred in the 1960s, [161, 162] initially for the development of sensor technologies and gave rise to a new field of research, known today as “Acoustofluidics”.

Acoustofluidics is a research field devoted to the study of acoustically actuated microfluidic systems, wherein the acoustic forces control the motion of the fluid itself or fluid-suspended objects (e.g. particles, biomolecules and cells) that respond to the force field based on their inherent mechanical properties (i.e. size, shape, density and compressibility). Acoustic force fields are highly versatile, with a wide range of use in mixing, concentration, sorting, filtration, pumping, and droplet production. Acoustically driven systems are simple in practice, yet complex in analysis. Designing effective systems to achieve the desired outcome, requires in-depth understanding of the acoustic forces and the underlying mechanisms that give rise to them.

Particles, cells and droplets suspended in an acoustic field are subjected to three steady-state forces; acoustic radiation forces, [146, 148] acoustic streaming induced drag forces, [163, 164] and Bjerknes forces. [165, 166] The first two will be discussed in details, while the latter force will be covered very briefly as it does not play an integral role in the methods employed within the systems discussed in this thesis.

2.3.1 Acoustic Radiation Forces

Introducing vibration to a fluid medium lead to the formation of a pressure field. The presence of a particle within this vibrating medium gives rise to three distinct inter-related scenarios; firstly, interaction of the incident acoustic wave with the particle; secondly, scattering of the wave from the particle; lastly, transmission of the wave into the particle. Depending on the particle’s mechanical properties (i.e. size, shape, density and compressibility), these scenarios influence the pressure field. This interactions with the sound wave yield a net resultant force, known as acoustic radiation force (ARF), arise and act directly on the particle.

2. Background, Theory & Fabrication

The derivation of radiation force relies on applying the perturbation theory to obtain the second-order governing equations based on the first-order pressure and velocity fluctuations. By assuming a very small perturbation parameter, ε to allow neglecting of the higher order terms; the pressure, P , velocity, \mathbf{v} , and density, ρ fields can be expanded as, [167]

$$P = P_0 + \varepsilon P_1 + \varepsilon^2 P_2 \quad (2.5a)$$

$$\rho = \rho_0 + \varepsilon \rho_1 + \varepsilon^2 \rho_2 \quad (2.5b)$$

$$\mathbf{v} = \mathbf{v}_0 + \varepsilon \mathbf{v}_1 + \varepsilon^2 \mathbf{v}_2 \quad (2.5c)$$

where, subscripts 0, 1 and 2 denote the order of the expression (i.e. initial, first and second-order). ε indicates perturbation parameter. $P_1 = \rho_1 c_0^2$ is given by the (isentropic) derivative $c_0^2 = (\partial P / \partial \rho)_s$.

We assume time-harmonic fields,

$$P_1 = P_1(x) e^{i\omega t} \quad (2.6a)$$

$$\rho_1 = \rho_1(x) e^{i\omega t} \quad (2.6b)$$

$$\mathbf{v}_1 = \mathbf{v}_1(x) e^{i\omega t} \quad (2.6c)$$

The relative slowness of the particle motion compared to the micron second time scale of the imposed high-frequency acoustic wave (in the order of kHz to MHz), means that particles respond to the time-averaged field. Thus, the radiation force averaged over a full oscillation cycle is considered,

$$\langle X \rangle = \frac{1}{T_{osc}} \int_0^{T_{osc}} X(t) dT_{osc} \quad (2.7)$$

where, T_{osc} represents the period of oscillation and t is time.

The excited vibrations are harmonic oscillations, thus, the first order pressure and velocity terms time-average to zero, while the second-order time-averaged terms have a

2. Background, Theory & Fabrication

non-zero magnitude. Now we consider the continuity and Navier-Stokes equations for density and velocity fields, respectively,

$$\frac{\partial \rho}{\partial t} = -\nabla \cdot (\rho \mathbf{v}) \quad (2.8a)$$

$$\rho \frac{\partial \mathbf{v}}{\partial t} = -\nabla P - \rho(\mathbf{v} \cdot \nabla) \mathbf{v} + \eta \nabla^2 \mathbf{v} + \left[\eta' + \left(\frac{4}{3} \right) \eta \right] \nabla(\nabla \cdot \mathbf{v}) \quad (2.8b)$$

where η and η' represents the shear and bulk viscosity coefficient for the fluid respectively. By operating far from the walls, we can assume inviscid conditions and therefore neglect the viscosity in the fluid ($\eta \approx 0$). Implementation of the perturbation theory (Eqn. 2.5) and $P_1 = \rho_1 c_0^2$ alongside the governing equations yields the first-order terms,

$$\frac{\partial \rho_1}{\partial t} = -\rho_0 \nabla \cdot \mathbf{v}_1 \quad (2.9a)$$

$$\rho_0 \frac{\partial \mathbf{v}_1}{\partial t} = -c_0^2 \nabla \rho_1 \quad (2.9b)$$

And the time-averaged second-order terms,

$$\nabla \langle \rho_1 \mathbf{v}_1 \rangle = -\rho_0 \nabla \cdot \langle \mathbf{v}_2 \rangle \quad (2.10a)$$

$$\langle \rho_1 \frac{\partial \mathbf{v}_1}{\partial t} \rangle + \rho_0 \langle (\mathbf{v}_1 \cdot \nabla) \mathbf{v}_1 \rangle = -\nabla \langle P_2 \rangle \quad (2.10b)$$

Finally, to get the time-averaged second-order pressure equation in terms of P_1 and v_1 , we use Eqn. 2.9b and Eqn. 2.10b,

$$\langle P_2 \rangle = \frac{1}{2\rho_0 c_0^2} \langle P_1^2 \rangle - \frac{1}{2} \rho_0 \langle v_1^2 \rangle \quad (2.11)$$

The integration of the second-order pressure field over the surface of spherical particle (denoted by $S(t)$, with the initial value of S_0) yields the acoustic radiation force exerted on the compressible particle suspended in an inviscid fluid.

$$\mathbf{F}_{\text{rad}} = \int_{S(t)} \langle P_2 \rangle (-\mathbf{n}) dS \quad (2.12)$$

The particle's surface experience slight translation and deformation caused by the applied force, thus it is considered to be a function of time. To compensate for the error caused by the surface's fluctuation, a convective momentum flux term is added. [168]

2. Background, Theory & Fabrication

$$\mathbf{F}_{\text{rad}} = \int_{S_0} \langle P_2 \rangle (-\mathbf{n}) dS - \int_{S_0} \rho \langle (\mathbf{v}\mathbf{n}) \cdot \mathbf{v} \rangle dS \quad (2.13)$$

By substituting Eqn. 2.11 we arrive at,

$$\mathbf{F}_{\text{rad}} = \frac{1}{2} \rho_0 \int_{S_0} [\langle \mathbf{v}_1^2 \rangle - \frac{1}{\rho_0^2 c^2} \langle P_1^2 \rangle] \mathbf{n} dS - \rho_0 \int_{S_0} \langle (\mathbf{n} \cdot \mathbf{v}_1) \mathbf{v}_1 \rangle dS \quad (2.14)$$

This expression was used to numerically model the system explained in chapter 3, wherein the half wavelength of the acoustic field approach particles dimensions ($\lambda_{\text{SAW}} \sim 2D$). In a scenario where the particle size is far smaller than the wavelength ($\lambda_{\text{SAW}} \gg D$), the expression for the time-averaged acoustic radiation force in a viscous fluid is given by, [169]

$$\mathbf{F}_{\text{rad}} = -\pi a^3 \left[\frac{2\kappa_0}{3} \Re[f_1^* P_1^* \nabla P_1] - \rho_0 \Re[f_2^* \mathbf{v}_1^* \cdot \nabla \mathbf{v}_1] \right] \quad (2.15a)$$

The asterisk indicates complex conjugates and $\Re[]$ the real part. Factors f_1 and f_2 are given by,

$$f_1 = 1 - \frac{\kappa_p}{\kappa_0} \quad (2.15b)$$

and

$$f_2 = \frac{2(1-\gamma)(\rho_p - \rho_0)}{2\rho_p + \rho_0(1-3\gamma)} \quad (2.15c)$$

where,

$$\gamma = -\frac{3}{2} \left[1 + i \left(1 + \tilde{\delta}_v \right) \right] \tilde{\delta}_v \quad (2.15d)$$

$$\tilde{\delta}_v = \frac{\sqrt{2\eta}}{a\sqrt{\omega\rho_0}} \quad (2.15e)$$

where $\kappa_0 = 1/(\rho_0 c^2)$ and κ_p denote the compressibility of the liquid and particle respectively, ρ_p represent density of the particles, η is the shear viscosity coefficient of the fluid, ω is the angular frequency of excitation and δ_v indicate the boundary layer. In chapter 4 and chapter 5, we make use of this expression to numerically predict the behaviour of particles suspended in a fluid exposed to a travelling surface acoustic wave.

2. Background, Theory & Fabrication

A particle suspended in a second-order time-averaged standing pressure field ($\langle P_2 \rangle$) is forced to move towards either local pressure nodal (i.e. $\langle P_2 \rangle$ is minimum) or antinodal (i.e. $\langle P_2 \rangle$ is maximum) regions, depending on a parameter, termed acoustic factor, [170] Φ

$$\begin{aligned}\Phi &= \frac{1}{3}f_1 + \frac{1}{2}f_2 \\ &= \frac{1}{3} \left[\frac{5\rho_p - 2\rho_f}{2\rho_p + \rho_f} - \frac{\kappa_p}{\kappa_f} \right]\end{aligned}\quad (2.16)$$

where, ρ and κ represent density and wave number with subscripts P and f denoting particle and fluid, respectively. As such, a positive or negative values of Φ direct the particle towards pressure node or antinode, respectively.

2.3.2 Acoustic Streaming induced Drag Forces

The propagation of acoustic waves through a viscous fluid medium induce a second-order nonlinear body force which acts on the fluid in the direction of the wave propagation. As a result, a net flow, termed acoustic streaming, is produced that tends to promote steady vortices. This mechanism fundamentally arises due to two phenomena. Firstly, the attenuation of acoustic beam as it propagates through the medium (i.e. liquid or gas) generate velocity gradient, such that the velocity amplitude decreases along the propagation direction. When time-averaged, this insert a net force to the fluid and therefore a net flow. In literature, this phenomenon is assumed a common occurrence in SAW actuated devices. [171] The second phenomenon arises due to viscous effects at the limits of the fluid volume. Conforming to the no-slip condition on the wall, the medium within the viscous boundary layer δ_v , represented in Eqn. 2.15e is forced to vibrate rotationally. This leads to the formation of a primary streaming vortex that is largely confined to this layer (as shown in Fig. 2.5 (a) and 2.5 (b)). The fluid outside of the boundary layer vibrates irrationally, though, the streaming in the layer offer sufficient force strength to drive acoustic streaming across the bulk medium. [170] (see Fig. 2.5 (c))

The ability of acoustic waves to exert momentum flux on the medium through which they are propagating was first observed by Lord Rayleigh. [157] Since then, it has been successfully employed for the rapid fluid mixing, [175, 176] pumping, [177, 178] and particle

2. Background, Theory & Fabrication

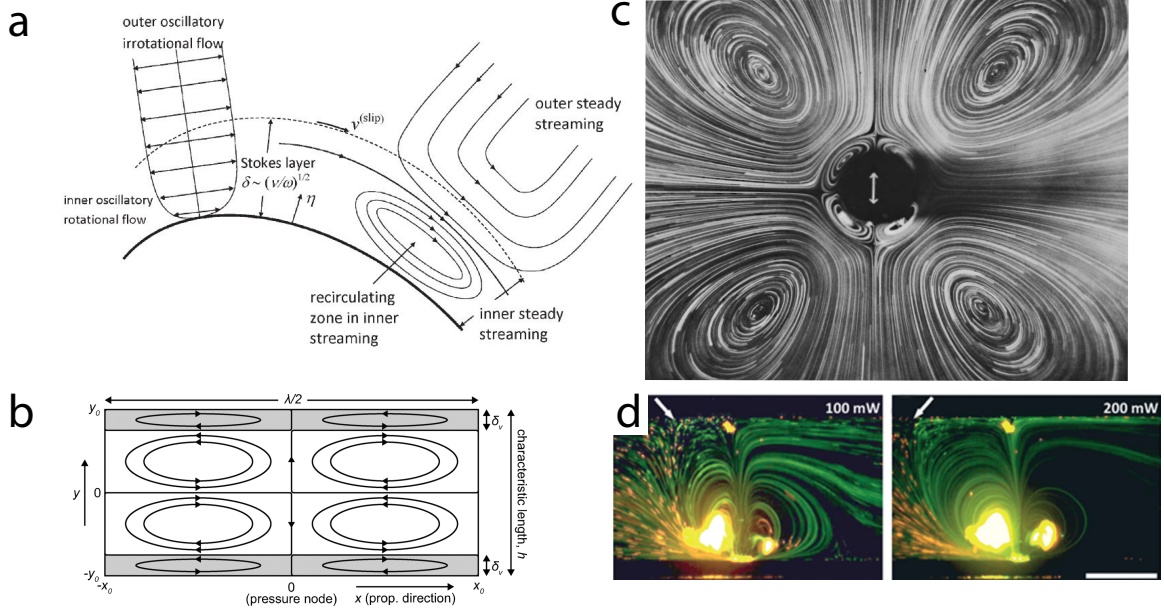


Figure 2.5: (a) Schematic illustrating the streaming arisen due to viscous effects at the limits of the fluid volume. Reproduced from [172] with permission from The Royal Society of Chemistry. (b) The cross-sectional view of the streaming within a microfluidic channel. Reproduced from [173] with permission from The Royal Society of Chemistry. (c) Streaming vortices formed in a bulk fluid by an oscillating cylinder in the centre. Reproduced from [172] with permission from The Royal Society of Chemistry. (d) Streaming within a microfluidic channel generated by surface acoustic waves (SAW), here is used for size-based sorting of particles. Scale bar is 200 μm . Reproduced from [174] with permission from The Royal Society of Chemistry.

concentration, [179–181] (Fig. 2.5 (d)) though there have also been significant efforts to suppress the streaming effects in acoustically-driven devices, as it can be disruptive to manipulation processes. [182]

To drive the expression of the driving force, we start from the continuity and Navier-Stokes equations for a compressible fluid,

$$\frac{\partial \rho}{\partial t} + \nabla \cdot (\rho \mathbf{v}) = 0 \quad (2.17\text{a})$$

$$\rho \left(\frac{\partial \mathbf{v}}{\partial t} + \mathbf{v} \cdot \nabla \mathbf{v} \right) = -\nabla p + \eta \nabla^2 \mathbf{v} + \left[\eta' + \left(\frac{4}{3} \right) \eta \right] \nabla (\nabla \cdot \mathbf{v}) \quad (2.17\text{b})$$

The combination of Eqn. 2.17a and the LHS of Eqn. 2.17b, equated to a body force (\mathbf{F}) yields,

$$\mathbf{F} = \frac{\partial(\rho \mathbf{v})}{\partial t} + \rho(\mathbf{v} \cdot \nabla) \mathbf{v} + \mathbf{v} \nabla \cdot \rho \mathbf{v} \quad (2.18)$$

2. Background, Theory & Fabrication

By time-averaging the body force we arrive at,

$$\langle \mathbf{F} \rangle = \langle \rho(\mathbf{v} \cdot \nabla) \mathbf{v} + \mathbf{v} \nabla \cdot \rho \mathbf{v} \rangle \quad (2.19)$$

The use of perturbation expansion theory (Eqn. 2.5) as previously yields the time-averaged second-order equations as,

$$\langle \mathbf{F} \rangle = \rho_0 \langle (\mathbf{v}_1 \cdot \nabla) \mathbf{v}_1 + \mathbf{v}_1 \nabla \cdot \mathbf{v}_1 \rangle \quad (2.20a)$$

$$\langle \mathbf{F} \rangle = -\nabla \langle P_2 \rangle + \left[\eta' + \left(\frac{4}{3} \right) \eta \right] \nabla (\nabla \cdot \mathbf{v}_2) + \eta \nabla^2 \mathbf{v}_2 \quad (2.20b)$$

Equation 2.20a and Equation 2.20b express the driving force of the acoustic streaming, whereby the second-order steady state velocity field \mathbf{v}_2 , known as streaming velocity, can be evaluated based on first-order velocity, \mathbf{v}_1 , and pressure fields, P_1 .

The fluid-suspended particles with an initial velocity of \mathbf{v}_p experience a drag force induced by the streaming velocity field, given by the Stokes drag equation,

$$\mathbf{F}_{\text{drag}} = 6\pi\eta a(\mathbf{v}_2 - \mathbf{v}_p) \quad (2.21)$$

where η indicates the fluid viscosity and a is the particle radius.

2.3.3 Bjerknes Forces

Bjerknes forces cause the mutual attraction or repulsion between individual particles or bubbles upon which the primary sound field is acting. [165] Scattering of the incident acoustic field off a particle alters the acoustic field experienced by nearby neighbouring particles. This interaction of one particle with the scattered wave of another gives rise to an inter-particle/bubble force termed Bjerknes forces. The strength of the Bjerknes force depends on the separation of the particles, as well as the ratio of size and acoustic wavelength, such that, the effect of these forces becomes increasingly significant as the particle size approaches the wavelength ($\lambda_{\text{SAW}} \sim D$). [183]

2. Background, Theory & Fabrication

2.4 Acoustic Excitation Methods

Acoustically driven microfluidic systems are mainly actuated using either bulk acoustic waves (section 2.4.1) or surface acoustic waves (section 2.4.2). These actuation methods fundamentally differ by the nature of their fluid-coupling mechanism. The bulk waves are excited across the fluid volume through resonating the entire microfluidic channel, whilst SAW is substrate-bound prior to coupling into the contacting fluid, thus can be readily oriented and localized, independent of channel boundaries. The use of each particular method offers specific advantages and limitations rendering them suitable for different applications as will be discussed in this section.

2.4.1 Bulk Acoustic Waves

In a typical BAW device (shown in Fig. 2.6), a piezoelectric transducer adhered to the fluid-filled channel is employed to generate vibrations within the system. By choice of an appropriate frequency to match the resonance criteria, acoustic waves are coupled to and resonate the fluid volume. Essentially, fluid is contained in a glass or silicon channel, highly reflective materials that assist with the formation of a standing field as the propagating and reflected bulk waves interfere. The channel's geometry, in particular the dimensions parallel to the wave propagation direction, have a significant influence on the performance of the system and formation of the desired standing field. To establish a resonant mode, the channels characteristic length should be designed to be multiple of half-wavelength [184] (see Fig. 2.6 (c)) As such the development of spatially one-dimensional, [185] and two-dimensional [186,187] standing fields require specific design of the system and appropriate choice of the channel width for 1D, and both width and length for 2D fields. The resultant acoustic radiation force, here, push suspended particles to the plains of either the pressure antinodes or nodes [188] (Fig. 2.6 (a) & (c)) depending on their acoustic contrast factor, Φ , (Eqn. 2.16) as discussed previously.

This actuation mechanism has been used in a wide range of manipulation applications; particle concentration, [190] separation, [191] and clustering in distinct lines, [185,192] grids, [186] and complex patterns. [21,193] The main limitation of BAW systems is that the pressure field is restricted to the resonant modes of the fluid medium. BAW devices typically operate at

2. Background, Theory & Fabrication

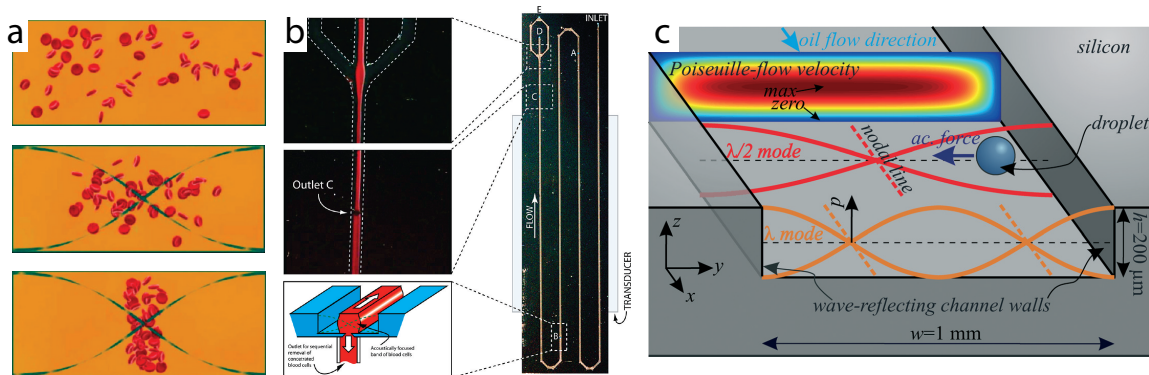


Figure 2.6: (a) Cross-sectional schematic of a standing acoustic field excited by a $\lambda_{acoustics}/2$ wavelength in a bulk acoustic wave (BAW) device depicting concentration of red blood cells in the pressure node. (b) A BAW device used for plasma separation. (a) & (b) are reprinted with permission from [189]. Copyright 2009 American Chemical Society. (c) Schematic of a BAW system and its working principle to manipulate particles. [184] - Published by The Royal Society of Chemistry.

kilohertz (kHz) to low megahertz (MHz) order frequencies which correspond to the wavelength of millimetre order. This length is several order of magnitude larger than the liquid-suspended objects (i.e. particles, cells and biomolecules), allowing for simultaneously positioning several clusters of particles in distinct locations, though, reducing the effectiveness and precision of manipulation on the order of individual particles. Furthermore, chip-integration of BAW systems may pose undesired effects on the other processes, demanding the need for a more lab on a chip compatible actuation technique. [160] As such, in our work, we have realised the advantages of SAW-driven systems to facilitate manipulation at a much finer length scale.

2.4.2 Surface Acoustic Waves

The phenomenon of wave propagation along the substrate surface was first reported by Lord Rayleigh in 1885. [163] In the following years, SAW continued to be the subject of several theoretical investigations, though their use in small scale applications had to wait for the availability of microfabrication technologies. The key technological advance to draw a surge of activity in the field of SAW was the invention of interdigitated transducers (IDT). However, the development of lithium tantalate (LT) and lithium niobate (LN) materials, serving as highly effective piezoelectric substrates for SAW, in the late 1960's played an important role in achieving the current advances. [162, 194] The initial widespread use of SAW was in telecommunication industry, [195] particularly for high-frequency signal processing, serving as bandpass filters and duplexers for radio frequency (RF) devices. [196] To date,

2. Background, Theory & Fabrication

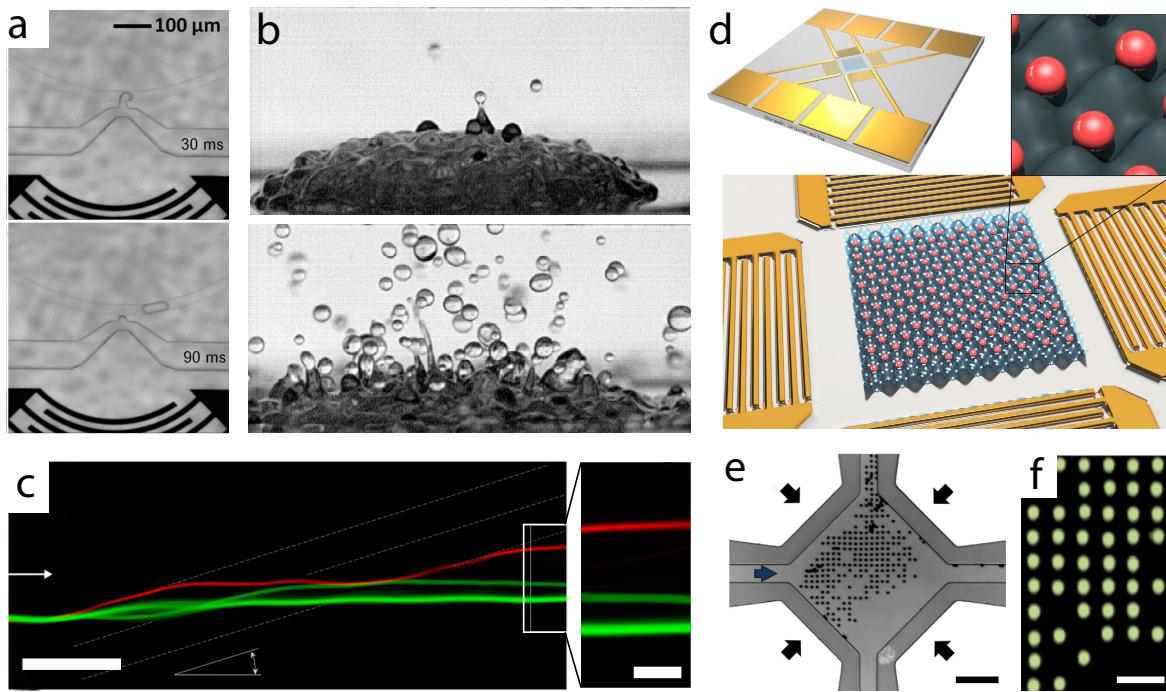


Figure 2.7: Representation of a few examples of surface acoustic wave (SAW) applications. (a) A SAW droplet maker device capable of producing picoliter droplets using a focused IDT. Reproduced from [46] with permission from The Royal Society of Chemistry. (b) Show the use of acoustics for atomization, [208]. Reproduced with permission. (c) A SAW cell sorter, separating 7.3 μm (green) and 9.9 μm (red) using straight IDT applied at an angle to the flow direction. Scale bar is 400 μm in the main image and 100 μm in the inset. [209] Copyright 2014 National Academy of Sciences. (d) Schematic of a SAW device capable of patterning single cells in a two-dimensional grid, (e) the experimental observation of the particle patterning. Scale bar is 100 μm (f) the patterning of particles when $\lambda/D = 3.33$. Scale bar is 30 μm . (d-f) reprinted from [86].

besides playing a critical role in RF communication, SAW has been successfully employed in bio-sensor technologies, [197] optical modulators, [198] touch sensitive screens, [199] and automotive windscreen raindrop sensors. [25]

Recently, the use of SAW in microfluidic technologies has received strong attention owing to its remarkable advantages over other lab on a chip actuation methods and have found application in droplet generation [200] (Fig. 2.7 (a)), merging, [201] and steering, [202, 203] atomization [204–206] (Fig. 2.7 (b)), size-based sorting [207] (Fig. 2.7 (c)), and particle patterning [86] (Fig. 2.7 (d) - (f)). SAW driven systems benefit from the concentrated mechanical displacement on the interface between the piezoelectric substrate and liquid resulting in the efficient coupling of energy to the liquid. Furthermore, by operating at Megahertz (MHz) frequencies SAW wavelengths can reach the dimension of individual micron sized particles, cells and biomolecules enabling high resolution and effective manipulation.

2. Background, Theory & Fabrication

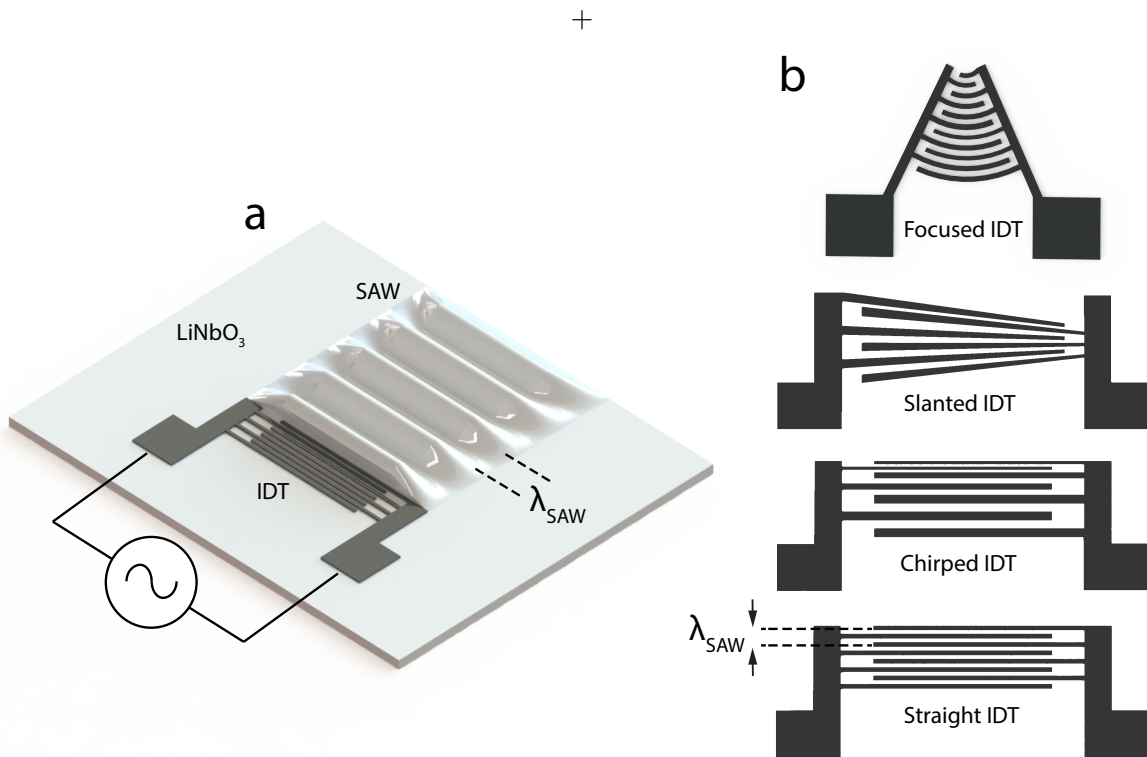


Figure 2.8: (a) A typical SAW device consists of a series of interdigitated transducers (IDT) patterned on a piezoelectric material, often Lithium Niobate (LiNbO_3 , LN). Upon actuation of the IDT at its resonant frequency, surface acoustic waves are produced and propagate on the substrate surface. It should be noted that illustration of the wavelength (λ_{SAW}) does not reflect their actual size. (b) Schematic of various configurations of the IDTs.

Theory

Piezoelectric properties in certain materials allow for conversion of electric charges to mechanical expansion or contraction, known as converse piezoelectric effect. [210] The predominant piezoelectric material used in typical SAW systems is Lithium Niobate (LN) due to several favourable parameters for this application including low acoustic attenuation, [196] high electromechanical coupling coefficient and high spontaneous polarization. [211, 212] The electromechanical coupling coefficient represents the efficiency of intrinsic electromechanical energy conversion by a particular material and is considered the most important coefficient of a piezoelectric material. [213] Spontaneous polarization indicates the electrical polarization possessed by the material in the absence of an external electric field. [214]

Surface acoustic waves are generated by a set of inter-locking comb-shaped conducting interdigitated transducers (IDT) patterned on the surface of a piezoelectric substrate (Fig.

2. Background, Theory & Fabrication

2.8 (a)). When an oscillating electrical signal is applied, IDTs are actuated at a frequency such that the mechanical displacement originated from one electrode constructively interfere with the waves emanating from the adjacent electrode resulting in the propagation of acoustic waves on the substrate surface, typically with the extent of one wavelength into the substrate. [215] The pitch of the electrodes, p , corresponds to the SAW wavelength dictating the optimum frequency, f of operation as given by,

$$f = \frac{C_{\text{SAW}}}{p} \quad (2.22)$$

where C_{SAW} is speed of sound in the substrate.

By the appropriate choice of wavelength, surface waves can be actuated at a range of frequencies from 10 MHz to 1 GHz. A major benefit over BAW systems is that the characteristics of propagating SAW can be modified to shape the resultant field as desired. This is made possible by simply changing the structure and pattern of the IDT. Several IDT configurations have been developed over time for use in a wide variety of applications. The most basic design, known as straight IDT, as shown in Fig 2.8 (b), consists of uniform electrode fingers, where each metal strip has a width of $\frac{1}{4}\lambda_{\text{SAW}}$. To generate SAW with higher intensity, concentric circular arc structure, termed focused IDT (Fig. 2.8 (b)), is used to laterally concentrate the displacement in a narrow region. [176, 216, 217] Other configurations include but not limited to, Chirped, [23] and slanted IDTs patterns [218] consisting of fingers with varying spacing and dimensions, respectively, to enable operation at a range of resonant frequencies (Fig. 2.8 (b)).

Widespread adoption of SAW to the portable microfluidics is only possible by optimisation of their power efficiency. The minimization and elimination of power loss require optimization of the IDT design by realising the importance of its electrical impedance. An electrically impedance matched circuit allow maximum power transition from the external power generator to the IDT and subsequently to the piezoelectric material and adjacent fluid. The IDT's electrical impedance is determined by several factors including the substrate and electrode materials, and the electrodes aperture, width and height. These factors are typically optimised by certain design parameters (e.g. operation frequency), thus cannot be simply modified. The

2. Background, Theory & Fabrication

number of finger pairs, though, can be appropriately chosen to adjust the impedance to match that of the excitation electronics, thus plays a critical role in achieving efficient operation. [219]

Upon encountering a fluid deposited on the substrate surface, SAW couples energy into the fluid in the form of longitudinal acoustic waves along an angle, termed the Rayleigh angle, θ_R , defined from a direction perpendicular to the substrate surface (see Fig. 2.9) and given by,

$$\theta_R = \sin^{-1}\left(\frac{C_l}{C_{\text{SAW}}}\right) \quad (2.23)$$

where C_{SAW} and C_l represent the sound speed in the substrate and in the liquid respectively.

The continuous leakage of energy into the fluid, as SAW propagates along the substrate-fluid interface, lead to the decay of surface waves with increasing distance from the SAW emanating source. The attenuation coefficient, α^{-1} , determining the length over which this phenomenon occurs (see Fig. 2.9) as given by, [220, 221]

$$\alpha^{-1} = \frac{\rho_s C_{\text{SAW}} \lambda_{\text{SAW}}}{\rho_0 C_l} \quad (2.24)$$

where ρ_s is the density of the substrate. The uniaxial propagation of the transmitted waves along the Rayleigh angle, θ_R , has a distinctly different attenuation length, defined as β^{-1} coefficient (see Fig. 2.9) given by, [221]

$$\beta^{-1} = \frac{\rho_0 C_l^3}{4\pi^2 f^2 \left(\frac{4}{3}\eta + \eta'\right)} \quad (2.25)$$

The acoustic streaming in SAW devices is often described as mainly being driven by the attenuation of propagating SAW beam through the fluid. [221] The other forms of energy loss (e.g due to friction) in an acoustically driven system are often considered small and therefore, typically neglected. Microfluidic SAW devices are mainly classified into travelling surface acoustic waves (TSAW) and standing surface acoustic waves (SSAW). These assumptions will be examined in the subsequent sections.

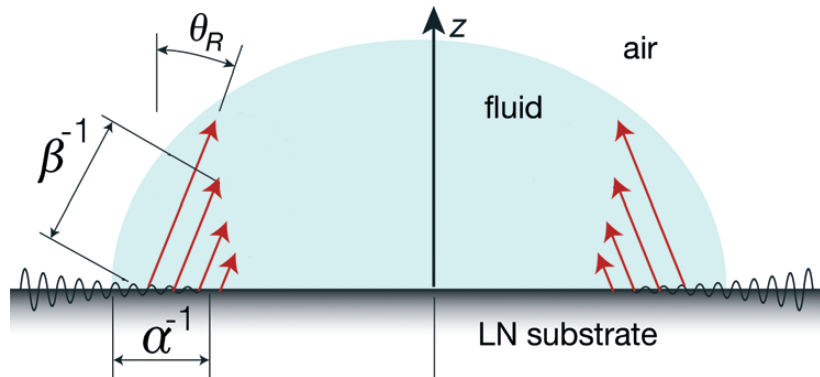


Figure 2.9: When surface acoustic waves (SAW) encounter an overlaying fluid, they are transmitted to the fluid along the Rayleigh angle θ_R . SAW attenuate along the substrate indicated with α^{-1} and along the fluid indicated with β^{-1} . Reproduced from [162] with permission from The Royal Society of Chemistry.

Travelling Surface Acoustic Waves

In a typical travelling wave system, one set of IDT generates a SAW propagating orthogonally to a microfluidic channel. The acoustic energy passes through the fluid media and interacts with the suspended matter (i.e. particle, cell and droplets), whereby particles are subjected to acoustic radiation force (section 2.3.1) and acoustic streaming induced drag forces (section 2.3.2), simultaneously. As such, the dominant force act to manipulate the particles. The acoustic radiation force is mostly assumed to push particles away from the SAW emanating source conforming to the present theoretical and experimental literature. This particular effect has found use in particle sorting, [222] droplet displacement, [223] chemical concentration gradient generation, [224] and on-chip fluorescence-activated cell sorting (FACTS). [225, 226] However, Destgeer *et al* show that there is an “anechoic corner” along the channel edge nearest to the SAW source where no migration takes place. In this region, acoustic streaming dominates and entrain particles in strong continues vortices. [227, 228] Only recently, Devendran *et al* have observed patterning behaviour in TSAW systems formerly only recognised in SSAW systems. [229] The patterning and migration of particles along with the streaming effects in a TSAW system are further explored and discussed in a numerical and experimental study in chapter 4, where it is realised that the dominant effect depends on the spatial location in the channel. Apart from location, particle size plays a critical role. The present literature determines the dominance of radiation or streaming forces based on a dimensionless number ($\kappa = ka$, k represent wave number and a is particle radius), defined in

2. Background, Theory & Fabrication

an experimental study that uses a different configuration than the conventional systems. [230] In a conventional TSAW system and by realising the patterning effect, chapter 5 of this thesis examine the role of size as a function of TSAW frequency and power.

Standing Surface Acoustic Waves

Standing surface acoustic wave (SSAW) is formed by interference of the SAW emanating from two opposing IDTs, operating at the same frequency. In this case, the resultant standing acoustic field is one-dimensional (an example is shown in Fig. 2.7 (c)). [216] Using two pairs of orthogonally opposing IDTs give rise to a two-dimensional standing field [231] (see Fig. 2.9 (d)). Both one-dimensional and two-dimensional fields consist of nodal and anti-nodal regions giving rise to ARF which act to trap particles in these regions based on their acoustic contrast, Φ , (Eqn. 2.16) to the fluid media. Most literature on precise particle manipulation reports the use of SSAW field, particularly when the particle size approaches that of the acoustic wavelength ($\lambda_{\text{SAW}} \sim D$). Some examples include patterning of particles as clusters, [231] or individually. [86, 183] By using frequency-matched counter propagating SAW, the standing field is often established across the entire channel area. However, SSAW fields have been established with pulsed actuation for spatially selective trapping location, [232] and by counter waves with slightly different frequencies to form an adjustable trapping location. [233] Chapter 3 of this thesis, represent a novel use of SSAW for a versatile and contactless filtration of particles whose size approaches that of the wavelength.

2.5 Fabrication

Essential to the development of microfluidic devices are the micro-technologies that enable fabrication of features on the scale of micrometre. Technologies based on etching/lithography/deposition can be applied in the range of scales between 0.2 μm and 500 μm , [53] thus the preferred method for the systems used in this thesis. Here, the SAW device (section 2.5.1) and the microfluidic channel (section 2.5.2) are fabricated separately, then bonded together (section 2.5.3) to produce a fully-functional device.

2. Background, Theory & Fabrication

2.5.1 SAW Device Fabrication

To produce a SAW device, the primary step is to design the IDT based on the intended application. A typical straight IDT consists of two sets of opposing connected metallic fingers, bus bar and electrode pads patterned on a piezoelectric substrate. In the design of a straight IDT, the most important factors include the width of each finger (corresponding to the required wavelength), IDT aperture (defined as the width of overlapping fingers) and the number of finger pairs (for an efficient operation). To design focused IDTs, besides finger width, IDT aperture and finger pairs numbers an extra element to consider is the focal length, f_{length} defined as:

$$f_{length} = \frac{R_f}{1 - 2b} \quad (2.26)$$

where R_f represents the finger curvature and b is anisotropy of the substrate material. Literature reports on the use of 10 MHz to 1 GHz range corresponding to 400 μm to 4 μm wavelength for an LN substrate in SAW driven microfluidics. This implies that features as small as 100 μm to 1 μm are required. Photolithography is a versatile and powerful tool to define micron and submicron features on the piezoelectric substrate. [234] In the work contained in this thesis, the piezoelectric substrate is 0.5 mm thick 128° Y-cut X-propagating lithium niobate wafer as this crystal orientation offer large electromechanical coupling coefficient, [235] desirable for an efficient electrical-mechanical energy conversion. The photolithography procedure consists of 4 steps (shown in Fig. 2.10 (a)(i)-(iv)): (1) the wafer is spin coated with a layer of photosensitive resist; (2) then heat treatment to remove the remaining solvent in photoresist; (3) by using a photomask placed on top of the wafer, the required features are selectively exposed to a uniform ultraviolet (UV) light (in case of a positive resist) or protected (in case of a negative resist); (4) then the features are realised on the wafer by dissolving the undesired regions, using an appropriate developer.

The IDTs are made up of conductive materials including Aluminium (Al) or Gold (Au), adhered to the LN substrate by the use of an adhesion layer comprising of chromium (Cr) or titanium (Ti). The choice for the overall thickness of the metal film is limited by the competition between efficient transmission of the electrical current to the IDT

2. Background, Theory & Fabrication

(acquired in thicker films) and low mass present of the substrate (in thinner films). As such, the total thickness is chosen so that the ratio of thickness, h and wavelength λ_{SAW} approximates to 1%. [162]

$$\frac{h}{\lambda_{\text{SAW}}} \approx 1\% \quad (2.27)$$

The metal layers are deposited on the wafer using high-vacuum electron-beam evaporation, as shown in Fig. 2.10 (a)(v) & (vi). In this deposition technique, a sample of metal is heated by an electron beam to reach evaporation, where individual atoms present at the surface gain sufficient energy to overcome the metallic bond and radiate along a straight path in all directions. Upon encountering the substrate surface, they are uniformly deposited to the surface and form a layer of metal film with a constant thickness. Modifying the thickness require adjustment of the metal temperature and the exposure time. This is followed by a lift-off procedure (Fig. 2.10 (vii)), wherein the wafer rests in a solvent that allows for removal of the photoresist underneath the deposited metal. This enables the creation of a metallic structure for the previously defined features. To protect the IDT fingers from degradation by corrosion and to promote adhesion of the chamber to LN wafer, a layer of SiO_2 is deposited (Fig. 2.10 (viii)). The final step is dicing the wafer to produce individual fully functional SAW-driven devices (Fig. 2.10 (ix)). Using a high-speed blade with a thickness reduced to approximately $20 \mu\text{m} \sim 35 \mu\text{m}$, the desired cuts are made along pre-defined lines that separate SAW-devices.

2.5.2 Chamber Fabrication

The use of Polydimethylsiloxane (PDMS) for microchannels is highly desirable. PDMS is a silicon-based organic polymer that offers several favourable properties for microfluidic applications. Apart from low cost, optical transparency, permeability to gases and excellent elasticity, PDMS is well known for its mould release properties, ease of fabrication and assembly to the microfluidic chip. [236] Fabrication of PDMS microchannels requires the use of the micro-moulding process, where photolithography along with deep reactive ion etching (DRIE) create the microchannel features on a silicon wafer. Here, the silicon wafer serves as a mould containing patterns, on top of which the liquid PDMS (mixed with 1:10 curing agent)

2. Background, Theory & Fabrication

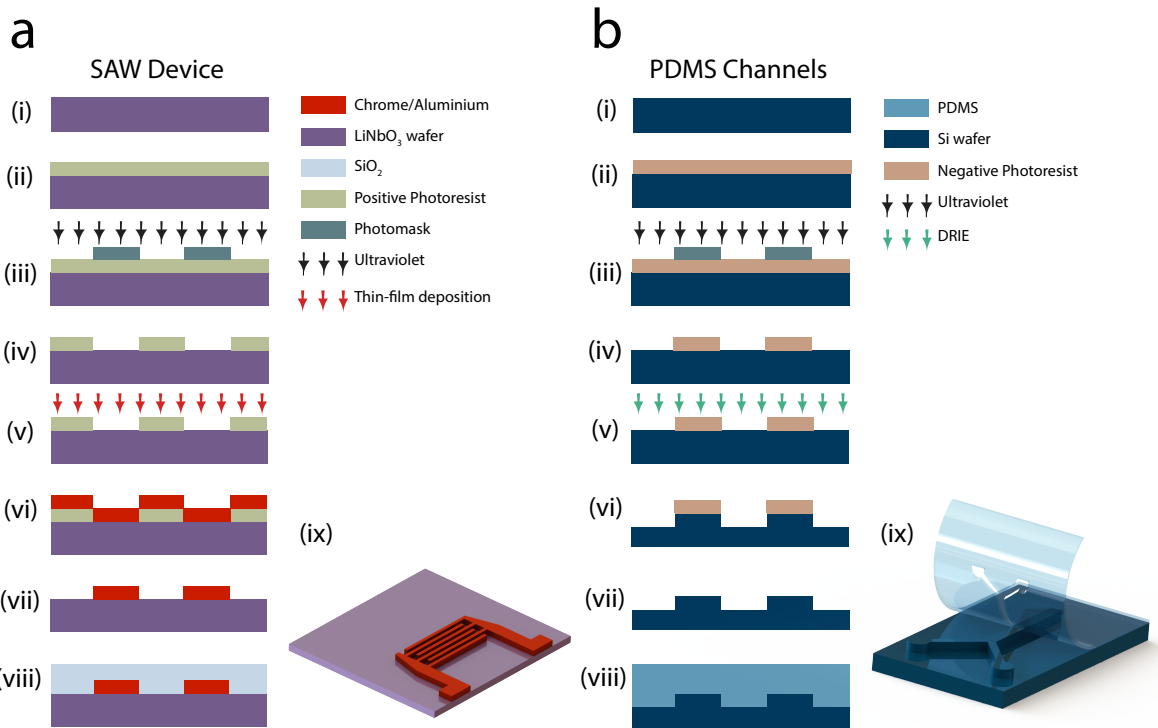


Figure 2.10: SAW device and PDMS channels are fabricated separately. The process diagram of the fabrication procedure for (a) the SAW device and (b) the PDMS channels are illustrated. The (a-i) LiNbO₃ wafer is (a-ii) spin coated with a positive photoresist (a-iii) then selectively exposed to the ultraviolet light by using a photomask. (a-iv) The patterned features are developed on the wafer. (a-v) & (a-vi) Metal layers are deposited by e-beam evaporation process (a-vii) patterned metals are realised on the wafer by lift off. Finally (a-viii) a layer of SiO₂ is deposited on the wafer. (ix) After dicing, fully functional SAW devices are produced. To fabricate the PDMS mould (b-i) & (b-ii) Si wafer is spin coated with a negative photoresist. (b-iii) Upon exposure to the ultraviolet light, and (b-iv) after dissolving the undesired photoresist, (b-v) & (b-vi) the wafer is etched using DRIE etching process to (b-vii) realise the mould features. (b-viii) Finally the PDMS is poured onto the mould and after heat treatment (b-ix) the desired channel features are imprinted within the cured PDMS.

is poured and after heat treating, cured (see Fig. 2.10 (b)(viii) & (ix)). As such, the inverse of silicon mould patterns is imprinted in the PDMS cast. With very low shrinkage during cure, PDMS offer the ability to replicate features down to micron and nano scales. [237] There are several methods to construct the silicon mould. In this thesis, the photolithography using a negative-tone UV photoresist was used to define the channel patterns on the Si wafer (Fig. 2.10 (b)(i)-(iv)). Here, the patterned photoresist serves as a mask for a selective deep reactive ion etching (DRIE). The exposed areas are isotropically etched by repeatedly applying the etchant (SF₆) and passivation (C₄F₈) plasma steps to create the patterns of required depth (Fig. 2.10 (b)(v)-(vii)). The rate of photoresist etching is relatively much less than that of the Si wafer, making this technique appropriate for the etch depths of up to 50 μm.

2. Background, Theory & Fabrication

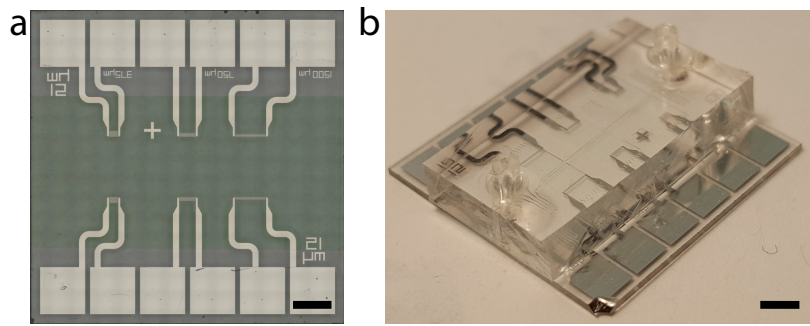


Figure 2.11: Illustration of the device (a) prior and (b) after its bonding to the PDMS channels. This device was used to conduct the experiments for the research presented in chapter 4 and chapter 5. Scale bars are 2 mm

2.5.3 Device Assembly

To produce a SAW actuated system with enclosed microfluidic channels, the SAW device and PDMS channels are assembled through a bonding process (see Fig. 2.11). In this process, the oxygen plasma exposure is used to activate the surface of LN and PDMS (on the imprinted side). By bringing these surfaces into contact, the increased concentration of hydroxyl (-OH) groups on the exposed surface of PDMS result in the formation of strong intermolecular bonds, [238–240] generating a waterproof and irreversible seal.

This chapter explores the role of elevated frequencies in SAW-driven systems, realised by reducing the acoustic half wavelength to the dimension of individual particles. In doing so a novel, highly sensitive, and high resolution membraneless filtration technique for filtration of micron particles is developed.

3

Virtual Membrane for Filtration of Particles

3.1 Overview

Sorting and filtration of a particular type of cells from a biological sample is fundamental for further analysis of the sample. Systems capable of automated filtration of particles and cells, facilitate essential biological studies and enable point-of-care diagnostic technologies. To date, numerous acoustically driven technologies actuated by either BAW or SAW perform particle sorting. Compared to the BAW systems, SAW actuated devices operate at a much higher frequency range potentially allowing particle manipulation at a much finer scale. In a unique manner, here we further reduce the wavelength to the dimension of individual particles and explore the effect of elevated frequencies in SAW systems and open up a new sorting mechanism.

In a novel approach, this work presents a sensitive particle sorting system which employs surface acoustic waves (SAW) to selectively filter particles with a specific size profile from a mixed population. Our device consists of two diagonally opposed pairs of radially focused interdigital transducers (FIDTs) oriented at a 60° angle relative to the flow direction. FIDTs permit the generation of a highly localized standing wave field (with a wavelength on the order of particle's size) which acts like as a “virtual membrane” filtering particular particle sizes based on two distinct phenomena. Firstly, particles that are greater than approximately 0.3 times of the acoustic half wavelength (i.e. $a > 0.3\lambda_{\text{SAW}}/2$), experience an overall force

3. Virtual Membrane for Filtration of Particles

that prohibits them from progressing further downstream, thus being filtered. These trapped particles are held in predetermined locations, which offer localised optical analysis potential. In contrast, the smaller particles will pass through the force field along the pressure nodes (akin to a filter pores), thus flowing through uninhibited, allowing for selective filtration of one particle type from a mixed population. The key to the high size selectivity of the presented virtual membrane is the contrast in the force fields experienced by particles of various sizes with respect to the acoustic wavelength. If the particle size is such that, at a given flow velocity and acoustic power, the repulsive acoustic force is dominant over the flow induced drag forces, the particles will be filtered out from the flow stream, otherwise it will progress downstream. The underlying mechanism of the deterministic particle filtration system was first established via numerical simulations, followed by experimental validation. Utilising high-frequency SAW at 258 MHz, 192.5 MHz and 129.5 MHz, filtration of 8 μm from 5 μm particles and 10.36 μm particles from 7 μm and 5 μm particles respectively is achieved.

3.2 Publication

The following publication was reproduced from [241] with kind permission from the Royal Society of Chemistry.



Lab on a Chip

PAPER

[View Article Online](#)

[View Journal](#) | [View Issue](#)



CrossMark
click for updates

Cite this: *Lab Chip*, 2016, **16**, 3515

Received 3rd May 2016,
Accepted 18th July 2016

DOI: 10.1039/c6lc00590j

www.rsc.org/loc

Virtual membrane for filtration of particles using surface acoustic waves (SAW)

Armaghan Fakhfouri,^a Citsabehsan Devendran,^a David J. Collins,^b Ye Al^b and Adrian Neild^{*a}

Surface acoustic wave (SAW) based particle manipulation is contactless, versatile, non-invasive and biocompatible making it useful for biological studies and diagnostic technologies. In this work, we present a sensitive particle sorting system, termed the virtual membrane, in which a periodic acoustic field with a wavelength on the order of particle dimensions permits size-selective filtration. Polystyrene particles that are larger than approximately 0.3 times the acoustic half-wavelength experience a force repelling them from the acoustic field. If the particle size is such that, at a given acoustic power and flow velocity, this repulsive force is dominant over the drag force, these particles will be prohibited from progressing further downstream (*i.e.* filtered), while smaller particles will be able to pass through the force field along the pressure nodes (akin to a filter's pores). Using this mechanism, we demonstrate high size selectivity using a standing SAW generated by opposing sets of focused interdigital transducers (FIDTs). The use of FIDTs permits the generation of a highly localized standing wave field, here used for filtration in $\mu\text{l min}^{-1}$ order flow rates at 10s of mW of applied power. Specifically, we demonstrate the filtration of 8 μm particles from 5 μm particles and 10.36 μm particles from 7.0 μm and 5.0 μm particles, using high frequency SAW at 258 MHz, 192.5 MHz, and 129.5 MHz, respectively.

Introduction

Separation and filtration of micron sized particles and cells is an essential step for various chemical and medical processes. In point-of-care diagnostic devices, for example, automated filtration of a specific type of cell from a biological sample is essential for further analysis, where microfluidic systems can perform this task with minimal reagent, time and cost. On-chip manipulation of suspended particles is accomplished using the advantageous characteristics of microscale flow, particularly the fluid viscous drag force. This is usually accompanied by the application of an external force including those arising from optical^{1,2} dielectrophoretic (DEP)^{3–5} and acoustophoretic fields.^{6–8} The interplay between these external forces and the drag forces induced by the flow field can be used to achieve particle separation. To date, the vast majority of these sorting strategies operate such that the particles are dragged through the force field by the flowing fluid but follow distinct trajectories based on their different responses to an externally applied field, as such the streamline

along which particles exit the force field is size dependent.^{9–16} In addition, external fields have also been used to non-selectively manipulate and trap suspended particles against a flow, and this has been demonstrated using mechanical,^{17,18} hydrodynamic,¹⁹ optical,^{20,21} magnetic actuation^{22,23} and acoustic^{24–26} techniques. Acoustic forces are particularly suitable for microfluidic actuation owing to their high biocompatibility^{27–30} and straightforward microfluidic integration.

Here, we combine these features (sorting within a flow and trapping against a flow) by selectively filtering particles with a specific size profile from a mixed population. The trapped particles are held in a pre-determined position, offering potential for localised optical analysis, while the untrapped particles are allowed to flow through and out of the chip permitting the selective dispensing of one particle type from a mixed population.

Acoustofluidics, *i.e.* the application of acoustic effects in microfluidic systems, utilises acoustic radiation forces (ARF) as a method for manipulating microparticles (suspended objects including cells). Particles immersed in a fluid with a different density and/or sound speed to the surrounding medium are subjected to ARF when they are exposed to an oscillating pressure and fluid displacement field. This effect arises from second order terms in the Navier-Stokes equation, which are non-zero when integrated over the particle's

^a Laboratory for Micro Systems, Department of Mechanical and Aerospace Engineering, Monash University, Clayton, Victoria 3800, Australia.
E-mail: Adrian.neild@monash.edu

^b Engineering Product Design Pillar, Singapore University of Technology and Design, Singapore

3. Virtual Membrane for Filtration of Particles

[View Article Online](#)

Paper

Lab on a Chip

surface and time-averaged over an acoustic cycle.^{31,32} The time scale of ARF-induced migration is, therefore, much larger than the time period of an acoustic oscillation, although the maximum particle migration distance in a standing wave field scales with the wavelength of the pressure field. Typical methods exploiting ARF for size-based particle filtration utilize actuation based on bulk acoustic waves (BAW) or surface acoustic waves (SAW). The former are produced through exciting a resonance within the fluid volume.^{33–39} ARF can be used for sorting by exploiting the difference in time (*i.e.* migration rate) required to move particles of various sizes to the pressure node in the standing wave field^{40–42} or the different behaviour of particles with differing material parameters,¹² where particles experience a difference in ARF magnitude based on their dimensions and physical properties. While the location and orientation of a BAW-generated wave is typically determined by the channel geometries and their acoustic properties (iso-impedance channel materials can be used to partially decouple the acoustic and channel interfaces³⁴), a SAW is substrate-bound prior to coupling into contacting materials and can thus be readily oriented and highly localized.^{43,44} A SAW is generated on a piezoelectric substrate by an alternating electrical current applied across a series of interdigital transducers (IDTs), whose micron-scale feature sizes result in 4–400 µm wavelengths that are directly comparable to typical microfluidic channel dimensions. Accordingly, SAW has been widely used in microfluidics for activities such as droplet production,³² merging⁴⁵ and steering,^{46,47} atomization,^{48–50} highly controllable particle manipulation^{43,51,52} and mixing.^{53,54} The key features of SAW actuation have been exploited in sorting applications to cause particles to follow size dependent trajectories through the force field. SAW is similarly suited for size-selective sorting applications because of its ability to create highly localized fields^{55,56} that are independent of the channel orientation⁶ and its ability to utilise standing wave⁵⁷ or travelling wave⁵⁸ mechanisms, or a combination of both.⁵⁹ In addition, SAW actuation allows operation across a wide range of wavelengths (~5–300 µm), the lower end of which means that wavelengths on the order of cell dimensions can be excited.

Here we exploit the ability to generate small wavelengths on the order of particle dimensions to selectively filter (and trap) one particle size from a mixed flowing particle suspension.

We utilize a standing pressure field established *via* actuation of counter-propagating focused SAWs oriented at an angle of 60° to the flow direction. It is known that particles considerably smaller than the acoustic wavelength will migrate along pressure nodes to locations of maximum field strength.³⁶ We show that if a particle has a diameter greater than 0.15λ_{SAW} the force along the nodal line switches sign and acts to repel the particle from the sound field. By balancing the acoustic power and flow rate, we show experimentally that particles with a diameter similar to or greater than half the wavelength (*i.e.* λ_{SAW}/2) are trapped statically,

while smaller particles pass through the sound field along pressure nodes. The alignment of smaller particles as they pass through the field are as if along virtual pores projecting perpendicularly to the acoustic propagation axis. Coupled with the size based trapping effect, we accordingly term this acoustic field and its acoustofluidic interactions the virtual membrane.

Using this SAW-based virtual membrane, we demonstrate continuous separation of 5 µm and 3 µm, 8 µm and 5 µm, 10.36 µm and 7.0 µm/5.0 µm, and 15 µm and 10 µm/8 µm diameter particles with actuation at 385.5 MHz, 258 MHz, 192.5 MHz, and 129.5 MHz, respectively. In each case, the frequency corresponds to a device pitch (λ_{SAW}/2) of the larger particle diameter.

Methodology

Experimental method

The device consists of a microfluidic channel, cast in polydimethylsiloxane (PDMS, 1:10 ratio of curing agent/polymer), and aligned on top of a SAW device. The SAW device is composed of two diagonally opposed pairs of radially focused interdigital transducers (FIDTs) on a lithium niobate (LiNbO₃) piezoelectric substrate (Fig. 1). In the experiments conducted, several devices with IDTs of varying wavelengths were used in order to conclusively demonstrate the effect of acoustic wavelength on particle filtration. Three different IDT designs were used: 40 finger pairs at 20 µm wavelength (λ_{SAW}), 38 finger pairs at 15 µm wavelength and 36 finger pairs at 10 µm wavelength, all spanning 26° with a geometric focal point 160 µm from the last finger pair. The 7/200 nm chrome/aluminium IDTs were deposited on a 0.5 mm thick, double side polished 128° *y*-cut *x*-propagating LiNbO₃ substrate. A 300 nm SiO₂ layer was further applied to prevent electrode degradation and to enhance adhesion of the substrate with the PDMS after exposure to air plasma. To improve separation efficiency, the FIDTs were arranged at a 60° angle relative to the centre line of a 200 µm wide, 24.6 µm high straight microfluidic PDMS channel.

Polystyrene particles (Magsphere, Pasadena, CA, USA) homogeneously suspended in solution (water diluted with 0.2% polyethylene glycol (PEG)) were continuously injected into the microfluidic chamber through a 20 µm wide perpendicular injection channel by using a syringe pump (KDS100, KD Scientific, Holliston, MA, USA). The electrical signal required to excite the SAWs was produced by an RF signal generator (Rohde & Schwarz HAMEG HM8134-3), amplified (Research (25A250A)) and applied to the opposing FIDTs. The experiments were conducted on the stage of a fluorescence microscope (Olympus BX43) with a light source (Olympus U-RFL-T) and imaged using a PixeLink (PL-B782U usb2) digital CCD colour camera.

Numerical simulation

The forces acting on a particle suspended in an acoustic field can be obtained analytically from knowledge of the pressure

3. Virtual Membrane for Filtration of Particles

[View Article Online](#)

Lab on a Chip

Paper

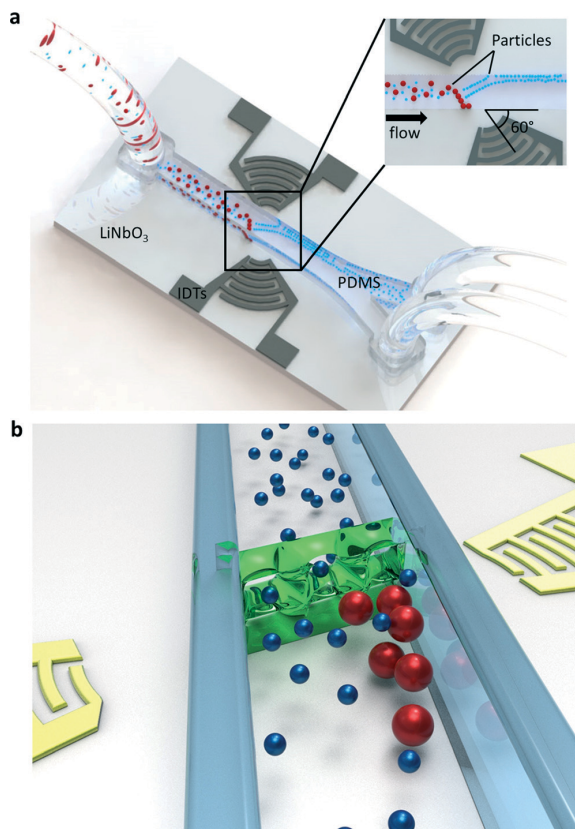


Fig. 1 (a) 3D rendered image of the virtual membrane for a particle filtration system structure and the operation of the device: two diagonally opposed pairs of radially focused interdigital transducers (FIDTs), arrayed on a lithium niobate (LiNbO_3) substrate, oriented at a 60° angle relative to the flow direction confined within a straight PDMS microfluidic channel. An aqueous solution containing various-sized suspended particles enters an acoustic field created by focused IDTs where particles are influenced by the 2nd order time averaged absolute pressure field. Larger particles are trapped at the beginning of the field, whereas smaller particles pass through pressure minima lines towards the upper boundary of the microfluidic chamber. (b) Zoomed-in image of the acoustic filtration region, whereby the virtual membrane (depicted in green) acts as a filter for the larger particles (red) while allowing the smaller particles (blue) to pass through the virtual pores.

field, provided the particle's size is much smaller than the acoustic wavelength.^{60,61} In this study, effects of standing surface acoustic waves (SSAW) on particles with sizes approaching half of the SAW wavelength are examined, for which a numerical method is required. The key to the virtual membrane concept is the difference in the force fields experienced by particles with different dimensions with respect to the acoustic wavelength. In order to demonstrate the proposed concept, a simplified 2D COMSOL Multiphysics 5.0 model has been developed. Experimentally, a standing acoustic pressure field is generated by using a pair of opposing FIDTs. Whilst a full 3D model of this would be desirable, it is not practical due to enormous computational cost. The 2D

model employed, however, is sufficient to clearly demonstrate the trends in the acoustic force field magnitude as the particle size approaches half an acoustic wavelength while minimizing computational load. The model consists of a fluid filled chamber, at each end of which the boundaries act as a radiating pressure source. These boundaries have a curved profile to mimic the production of a focused standing acoustic pressure field (Fig. 2) imposed by the FIDTs. The acoustic wavelength used in the numerical simulations are equated to that of the experimentally applied SAW wavelength λ_{SAW} .

The presence of a particle in an acoustic field scatters and diffracts incident sound waves. To avoid multiple reflections of the scattered component, matched impedance boundary conditions were imposed on the upper and lower edges of the fluid volume, mimicking the continuous channel used experimentally. In order to simulate the acoustic energy loss due to SAW amplitude decay along the substrate/fluid interface, the model incorporates acoustic attenuation ($\alpha_{\text{SAW}} = 1/(9.2 \times \lambda_{\text{SAW}})$ Nepers per m).⁶² Having imposed the conditions required to generate a representative pressure field, the acoustic radiation force (ARF) exerted on a compressible particle is calculated^{59,63} using:

$$F_{\text{rad}} = \frac{1}{2} \rho_f \int_{s_0} \left[\langle v_i^2 \rangle - \frac{1}{\rho_i^2 C_f^2} \langle p_i^2 \rangle \right] n dS - \rho_f \int_{s_0} \langle (n \cdot v_i) v_i \rangle dS \quad (1)$$

where ρ_f and C_f represent the density and sound speed of the fluid with values of 1000 kg m^{-3} and 1490 m s^{-1} , respectively, for water. The parameters $\langle p_i^2 \rangle$ and $\langle v_i^2 \rangle$ are the mean square fluctuation of the pressure and velocity, respectively. For the fluorescent polystyrene particles used, the density (ρ_p) is 1050 kg m^{-3} and the speed of sound (C_p) is 2350 m s^{-1} . In line with previous studies, for the purpose of modelling the acoustic forces, the fluid is assumed to be inviscid. The radiation forces calculated, as obtained from the numerical model in COMSOL, have been benchmarked against cases studied by Dual

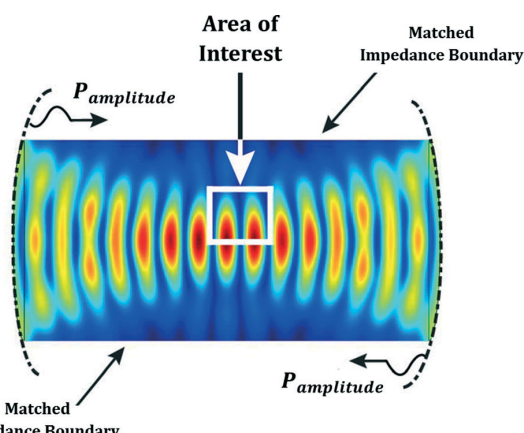


Fig. 2 FEA model of the system illustrating the 2nd order time averaged absolute pressure distribution as well as the applied boundary conditions. The area of interest depicts the region where the lateral forces are evaluated.

3. Virtual Membrane for Filtration of Particles

[View Article Online](#)

Paper

Lab on a Chip

et al.⁶³ The spatial variation in the forces (x and y components) are found by moving the particles to various locations, and this is carried out along defined lines of interest over a distance of λ_{SAW} with a step size of $\lambda_{SAW}/9$. Particles in a standing wave field that are denser and stiffer than the surrounding medium will migrate to the pressure nodes; forces are therefore examined along the line (AB) in Fig. 3a that cuts through the nodes and antinodes of the standing wave. Furthermore, for a standing wave with lateral intensity variation, small particles can be expected to migrate towards pressure nodes but also towards the lateral location along which there is maximum pressure fluctuation,³⁷ which occurs here at the

centre of our focused field. To explore how this behaviour varies with particle size, the second line of interest is defined as being along the length of the central pressure node (line CD in Fig. 3a).

Results and discussion

Numerical results

Particles are brought towards the edge of acoustic field by the fluid flow. With an initial random distribution across the width of the channel, they can encounter any part of the standing wave from the node to the antinode; as such, the forces have been calculated along line AB (Fig. 3a) which stretches from one antinode to the next.

The forces are derived from eqn (1) and are the integral of forces on the surface of the particles shown in Fig. 3(b) and (c). The results are shown in Fig. 3(d) and (e) for the forces in the x (along AB) and y (along CD) directions, respectively. Fig. 3d demonstrates that the forces in the x -direction act to move the particles towards the pressure node regardless of particle size (over the range examined), although the magnitude of these forces does vary. The force components in the y direction (perpendicular to the nodes), as shown in Fig. 3e for particles located along AB, however, show a variation in both magnitude and sign. For the case of the smaller 2 μm particle, the force fluctuates in sign along AB, becoming negative (directed into the sound field) as the particle approaches the nodal position. As such, smaller particles are pushed laterally towards the node, a location at which they are then drawn into the acoustic field. This is in agreement with analytical expressions and experimental data for particles substantially smaller than the wavelength.³⁶ However, the force acting on the 10 and 5 μm particles ($\lambda_{SAW} = 20 \mu\text{m}$) is positive along the whole length of AB and as such acts to prevent the particles from entering the sound field.

The force field is further examined by considering the forces along line CD in the y -direction (in the x -direction, they are as close to zero as allowed numerically). As shown in Fig. 3f, the smaller particles are drawn to the location $y = 0$ along the nodal line, again in line with expectations.³⁶ However, a positive (repulsive) force is shown to be present along the length of line CD for larger particles, preventing them from travelling along the node.

The simulations show that the sound field will repulse particles whose dimensions approach the half wavelength of the acoustic field and can thus counteract flow induced fluid drag. To define what is meant by a “larger” particle, Fig. 3g shows the value of F_y at a single location along CD for varying particle diameters (scaled based on each of the three wavelengths used). The data for each wavelength don’t collapse onto a single line due to wavelength dependent differences in the degree of lateral focusing in the sound field. For each of the wavelengths at small particle sizes, the force is negative, i.e. the particle is drawn into the field, whilst for larger particle sizes this becomes positive indicating rejection from the field. The crossover in the sign of the force occurs over

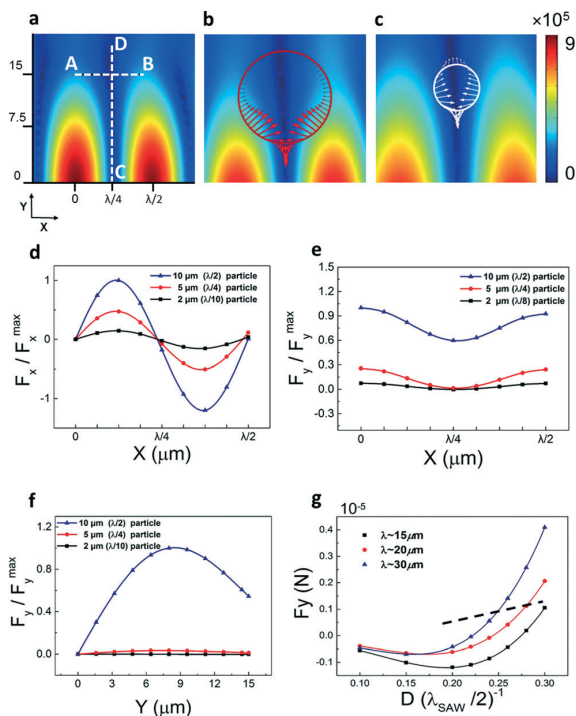


Fig. 3 (a) FEA model of the 2nd order time averaged absolute pressure distribution ($\lambda_{SAW} = 20 \mu\text{m}$) with no particles present. λ here represents λ_{SAW} . The dashed black line (AB) (from $x = 0$ to $x = \lambda/2$ at $y = 15 \mu\text{m}$) represents the path across which the spatial forces acting on particles have been assessed. Spatial force field with (b) 10 and (c) 5 μm particles. The resultant forces, once integrated over the surface area, are shown in the (d) x component of the lateral force, normalized by the maximum F_x , along the dashed line (AB) shown in part a. (e) y component of the lateral force, normalized by the maximum F_y , along the dashed line (AB). (f) y component of the lateral force, normalized by the maximum F_y , along the pressure minima line (CD). The y component (g) of the acoustic force acting on a particle at a single location along CD shows a transition between negative (acceptance into the sound field) and positive (rejection from the sound field) forces at approximately $D(\lambda/2)^{-1} = 0.3$. The repulsive force rises rapidly with increasing particle diameter, as does a fluid flow induced drag that is of a similar magnitude to the acoustic forces – here notionally shown as the dotted line at a strength equal to that of a 8 μm particle and proportional to the radius. Smaller particles are drag dominated and larger ones are acoustic force dominated, giving rise to the possibility of filtering.

3. Virtual Membrane for Filtration of Particles

[View Article Online](#)

the range of $D(\lambda_{\text{SAW}}/2)^{-1}$ between 0.22 and 0.27, for the two dimensional particles modelled. Above these values, the forces rise rapidly with particle size. This indicates the possibility of sorting when combined with fluid flow induced drag, when the strength of the acoustic field and flow field is such that the acoustic force is of similar or greater magnitude to that induced by fluid drag. We have considered this scenario in Fig. 3g, in which the dotted line represents the notional drag force, the amplitude of which is selected to cross the line (for $\lambda_{\text{SAW}} = 20 \mu\text{m}$) at the point corresponding to an example 8 μm particle. The dotted line is constantly sloped as the drag force is proportional to the particle diameter. Two outcomes are predicted by this scenario, the first is for particles larger than 8 μm for which the acoustic repulsion force is larger than the drag force, so that the particles are prevented from traversing the acoustic field, and the second is for particles smaller than 8 μm for which the drag force is dominant where these particles migrate to the local nodal locations by F_x and are dragged through the sound field along the nodal lines. It is this alignment of the smaller particles along the nodes as they pass through the field which is reminiscent of a series of filtering pores.

Experimental results

Having established the underlying mechanism *via* numerical simulation, we now demonstrate selective trapping of particles experimentally. Fig. 4 illustrates the difference in behaviour of 7 μm and 10.36 μm particles separately (blue and red, respectively), which enter (from the left) a sound field with a surface acoustic wavelength of 20 μm . At very low powers (Fig. 4a and d), neither particle size is affected by the sound field; instead, the viscous drag forces ($F_{\text{drag}} =$

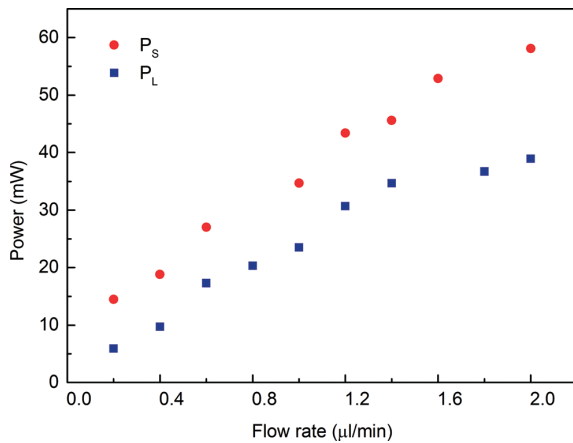


Fig. 5 Applied power as a function of flow rate. As shown in Fig. 4, P_S indicates the power at which $95 \pm 5\%$ of smaller particles (7 μm) are able to pass through the force field, whilst $85 \pm 5\%$ of the larger particles (10.36 μm) get trapped. P_L , on the other hand, is the power to capture the larger particles and allow $75 \pm 5\%$ of particles of smaller diameter to be drawn into the force field without being interrupted by the streaming induced drag force.

$6\pi\mu rU$, where r is the particle radius, μ is the viscosity and U is the relative velocity of the particle and fluid) imposed by the flowing fluid are dominant. However, when the applied acoustic force is sufficient to counter the fluid drag forces for larger particles, it is observed that when they reach the standing acoustic pressure field, particles are trapped at its periphery, as predicted by the positive nature of F_y in Fig. 3e and f. In addition, influenced by the drag of the fluid and the fact that the sound field has been angled towards the flow field, they are collected at the lower

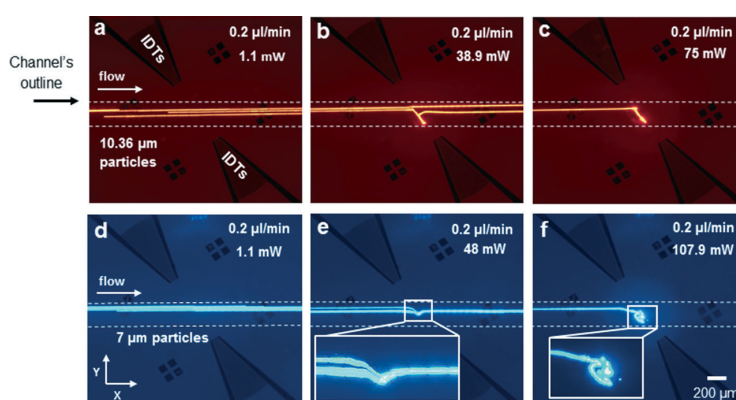
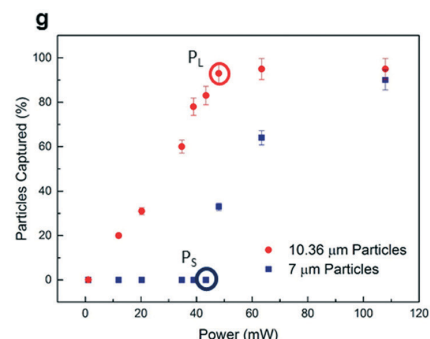


Fig. 4 Experimental images of particle manipulation and sorting efficiency at different applied powers. The figure shows optical fluorescence images of 10.36 μm particles (a–c) where (a) particles are not affected by the field at 1.1 mW applied power, and (b) $78 \pm 3.9\%$ of particles at 38.9 mW applied power and (c) $95 \pm 5\%$ of particles at 75 mW applied power (all with $0.2 \mu\text{l min}^{-1}$ lateral flow rate) are trapped/filtered once they reach the field. The sorting behaviour of 7.0 μm particles is shown in (d)–(f) where these particles (d) continue in the direction of the flow at 1.1 mW applied power, (e) are laterally displaced upon entering the field as they are affected by the acoustic force, and (f) are trapped at the start of the field as they are subjected to acoustic streaming and move along circular paths. (g) Capture efficiency as a function of power, with higher power resulting in greater capture efficiency; the cut-off power is where the greatest number of larger particles are captured while smaller particles are able to pass through the field (circled). P_L and P_S represent powers at which $95 \pm 5\%$ of large particles and $5 \pm 5\%$ of smaller particles are captured, respectively. These powers are utilized to obtain the results shown in Fig. 5.



3. Virtual Membrane for Filtration of Particles

[View Article Online](#)

Paper

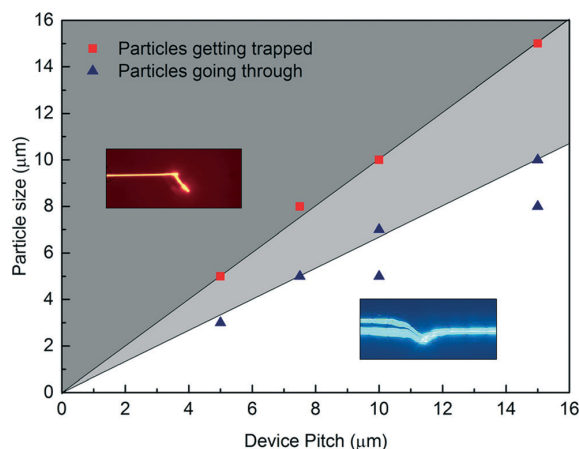


Fig. 6 The effective critical particle diameter is a function of the acoustic wavelength. The cut-off in behaviour is examined here across multiple device pitches ($\lambda_{\text{SAW}}/2 \mu\text{m}$). The particles within the dark grey area are trapped statically, with the red squares being the smallest particles to be captured. The slope of the line, separating the dark grey area was found to be very close to 1. The particles located in the light grey area show a mixture of behaviour. In the white section, particles are able to pass through the field at powers at which the larger particles are trapped.

(in the image plane) edge of the channel (Fig. 4b and c). In contrast, at low powers (Fig. 4e), the smaller particles are able to be drawn into the force field, along the nodal lines – as shown by a clear perturbation in the trajectory. Once at the nodes, the fluid viscous drag force draws them through the field and along the channel. As the applied power is further increased, the smaller particles can also be captured; this occurs due to a different mechanism than that used to capture the larger particles. For these smaller particles, the trapping results in particle clusters which are in constant motion, which indicates that the particles are located in a vortex induced by acoustic streaming^{44,64} (Fig. 4f). The effect of streaming wasn't included in the model as it would require a 3D model which is currently computationally prohibitive; instead, this is characterised experimentally. Fig. 4g quantifies the role that the applied power plays in the capturing of particles of a given size. It can be seen that, at the higher applied power levels and concordant higher acoustic pressure amplitudes, the magnitude of lateral acoustic forces becomes more dominant compared to the drag force for the larger particles (10.36 μm); hence, a larger proportion is captured; 75 mW is sufficient to trap $95 \pm 5\%$ of the particles (where the uncertainty is one standard error). For low powers, the smaller particles (7 μm) aren't trapped in the force field; however, above a certain power level (50 mW), their trajectories become increasingly dominated by fluid drag resulting from acoustic streaming. These data sets suggest that selective trapping can be achieved at powers between 43.4 mW (where $83 \pm 4.15\%$ of 10 μm particles are captured whilst 100% of smaller particles pass through the acoustic pores)

Lab on a Chip

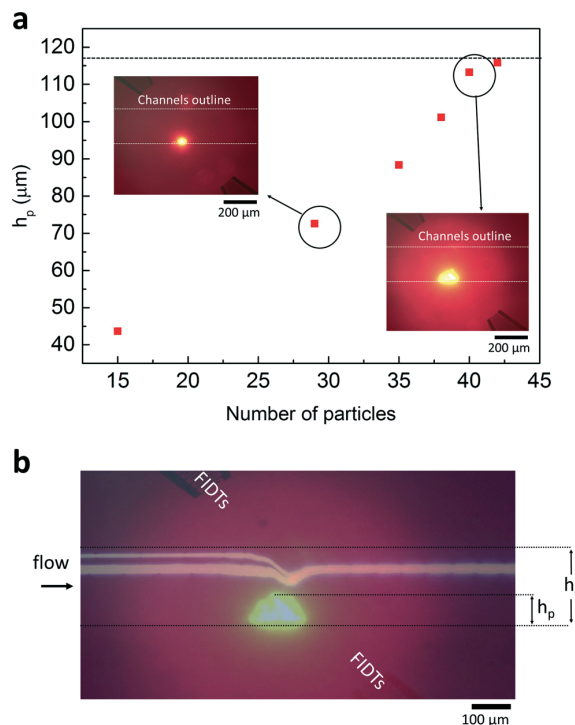


Fig. 7 (a) As time progresses, the size of the bolus of 10.36 μm particles grows, and the width across the channel is plotted against the number of particles captured (each data point is equally spaced temporally). (b) A composite image of the trajectories of small particles (7 μm) entering along the edge of the channel and the growing bolus of large particles; once the tip of the bolus impedes this trajectory, the filter will cease to perform efficiently; the height at which that occurs is marked as a dotted line in (a).

and 49 mW (where $95 \pm 5\%$ of 10 μm particles are captured, but only $36 \pm 3.2\%$ of smaller 7 μm particles pass through).

Fig. 5 further investigates the influence of power, as a function of flow rate, on desired capture and separation of particles. Two parameters have been defined: P_L , the lowest power at which all of the large particles are trapped, and P_S , the highest power at which the small particles pass through the field. It can be seen that the difference in these values at $0.2 \mu\text{l min}^{-1}$, the flow rate used in Fig. 4, remains the same up to in excess of $1.0 \mu\text{l min}^{-1}$.

Because the sorting efficiency is dependent on the similarity of P_S and P_L , it is beneficial for the transition from 0% to 100% capture of a given particle type to take place over a narrow power range; if the slope along which the red squares are located in Fig. 4g were less steep, P_L would be larger and the sorting efficiency lower. Similarly, Fig. 4g demonstrates that the capture rate for increasing applied power is steeper for larger particles (acoustic radiation force trapped) than the smaller ones (acoustic streaming trapped); an increase of 50 mW in power is needed to increase the collection by streaming from 65% to 90%. In streaming fields, the movement of

3. Virtual Membrane for Filtration of Particles

[View Article Online](#)

Lab on a Chip

Paper

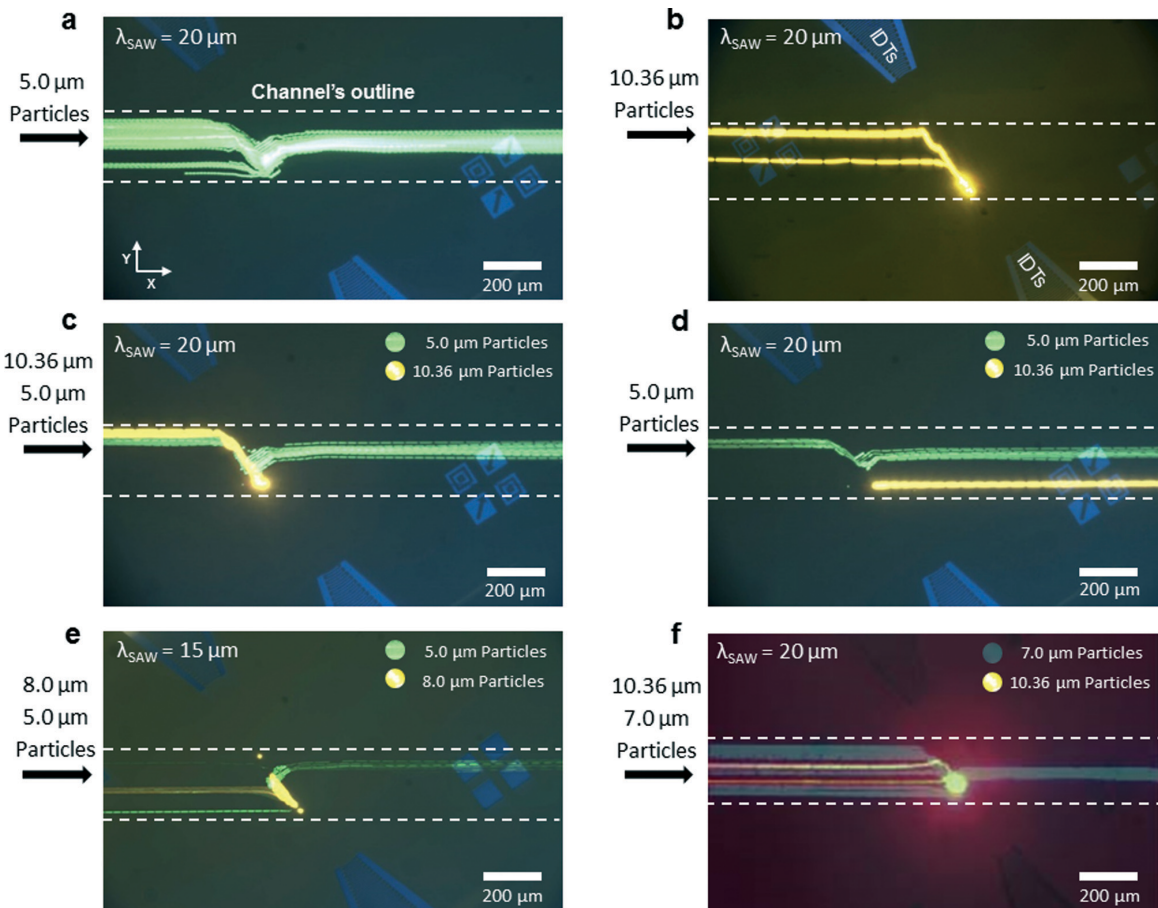


Fig. 8 Particle sorting using an acoustic filter. Trajectories of fluorescent polystyrene particles of 5 μm (green) and 10.36 μm (yellow) diameter entering the microfluidic chamber at the flow rate of $2 \mu\text{l min}^{-1}$ through the left side entrance. Here, the focused IDTs, composed of $\lambda_{SAW} = 20 \mu\text{m}$ finger pairs operating at 194 MHz, are acting at a 45° angle relative to the microfluidic channel. Once particles reach the standing acoustic pressure field (in the middle of the chamber), established by a pair of counter-propagating SAW devices (a) particles of diameter $D_p < D_{\text{critical}}$ are laterally displaced and pass through the potential force minima lines towards the upper edge of the chamber and then to the exit, (b) particles of $D_p \geq D_{\text{critical}}$ are trapped at the last possible pressure nodes and are directed towards the lower edge of the chamber due to fluid drag. (c) The combination of these two sorting behaviours is illustrated where simultaneous separation of particles occurs. (d) Release of 10.36 μm particles once the application of SAW is stopped; (e) separation of 8 μm (yellow) and 5 μm (green) particles with $\lambda_{SAW} = 15 \mu\text{m}$. (f) Separation of 7 μm (blue) and 10.36 μm (red) particles using a $\lambda_{SAW} = 20 \mu\text{m}$ device in a composite picture of videos taken from the same device under identical experimental conditions.

the particles leads to particle-particle and particle-wall interactions that can lead to particles being expelled out of the streaming vortex,⁶⁴ possibly responsible for the relatively inefficient collection for the streaming based mechanism relative to that induced by the acoustic force. Accordingly, acoustic radiation forces are the preferential particle capture mechanism. In Fig. 6, four individual devices have been examined with pitches of 5 μm , 7.5 μm , 10 μm and 15 μm ($\lambda_{SAW} = 10, 15, 20$ and 30 μm). In each device, we varied the power whilst examining which particle sizes could be captured. This was possible for the larger particle sizes marked with red squares (located within the dark grey area) and not for those smaller particles marked with blue triangles (located in the white area). Then, a power was found at which the larger par-

ticles where captured for each experimental condition, whilst the smaller ones passed through the field – the two insets show this occurring. Interestingly, it can be seen that for particles held statically, they must have a diameter which is greater than the pitch of the IDTs. Whilst the mechanism for this is not understood, the experimental characterisation gives rise to a simple design rule for these sorting devices and the mechanism can be considered to be tuneable based on the IDT pitch.

The number of particles that can be successfully trapped, even for those larger than half the acoustic wavelength, is limited by volumetric constraints as the bolus of trapped particles extends across the channel width. Whilst the devices presented here have not been optimised for maximum

3. Virtual Membrane for Filtration of Particles

Paper

[View Article Online](#)

Lab on a Chip

particle capture, they can give an indication of the limitations involved. As small particles enter the channel at the edge of the channel, which can be arranged simply with a buffer flow, the trajectories can be seen in Fig. 7b; the small particles pass through the centre part of the channels, as with any membrane when the larger particles obstruct the pathway of the smaller particles, filtration performance is hindered. As such, the bolus must be limited in size such that it doesn't hinder this trajectory; the number of 10 μm particles (the largest used in these experiments) trapped is plotted against the height of the bolus in Fig. 7a, and the volume of these trapped particles represents almost perfect packing. Clearly, additional trapping capacity would be expected with wider channels or potentially by offsetting the focal region of the acoustic field away from the centre of the channel to divert the trajectory of the small particles.

Particle sorting of mixed particle inputs is demonstrated in Fig. 8, including 10.36 μm and 5.0 μm particles (yellow and green), using a $\lambda_{\text{SAW}} = 20 \mu\text{m}$ wavelength device operating at 194 MHz. In Fig. 8(a)–(c), the applied power and flow rate have been specifically adjusted to capture the greatest number of larger particles ($95 \pm 5\%$), whilst all the smaller particles pass through the field. As seen in Fig. 8(c), once the mixture consisting of 10.36 μm and 5.0 μm particles (flowing from left to right) arrive to the established standing pressure field, the larger particles are selectively retained. As discussed previously and as indicated in the numerical model, the larger 10.36 μm particles are captured and follow the outer edge of the sound field (inclined to the flow field) to the lower edge of the chamber, while the smaller 5.0 μm particles pass through the sound field along the pressure nodes. Once the sound field is turned off, the trapped particles are released (Fig. 8d). The released larger particles will follow a path adjacent to the lower side of the chamber; as such, they could be collected from multiple outlets downstream. However, we envisage that the primary use of this function is the dispensing of the smaller particles from an open ended channel, followed by release and dispensing of the larger particles.

To emphasise the scalability of the system, in Fig. 8(e and f), different populations of mixed particle sizes are sorted: firstly, 8 μm particles are sorted from 5 μm using a 15 μm wavelength device, corresponding to a 7.5 μm device pitch. Similarly, 10.36 μm particles are sorted from 7 μm particles using a device pitch of 10 μm (in this case, a composite image consisting of two images is shown due to the need to switch optical filters).

Conclusions

A deterministic SAW-based sorting and filtration mechanism has been demonstrated. It utilises high frequency standing acoustic pressure fields, established by the generation of counter-propagating focused surface acoustic waves. In the regime where the surface acoustic wavelength approaches that of the particle diameter, a novel behaviour has been

identified and utilized for selective particle filtration. Particles smaller than the critical diameter, dictated by a balance between acoustic power and flow rate, are permitted to pass through the virtual pores formed at acoustic nodal locations that translate through the field. Larger particles, however, are retained at the leading edge of the sound field by acoustic radiation forces.

Acknowledgements

The authors would like to thank the Australian Research Council (No. DP160101263) for their kind support of this research. All devices used in this work were fabricated at the Melbourne Centre for Nanofabrication (MCN).

References

- B. Landenberger, H. Hofemann, S. Wadle and A. Rohrbach, *Lab Chip*, 2012, **12**, 3177–3183.
- M. P. MacDonald, G. C. Spalding and K. Dholakia, *Nature*, 2003, **426**, 421–424.
- P. R. C. Gascoyne and J. Vykoukal, *Electrophoresis*, 2002, **23**, 1973–1983.
- S. Park, Y. Zhang, T. H. Wang and S. Yang, *Lab Chip*, 2011, **11**, 2893–2900.
- H. Shafiee, M. B. Sano, E. A. Henslee, J. L. Caldwell and R. V. Davalos, *Lab Chip*, 2010, **10**, 438–445.
- D. J. Collins, T. Alan and A. Neild, *Lab Chip*, 2014, **14**, 1595–1603.
- J. Nam, Y. Lee and S. Shin, *Microfluid. Nanofluid.*, 2011, **11**, 317–326.
- J. Nam, H. Lim, D. Kim and S. Shin, *Lab Chip*, 2011, **11**, 3361–3364.
- P. Li, Z. Mao, Z. Peng, L. Zhou, Y. Chen, P.-H. Huang, C. I. Truica, J. J. Drabick, W. S. El-Deyri and M. Dao, *Proc. Natl. Acad. Sci. U. S. A.*, 2015, **112**, 4970–4975.
- M. Hejazian, W. Li and N.-T. Nguyen, *Lab Chip*, 2015, **15**, 959–970.
- C. W. Shields IV, C. D. Reyes and G. P. López, *Lab Chip*, 2015, **15**, 1230–1249.
- J. Nam, H. Lim, C. Kim, J. Y. Kang and S. Shin, *Biomicrofluidics*, 2012, **6**, 024120.
- J. Shi, H. Huang, Z. Stratton, Y. Huang and T. J. Huang, *Lab Chip*, 2009, **9**, 3354–3359.
- F. Petersson, A. Nilsson, C. Holm, H. Jonsson and T. Laurell, *Lab Chip*, 2005, **5**, 20–22.
- X. Ding, Z. Peng, S. C. Lin, M. Geri, S. Li, P. Li, Y. Chen, M. Dao, S. Suresh and T. J. Huang, *Proc. Natl. Acad. Sci. U. S. A.*, 2014, **111**(36), 12992–12997.
- J. Behrens, S. Langelier, A. R. Rezk, G. Lindner, L. Y. Yeo and J. R. Friend, *Lab Chip*, 2015, **15**, 43–46.
- F. Beyeler, A. Neild, S. Oberti, D. J. Bell, Y. Sun, J. Dual and B. J. Nelson, *J. Microelectromech. Syst.*, 2007, **12**.
- A. Neild, S. Oberti, F. Beyeler, J. Dual and B. J. Nelson, *J. Micromech. Microeng.*, 2006, **16**, 1562–1570.
- P. J. Lee, P. J. Hung, R. Shaw, L. Jan and L. P. Lee, *Appl. Phys. Lett.*, 2005, **86**, 223902.

3. Virtual Membrane for Filtration of Particles

[View Article Online](#)

Lab on a Chip

Paper

- 20 D. J. Grier, *Nature*, 2003, **424**, 810–816.
- 21 A. H. Yang, S. D. Moore, B. S. Schmidt, M. Klug, M. Lipson and D. Erickson, *Nature*, 2009, **457**, 71–75.
- 22 E. Mirowski, J. Moreland, S. Russek, M. Donahue and K. Hsieh, *J. Magn. Magn. Mater.*, 2007, **311**, 401–404.
- 23 E. Mirowski, J. Moreland, A. Zhang, S. E. Russek and M. J. Donahue, *Appl. Phys. Lett.*, 2005, **86**, 243901.
- 24 D. J. Collins, T. Alan and A. Neild, *Appl. Phys. Lett.*, 2014, **105**, 033509.
- 25 S. Oberti, D. Moller, A. Neild, J. Dual, F. Beyeler, B. J. Nelson and S. Gutmann, *Ultrasonics*, 2010, **50**, 247–257.
- 26 P. Rogers and A. Neild, *Lab Chip*, 2011, **11**, 3710–3715.
- 27 D. J. Collins, B. Morahan, J. Garcia-Bustos, C. Doerig, M. Plebanski and A. Neild, *Nat. Commun.*, 2015, **6**, 8686.
- 28 M. Wiklund, *Lab Chip*, 2012, **12**, 2018–2028.
- 29 D. Bazou, R. Kearney, F. Mansergh, C. Bourdon, J. Farrar and M. Wride, *Ultrasound Med. Biol.*, 2011, **37**, 321–330.
- 30 J. Hultstrom, O. Manneberg, K. Dopf, H. M. Hertz, H. Brismar and M. Wiklund, *Ultrasound Med. Biol.*, 2007, **33**, 145–151.
- 31 B. T. Chu and R. E. Apfel, *J. Acoust. Soc. Am.*, 1982, **72**, 1673–1687.
- 32 D. J. Collins, T. Alan, K. Helmerson and A. Neild, *Lab Chip*, 2013, **13**, 3225–3231.
- 33 I. Leibacher, P. Reichert and J. Dual, *Lab Chip*, 2015, **15**, 2896–2905.
- 34 I. Leibacher, S. Schatzer and J. Dual, *Lab Chip*, 2014, **14**, 463–470.
- 35 P. Hahn, I. Leibacher, T. Baasch and J. Dual, *Lab Chip*, 2015, **15**, 4302–4313.
- 36 M. Antfolk, P. B. Muller, P. Augustsson, H. Bruus and T. Laurell, *Lab Chip*, 2014, **14**, 2791–2799.
- 37 A. Neild, S. Oberti and J. Dual, *Sens. Actuators, B*, 2007, **121**, 452–461.
- 38 A. Neild, S. Oberti, A. Haake and J. Dual, *Ultrasonics*, 2006, **44**(Suppl 1), e455–e460.
- 39 P. Glynne-Jones, C. E. Demore, C. Ye, Y. Qiu, S. Cochran and M. Hill, *IEEE Trans. Ultrason. Ferroelectr. Freq. Control*, 2012, **59**, 1258–1266.
- 40 M. Antfolk, C. Magnusson, P. Augustsson, H. Lilja and T. Laurell, *Anal. Chem.*, 2015, **87**(18), 9322–9328.
- 41 P. Augustsson, C. Magnusson, M. Nordin, H. Lilja and T. Laurell, *Anal. Chem.*, 2012, **84**, 7954–7962.
- 42 F. Petersson, L. Åberg, A.-M. Swärd-Nilsson and T. Laurell, *Anal. Chem.*, 2007, **79**, 5117–5123.
- 43 D. J. Collins, A. Neild and Y. Ai, *Lab Chip*, 2016, **16**, 471–479.
- 44 D. J. Collins, Z. Ma and Y. Ai, *Anal. Chem.*, 2016, **88**, 5513–5522.
- 45 M. Sesen, T. Alan and A. Neild, *Lab Chip*, 2014, **14**, 3325–3333.
- 46 L. Schmid and T. Franke, *Appl. Phys. Lett.*, 2014, **104**, 133501.
- 47 M. Sesen, T. Alan and A. Neild, *Lab Chip*, 2015, **15**, 3030–3038.
- 48 C. Cortez-Jugo, A. Qi, A. Rajapaksa, J. R. Friend and L. Y. Yeo, *Biomicrofluidics*, 2015, **9**, 052603.
- 49 K. Tveen-Jensen, F. Gesellchen, R. Wilson, C. M. Spickett, J. M. Cooper and A. R. Pitt, *Sci. Rep.*, 2015, **5**, 9736.
- 50 D. J. Collins, O. Manor, A. Winkler, H. Schmidt, J. R. Friend and L. Y. Yeo, *Phys. Rev. E: Stat., Nonlinear, Soft Matter Phys.*, 2012, **86**, 056312.
- 51 L. Ren, Y. Chen, P. Li, Z. Mao, P.-H. Huang, J. Rufo, F. Guo, L. Wang, J. P. McCoy and S. J. Levine, *Lab Chip*, 2015, **15**, 3870–3879.
- 52 A. A. Nawaz, Y. Chen, N. Nama, R. H. Nissly, L. Ren, A. Ozcelik, L. Wang, J. P. McCoy, S. J. Levine and T. J. Huang, *Anal. Chem.*, 2015, **87**(24), 12051–12058.
- 53 R. Shilton, M. K. Tan, L. Y. Yeo and J. R. Friend, *J. Appl. Phys.*, 2008, **104**, 014910.
- 54 A. R. Rezk, A. Qi, J. R. Friend, W. H. Li and L. Y. Yeo, *Lab Chip*, 2012, **12**, 773–779.
- 55 L. Schmid, D. A. Weitz and T. Franke, *Lab Chip*, 2014, **14**, 3710–3718.
- 56 V. Skowronek, R. W. Rambach, L. Schmid, K. Haase and T. Franke, *Anal. Chem.*, 2013, **85**, 9955–9959.
- 57 J. Shi, X. Mao, D. Ahmed, A. Colletti and T. J. Huang, *Lab Chip*, 2008, **8**, 221–223.
- 58 G. Destgeer, B. H. Ha, J. H. Jung and H. J. Sung, *Lab Chip*, 2014, **14**, 4665–4672.
- 59 C. Devendran, N. R. Gunasekara, D. J. Collins and A. Neild, *RSC Adv.*, 2016, **6**, 5856–5864.
- 60 L. P. Gor'kov, *Sov. Phys. Dokl.*, 1962, **6**, 773.
- 61 M. Settnes and H. Bruus, *Phys. Rev. E: Stat., Nonlinear, Soft Matter Phys.*, 2012, **85**, 016327.
- 62 S. Shiokawa, Y. Matsui and T. Ueda, Liquid streaming and droplet formation caused by leaky Rayleigh waves, *Proc. - IEEE Ultrason. Symp.*, 1989, 643–646.
- 63 J. Dual, P. Hahn, I. Leibacher, D. Moller, T. Schwarz and J. Wang, *Lab Chip*, 2012, **12**, 4010–4021.
- 64 H. V. Phan, M. Sezen, T. Alan and A. Neild, *Appl. Phys. Lett.*, 2014, **105**, 193507.

This chapter aims to seek an in-depth understanding of the effects arising due to the incidence of a travelling surface acoustic wave (TSAW) through a microfluidic channel. As opposed to the literature that broadly overlook the influence of diffraction, here we explore the significance of diffractive patterns in a travelling SAW system.

4

Diffraction Driven Mechanisms

4.1 Overview

Chapter 3 explores the effect of elevated frequencies in a SAW-actuated system and in doing so aims to exploit a capability that is hard, if at all possible, to achieve with BAW systems. By reducing the SAW wavelength to the dimension of an individual particle, a novel and highly sensitive filtration system was developed to trap particles of a certain size profile against a flow. In this chapter, another facet of SAW is explored which is not available in BAW systems. Here, a single SAW is used to create a travelling sound field in microfluidic channel, and the resulting manipulation is studied. Under the effect of travelling SAW field, the current literature mainly reports continuous unidirectional migration of particles in the SAW propagation direction. Here, we realise that this mono-directional particle translation is one effect amongst many. By considering the influence of diffractive effects, a significant phenomenon that is broadly overlooked in the present theoretical and experimental literature, a scenario is realised wherein trapping of particles into stable locations occur in a travelling SAW system. By numerically modelling and experimentally characterising a travelling SAW system, we have identified five distinct mechanisms in an individual system. Firstly, diffractive effects on the substrate and at the intersection of LN-channel give rise to a pressure field with complex amplitude patterns. The resultant ARF act to trap particles orthogonal (due to substrate diffraction) and parallel (due to LN-channel diffraction) to the propagation direction. Secondly, the acoustic streaming gives rise to fluid swirling in two orthogonal

4. Diffraction Driven Mechanisms

planes; lateral vortices at the peripheral regions, and vertical vortices within the extent of the SAW beam. Finally, the migration of particles along the propagation direction.

4.2 Publication

The following publication was reproduced from [242] with kind permission from the Royal Society of Chemistry.



Lab on a Chip

PAPER

[View Article Online](#)

[View Journal](#) | [View Issue](#)



Cite this: *Lab Chip*, 2018, **18**, 2214

Received 8th March 2018,
Accepted 20th June 2018

DOI: 10.1039/c8lc00243f

rsc.li/loc

Surface acoustic wave diffraction driven mechanisms in microfluidic systems†

Armaghan Fakhfouri, ^a Citsabehsan Devendran, ^a Thomas Albrecht,^b David J. Collins, ^{cde} Andreas Winkler,^f Hagen Schmidt^f and Adrian Neild ^{*a}

Acoustic forces arising from high-frequency surface acoustic waves (SAW) underpin an exciting range of promising techniques for non-contact manipulation of fluid and objects at micron scale. Despite increasing significance of SAW-driven technologies in microfluidics, the understanding of a broad range of phenomena occurring within an individual SAW system is limited. Acoustic effects including streaming and radiation force fields are often assumed to result from wave propagation in a simple planar fashion. The propagation patterns of a single SAW emanating from a finite-width source, however, cause a far richer range of physical effects. In this work, we seek a better understanding of the various effects arising from the incidence of a finite-width SAW beam propagating into a quiescent fluid. Through numerical and experimental verification, we present five distinct mechanisms within an individual system. These cause fluid swirling in two orthogonal planes, and particle trapping in two directions, as well as migration of particles in the direction of wave propagation. For a range of IDT aperture and channel dimensions, the relative importance of these mechanisms is evaluated.

1. Introduction

Manipulation of particles is key for tasks such as sorting, patterning and concentration within microfluidic chips. Manipulation can take place using passive physical features to give rise to hydrodynamic interaction which result in motion along fluid streamlines.^{1–4} Alternatively, active methods employ external force fields, arising from magnetic,^{5,6} dielectrophoretic (DEP),^{7,8} optical^{9,10} or acoustical¹¹ effects, to act on the suspended objects.

Ultrasonic excitation generates acoustic forces acting both on suspended matter and the fluid itself. In addition, the straightforward on-chip integration, non-contact and biocompatible nature¹² of acoustic methods has made them particularly interesting for biologically oriented microfluidic

systems.^{13–15} Two key approaches have been established, the use of bulk acoustic waves^{16–18} (BAW) and surface acoustic waves^{19–22} (SAW). In BAW systems, a piezoelectric component which is adhered to the microfluidic chip is used as an excitation source. Waves couple into the fluid, which is typically contained within materials such as silicon and glass, in which strong reflections occur. By choice of a suitable excitation field, the resulting standing wave will become resonant, yielding sufficient forces to push particles to the planes of either the pressure nodes or antinodes. This means that the pressure field is restricted to the resonant modes of the fluid volume.^{23–26}

SAWs are excited by a pair of comb-shaped electrodes on a piezoelectric substrate. By selecting a suitable frequency of oscillation, the waves which propagate from each electrode along the surface of the substrate interfere constructively. As the resonance required to maximise the amplitudes of excitation occurs due to this constructive interference, the frequency of operation is dictated by the pattern and spacing of the electrodes and not the fluid volume dimensions. Thus, it is not necessary to include interfaces which ensure high degrees of reflection; typical SAW systems use a fluid volume contained in polydimethylsiloxane (PDMS), a material which has lower acoustic impedance to that of water. Accordingly, a travelling surface acoustic wave²⁷ (TSAW) can be excited, where acoustic energy passes through the fluid and into the PDMS bulk, in which it is then damped. In contrast, standing surface acoustic waves^{28,29} (SSAW) can be excited by the use

^a Laboratory for Micro Systems, Department of Mechanical and Aerospace Engineering, Monash University, Clayton, Victoria 3800, Australia.

E-mail: Adrian.neild@monash.edu

^b Department of Mechanical and Aerospace Engineering, Monash University, Clayton, Victoria 3800, Australia

^c Pillar of Engineering Product Development, Singapore University of Technology and Design, Singapore 487372, Singapore

^d Department of Biological Engineering, Massachusetts Institute of Technology, Cambridge, Massachusetts 02139, USA

^e Department of Electrical Engineering and Computer Science, Massachusetts Institute of Technology, Cambridge, MA 02139, USA

^f SAWLab Saxony, IFW Dresden, Dresden, D-01069 Germany

† Electronic supplementary information (ESI) available. See DOI: [10.1039/c8lc00243f](https://doi.org/10.1039/c8lc00243f)

4. Diffraction Driven Mechanisms

[View Article Online](#)

Lab on a Chip

Paper

of counter-propagating TSAWs. SAW-driven systems have found applications in droplet generation,³⁰ merging,³¹ steering³² and splitting,³³ atomization,^{34,35} particle patterning,^{36,37} size-based sorting^{38–40} and filtration.⁴¹

Ultrasonic manipulation of particles requires the use of steady state forces, these arise through two main mechanisms. The propagation of a sound field in a fluid results in body forces being exerted on the fluid, giving rise to acoustic streaming,^{42–44} where the resulting circulating flows entrain suspended particles.^{45,46} The ultrasonic field also generates acoustic radiation forces⁴⁷ (ARF) which act directly on the suspended matter. The force field in a travelling wave coupled into the fluid, pushes particles in the direction of wave propagation,⁴⁸ whilst in a standing wave particles are pushed towards pressure nodes⁴⁹ or antinodes⁵⁰ depending on the acoustic contrast of the suspended particle in a given surrounding medium. As the force profiles are different for each mechanism, establishing the dominant force is key to understanding the resulting behaviour. In the case of BAW systems, the sound field has been modelled,^{51–54} the streaming flows predicted,^{44–46} and the size dependent nature of the force dominance has been described; there being a minimum particle size above which collection occurs within the standing wave.⁴⁴

However, the complexity of SAW systems is still being elucidated. For example, a recent study examined the dominant force affecting particle behaviour outcomes in a SSAW, showing that the dominant effect is both size and location dependent;⁴⁵ this location dependence is not present in BAW. In addition, many recent studies, have added depth to the approximations made about SAW-driven microfluidics and challenged some of the assumptions commonly made. Firstly, in TSAW systems it is assumed that particles migrate away from the ultrasonic source. However, through a series of experiments, Destgeer *et al.* showed that an anechoic corner exists in which no migration of particles is observed.^{55–57} Secondly, diffraction of the ultrasonic wave arising from a discontinuity introduced by the channel wall, means that particles can be held in spatial periodic patterns within a TSAW system,^{58,59} whereas the periodic nature of this outcome is usually only expected for SSAW excitation. Thirdly, the counter-propagation of two waves excited by separate sets of electrodes need not lead to standing waves and so periodic patterning. Rather, it can result in a single, movable, trapping location if two slightly different frequencies are used.⁶⁰ Finally, the distinction between SSAW and TSAW systems has been challenged, with the attenuation of each counter-propagating TSAW (used to establish a SSAW) meaning that different parts of a channel can be dominated by TSAW or SSAW, a fact that yields an accurate sorting mechanism.⁶¹

In light of these developments, which have highlighted the complexity of SAW systems and in each case used them advantageously, this work carefully examines the behaviour of particles in a TSAW field. In doing so, this study expounds the key features of a complex acoustic field resulting from diffraction patterns of a travelling SAW through a three-dimensional spatial system. The outcomes are discussed in

terms of diffraction effects which lead to multiple distinct particle patterning behaviours in the propagation and lateral directions under the influence of ARF. Additionally, streaming effects occur both at the sides of the TSAW beam and within its extent. The relative influence of these effects are compared for high frequency acoustic beams produced by a series of finite-width interdigitated transducers (187.5 μm, 375 μm, 750 μm, 1500 μm wide), in channels of a range of dimensions (100 μm and 200 μm width and 26 μm, 35 μm and 46.5 μm height) and increasing distances from the IDT (680 μm, 1400 μm and 2050 μm).

2. System mechanics

Application of an oscillating electrical signal to each electrode patterned on the piezoelectric substrate is used to generate substrate waves. An interdigitated transducer (IDT) is formed by patterning multiple electrodes in a periodic pattern dictated by the intended frequency of operation. Exciting the system at the synchronous frequency will result in each electrode's vibration to constructively interfere and generate a surface acoustic wave to propagate across the surface of the piezoelectric substrate. A TSAW couples into an overlying fluid in the form of a plane wave propagating at the Rayleigh angle $\theta_R = \arcsin(c_0/c_s)$ where c_0 and c_s represent the speed of sound in the liquid and the SAW phase velocity of the substrate, respectively. However, a complete description of the ensuing sound field must also consider the inherent diffraction of the waves. This is important in determining the spatial amplitude of the wavefront; this is true for both the SAW in the substrate and the wave coupled into the fluid. Diffraction can be accounted for by the Huygens–Fresnel principle.⁶² This describes each vibrating point as a source of a spherical wavefront which interfere with each other, resulting in spatial amplitude variations. Typically, the impulse response of a system describes geometrically the arrival of each wavefront from all source locations, which is then convolved with the actual excitation waveform.^{62,63} The locations in the sound field of maximum amplitude are those at which these secondary wavefronts constructively interfere. An alternative description, using a mathematical simplification, considers a source as consisting of an emitter of a plane wave and edge waves from the perimeter of the aperture.^{58,63} These diffraction effects can strongly influence acoustic streaming and ARF, as these forces depend on the amplitude and gradient of the pressure field.

The acoustic radiation force acts directly on particles exposed to an ultrasonic field. For a particle radius much smaller than the acoustic wavelength ($a \ll \lambda_{\text{SAW}}$) the time-averaged resultant radiation force is given by eqn (1),^{45,64} derived using perturbation theory, considering continuity and the Navier–Stokes equation:

$$\mathbf{F}_{\text{ARF}} = -\pi a^3 \left[\frac{2\kappa_0}{3} \mathbb{R} [\mathbf{f}_1^* \mathbf{P}_1^* \nabla \mathbf{P}_1] - \rho_0 \mathbb{R} [\mathbf{f}_2^* \mathbf{v}_1^* \nabla \mathbf{v}_1] \right] \quad (1)$$

4. Diffraction Driven Mechanisms

Paper

[View Article Online](#)

Lab on a Chip

where the asterisk indicates complex conjugates and $\Re[\cdot]$ the real part. P_1 and v_1 are the first order pressure and velocity field and factors f_1 and f_2 are given by:

$$f_1 = 1 - \frac{\kappa_p}{\kappa_0} \quad (2a)$$

and

$$f_2 = \frac{2(1-\gamma)(\rho_p - \rho_0)}{2\rho_p + \rho_0(1-3\gamma)} \quad (2b)$$

where,

$$\gamma = -\frac{3}{2} [1 + i(1 + \tilde{\delta}_v)] \tilde{\delta}_v \quad (2c)$$

$$\tilde{\delta}_v = \frac{\sqrt{2\eta}}{a\sqrt{\omega\rho_0}} \quad (2d)$$

$\kappa_0 = 1/(\rho_0 c_0^2)$ and κ_p denote the compressibility of the liquid and particle respectively, ρ_0 and ρ_p represent density of liquid and particles respectively, ω is the angular frequency of excitation and η is the shear viscosity coefficient of the fluid. As can be seen in eqn (1), both terms are a measure of the sound field (either pressure or fluid particle velocity) and the gradient of that term. The effect of taking the complex conjugate of these two terms means that the time variations, due to the oscillation of the harmonic sound field, are removed. Accordingly, the acoustic radiation force is a steady state force which acts to translate or capture particles over a much longer time scale than the time period of the excitation. The most common description of particle behaviour resulting from exposure to a travelling wave is migration in the direction of propagation. However, in this work, we will also investigate the role of diffraction in generating forces to trap particles in both lines parallel to the microfluidic channel edge (we term this parallel trapping) and into clumps along the channel length (orthogonal trapping), as depicted in Fig. 1a.

An additional mechanism, acoustic streaming is a steady flow driven by Reynolds stresses. Reynolds stress is the body force, given in eqn (3a),^{45,65} that arises as a result of the time-averaged first-order acoustic momentum flux gradient. Acoustic streaming velocity, v_2 , is obtained by equating the Reynolds stress to the time-averaged second order terms given in eqn (3b).^{45,65} Acoustic streaming in turn induces a drag force on a suspended particle that affects particle migration behaviour. For a spherical particle, this is governed by the Stokes drag equation (eqn (3c)).

$$\langle F \rangle = \rho_0 \langle (v_1 \cdot \nabla) v_1 + v_1 \nabla \cdot v_1 \rangle \quad (3a)$$

$$\langle F \rangle = -\nabla \langle P_2 \rangle + \left[\eta' + \left(\frac{4}{3} \right) \eta \right] \nabla (\nabla \cdot v_2) + \eta \nabla^2 v_2 \quad (3b)$$

$$F_{\text{drag}} = 6\pi\eta a(v_2 - v_p) \quad (3c)$$

where P_2 and v_2 are the second-order (steady state) pressure and velocity field respectively. η' represents the bulk viscosity coefficient and v_p is particle's velocity. Again, as with the acoustic radiation force, the time-averaged force magnitude scales with the spatial gradient of the pressure and velocity fields.

In this work, the excitation of a travelling wave gives rise to a steady swirling flow at the periphery of the finite-width SAW beam due to the large velocity gradient at this location in the width (x) direction (which we term peripheral streaming). In addition, due to the diffraction lobes in the plane orthogonal to the electrodes ($x-z$ plane), a significant swirling motion is observed within the aperture of the IDT. These vortices occur about an axis parallel to the channel length (lobe streaming). These streaming based mechanisms are also depicted in Fig. 1a. Here, we examine the interactions of particles with a combined influence of ARF and streaming in a travelling wave system and how the relative influence of the effects depend on channel geometry, channel position and actuation power. This excitation gives rise to five distinct acoustofluidic actuation mechanisms beyond the standard propagation driven migration (Fig. 1a); an example of the results of streaming and ARF is shown in Fig. 1b. Fig. 1c depicts the streaming-driven vortices.

3. Methods

The device used in this work consists of a narrow microfluidic channel which is bonded onto a piezoelectric SAW device as shown in Fig. 1d. SAWs are produced using a straight interdigital transducer (IDT) designed with sets of 19, 14, 9, and 7 connected metallic finger pairs with overlapping width (aperture) of 187.5 μm, 375 μm, 750 μm and 1500 μm respectively. The IDT, with 21 μm pitch (operating at 180 MHz), are composed of a conductive 200 nm aluminium layer on top of a chromium adhesion layer deposited on a piezoelectric 128° rotated *Y*-cut *X* propagating lithium niobate (LiNbO₃; LN) substrate using an e-beam evaporator. A 270 nm thick layer of SiO₂ was then deposited to insulate the electrodes from corrosion and to promote PDMS-LN bonding.

The experiments used a quiescent homogenous solution of fluorescent 1 μm polystyrene particles (Magsphere, Pasadena, CA, USA) and water diluted with 0.2% polyethylene glycol (PEG), which filled the rectangular microfluidic channel. To study the influence of channel geometry on the streaming flows and particle patterning within the system, 100 μm and 200 μm wide (along x -direction, see Fig. 1a) and 26 μm, 35 μm and 45.6 μm high (along z -direction) microfluidic channels casted in polydimethylsiloxane (PDMS, 1:10 ratio of curing agent/polymer) were utilized. Upon application of an AC signal using a signal generator (Rohde and Schwarz HAMEG HM8134-3), particle behaviour was visualized via a fluorescence microscope (Olympus BX43) coupled with compatible light source (Olympus UFL-T). A PixeLink (PL-B782U usb2) CCD

4. Diffraction Driven Mechanisms

[View Article Online](#)

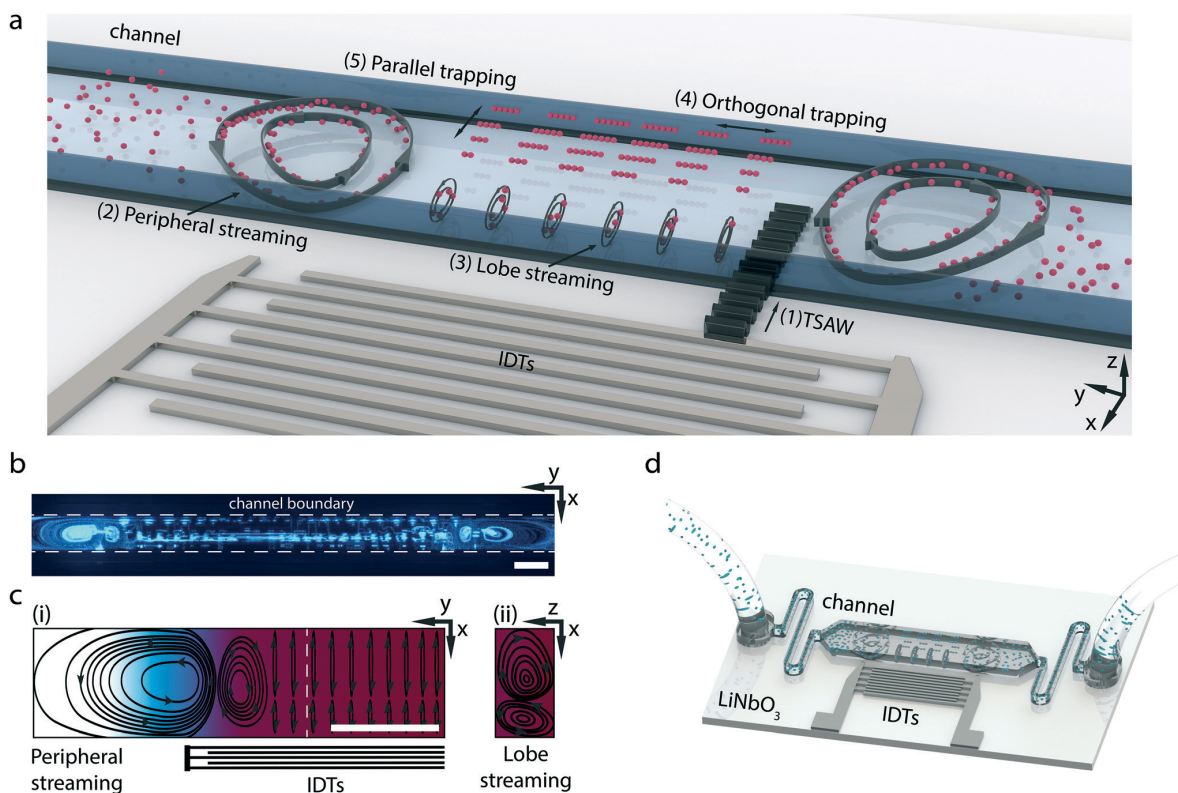


Fig. 1 Visualisation of the combined acoustic streaming field and acoustic radiation force resulting from incidence of fluid and a TSAW generated by a finite-width set of IDT. (a) Conceptual illustration of particle behaviour upon interaction with the SAW-field depicting five distinct key mechanisms; (1) migration of particles in the direction of TSAW propagation, (2) peripheral streaming vortex (x - y plane) at the SAW beam's edges, (3) lobe streaming vortices (x - z plane) within the extent of SAW beam, (4) orthogonal trapping of particles along the y -direction due to diffraction patterns on the oscillating LN substrate along the TSAW propagation, (5) parallel trapping of particles (along the x -direction) as a result of diffraction in the fluid arising from the knife edge at the far end. (b) The mechanisms are experimentally visualized within an aqueous quiescent solution of $1\text{ }\mu\text{m}$ polystyrene particles subjected to a TSAW. (c) Streamlines of the acoustic streaming field generated by the TSAW-beam. Within (i)-top view the red region indicates high acoustic intensity which decreases as the colour fades to blue, and subsequently white (minimum intensity). The vertical vortices in the x - z plane shown in (ii)-cross-sectional view are extracted from the dashed white lines in fig. (i). (d) 3D rendered image of the experimental setup depicting key resultant mechanisms. Scale bars are $100\text{ }\mu\text{m}$.

colour camera was used to capture the migration behaviour digitally. All spatial 2D measurements of particle collection were conducted *via* image intensity analysis using MATLAB.

To further investigate the effects of the system, a simplified 2-dimensional fully coupled LN substrate and a fluid domain was modelled using COMSOL Multiphysics v5.1. The relevant LN substrate properties were rotated to accommodate for the particular crystal cut orientation used experimentally. The single set of IDT were represented by equipotential lines on the piezoelectric solid domain, mimicking the IDT patterns used in the experiments, excited with a harmonic voltage potential (using a coupled electrostatic module) oscillating at the frequency of operation. This was then fully coupled to the fluid domain, modelled using the thermoviscous set of equations (thermoacoustic module within COMSOL Multiphysics) to accurately capture the pressure and velocity fluctuations. This approach is similar to that of previous publications^{44,45} with the exception that an

assumed input displacement/velocity profile is not needed, as the coupled solid LN substrate is present. The PDMS ceiling of the fluid domain was modelled using an impedance boundary condition (this assumes that the thickness of the PDMS cover exceeds the attenuation length; as with the experimental device). However, the PDMS side walls were modelled with a coupled acoustic pressure domain consisting of a PDMS block $50\text{ }\mu\text{m}$ wide on either side (similar to that of the PDMS wall thickness in experiments). The floor of the PDMS blocks were coupled to the solid LN substrate, which allows for the SAW displacement amplitude decay as well as any effects that arise due to the acoustic transmission through the PDMS wall into the fluid. There is no significant influence on the pressure field in the fluid domain arising from the pressure field in the PDMS block on either side, in line with observations reported by Collins *et al.*^{59,66}

To obtain the second order streaming fields (*i.e.* v_2), a laminar flow stationary study is carried out. The known first

4. Diffraction Driven Mechanisms

[View Article Online](#)

Paper

Lab on a Chip

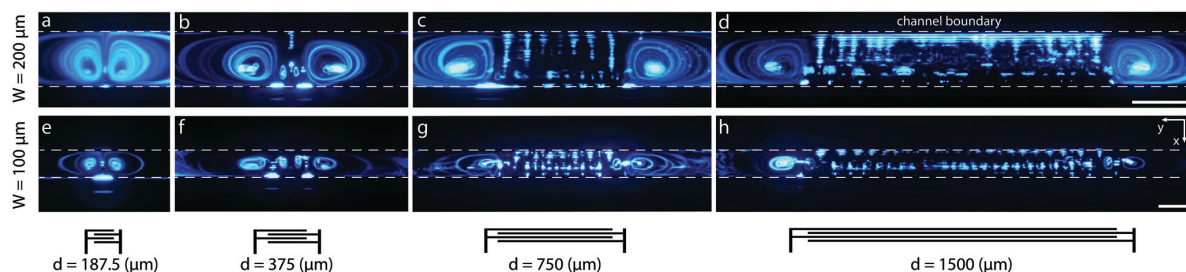


Fig. 2 Experimental results of cross-over between streaming dominated to acoustic radiation dominated migration of $1\text{ }\mu\text{m}$ particles, corresponding to distinct IDT apertures (d) as well as channel widths (W). $21\text{ }\mu\text{m}$ wavelength TSAW (at 180 MHz frequency and 15 dBm generator power level) vary in their aperture sizes. Peripheral streaming dominated translation of particles is visualized in fig. (a and b) and (e and f). In between the peripheral streaming, ARF dominates and orthogonal as well as parallel trapping occurs as visualized in systems driven by $1500\text{ }\mu\text{m}$ (d & h) and $750\text{ }\mu\text{m}$ (c & g) aperture IDTs. All channels have a dimension $H = 35\text{ }\mu\text{m}$ high. Scale bar is $200\text{ }\mu\text{m}$ in (a-d) and $100\text{ }\mu\text{m}$ in (e-h).

order velocity fields from the solved thermoviscous set of equations are utilised to calculate the body force (*i.e.* Reynolds' stress) as in eqn (3a), which in turn is used to drive the fluid flow, resulting in the acoustic streaming fields. All the relevant parameters and properties used in the model are given in Table S1 provided in ESI.[†]

4. Results and discussion

In a typical travelling wave system, whereby the wave is propagating orthogonally to a microfluidic channel and interacts with suspended matter (*i.e.* particles or droplets), the matters are pushed in the direction of wave propagation, conforming to present theoretical⁶⁷ and experimental literature. This effect has been used for sorting,⁶⁸ droplet displacement⁶⁹ and on-chip fluorescence-activated cell sorting (FACS).^{57,70,71}

Similarly, we observe monodirectional translation of the particles, but our experiments show that it is one effect amongst many. When particles within a static aqueous solution are exposed to a finite-width TSAW beam they also experience acoustic radiation force due to the complex amplitude pattern caused by diffraction, as well as a drag force induced by acoustic streaming. The relative strength of these two forces, which varies spatially, dictates particle translation behaviour. As such, we describe a total of five distinct mechanisms that occur within a SAW system. These are, firstly, migration in the direction of TSAW propagation. Secondly, peripheral streaming, which consists of lateral streaming vortices at the vicinity of the SAW beam (x - y plane). These extend across the entire width of the microfluidic channel (x -direction). Thirdly, lobe streaming which causes vertical vortices (x - z plane) along the channel length (y -direction). These occur at the channel edge closest to the SAW-beam source and (in our experiments) are at a much smaller length scale compared to peripheral streaming. Fourthly, orthogonal trapping which creates particle aggregation in clumps along the length of channel (y -direction), and finally, parallel trapping, which forms periodic particle patterning across the microfluidic channel width (x -direction).

Whereas previous numerical and experimental studies have focused on some of these mechanisms individually, here we capture all these effects simultaneously in a single experimental set up, as shown in Fig. 2. This allows us to examine the underlying mechanisms and the alteration in particle behaviour (corresponding to geometric parameters of

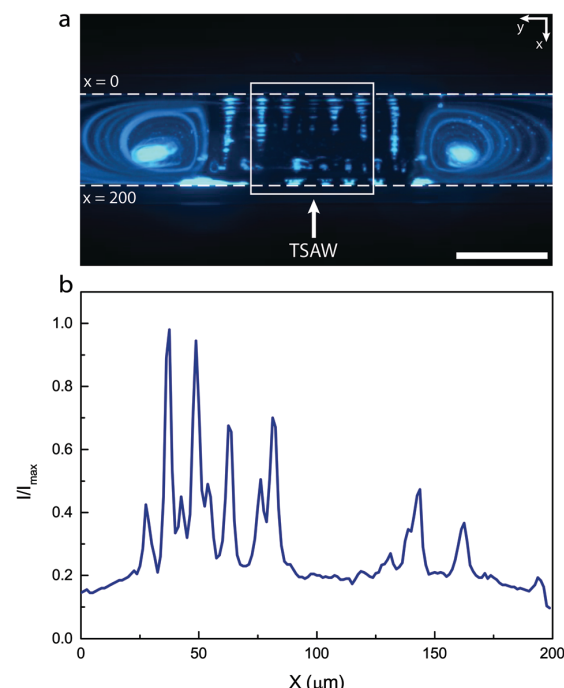


Fig. 3 Travelling SAW results in particle migration in the propagation direction. (a) Experimental visualisation of $1\text{ }\mu\text{m}$ particle behaviour existing within a channel ($H = 35\text{ }\mu\text{m}$, $W = 200\text{ }\mu\text{m}$), as a $21\text{ }\mu\text{m}$ wavelength TSAW (at 180 MHz frequency and 15 dBm generator power level) interacts with the particles. (b) Normalized mean image intensity along the x direction of the area bounded within the white square in (a) as a function of x location indicating that most particles are located away from the IDT, *i.e.* as we move from $x = 200\text{ }\mu\text{m}$ towards $x = 0$, showing that particles are displaced in the direction of TSAW propagation. Scale bar is $200\text{ }\mu\text{m}$.

4. Diffraction Driven Mechanisms

[View Article Online](#)

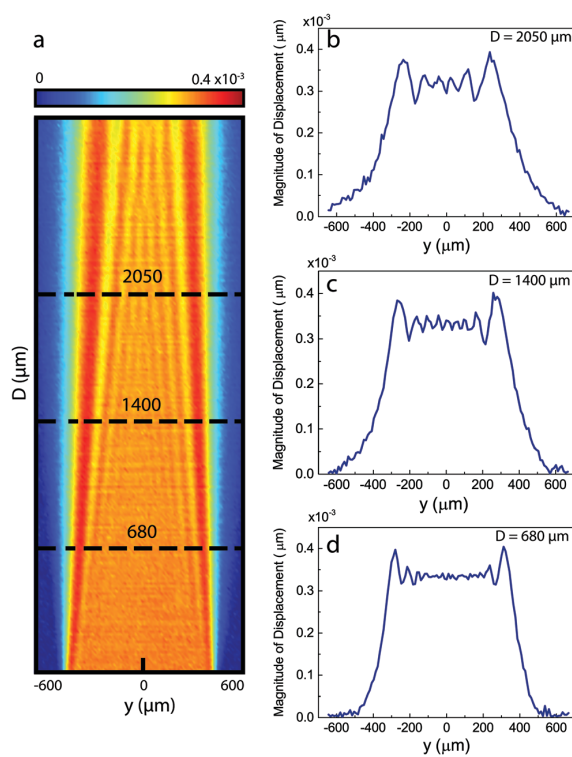


Fig. 4 (a) Amplitude distribution of surface-normal displacement patterns on the LN substrate extending across IDT aperture measured via laser Doppler vibrometer (LDV). An IDT (consisting of 7 finger pairs) with $d = 750 \mu\text{m}$ was used here (operating at applied generator voltage = 2.5 V and the frequency = 180 MHz). Dashed lines represent distinct channel locations used experimentally. (b)–(d) Magnitude of substrate-normal displacement as a function of y location. The displacement have unit of μm .

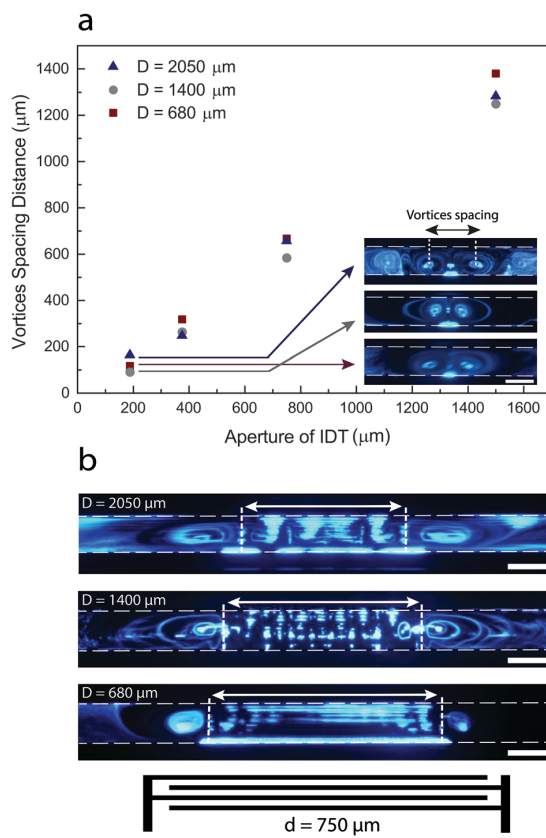


Fig. 5 (a) Spacing between the center of each peripheral vortex for four different IDT aperture (d) and three different channel locations (D). The experimental images from (a) 187.5 μm and (b) 750 μm IDT are presented. (b) The spacing between inner edge of the peripheral vortices (shown with a double arrow between dashed lines) are 573 μm 468.6 μm and 428.3 μm for D of 680 μm , 1400 μm and 2050 μm respectively. Scale bar is 100 μm .

transducers as well as the channel dimensions) in the following subsections.

4.1. Propagation migration

The most commonly described effect of TSAW is the migration of particles in the direction of propagation. This has been very effectively used for sized-based particle separation.^{48,68,72} Destgeer *et al.*⁵⁵ describe an area of the channel, along the channel edge nearest the ultrasound source, in which this doesn't occur, which they term an anechoic corner. Our work will show that behaviour in this area is dominated by streaming (lobe streaming), however outside this area we see a rich range of particle behaviour.

Nonetheless, underlying this, we do see an increase in particle concentration at the channel edge furthest from the IDT, consistent with migration in the direction of wave propagation. Fig. 3 shows the fluorescence intensity measured across the width of the channel, clearly showing an increase in particle numbers away from the source. For this particle size, the intensity is periodic arising from an additional

mechanisms that we have identified, however, if the channel width were increased this would diminish⁶⁵ and propagation migration would dominate.

4.2. Peripheral streaming

At the edges of the ultrasonic beam, substantial lateral vortices (within the x - y plane) occur. In this location, large spatial gradients in pressure can be expected which will generate significant body forces on the fluid, according to eqn (3a). These vortices have previously been used for nanoparticle manipulation,^{42,73,74} making use of the tendency for particles to be diverted into inner rotating streamlines and eventually focus them at the centre of the swirling fluid. This feature can be seen at each end of the channel along the length direction (besides the IDT aperture) in Fig. 2, with the size of the vortex extending the full width of the channel.

The formation of the ultrasonic SAW beam occurs in the substrate, hence, a laser Doppler vibrometer (LDV) scan has

4. Diffraction Driven Mechanisms

[View Article Online](#)

Paper

Lab on a Chip

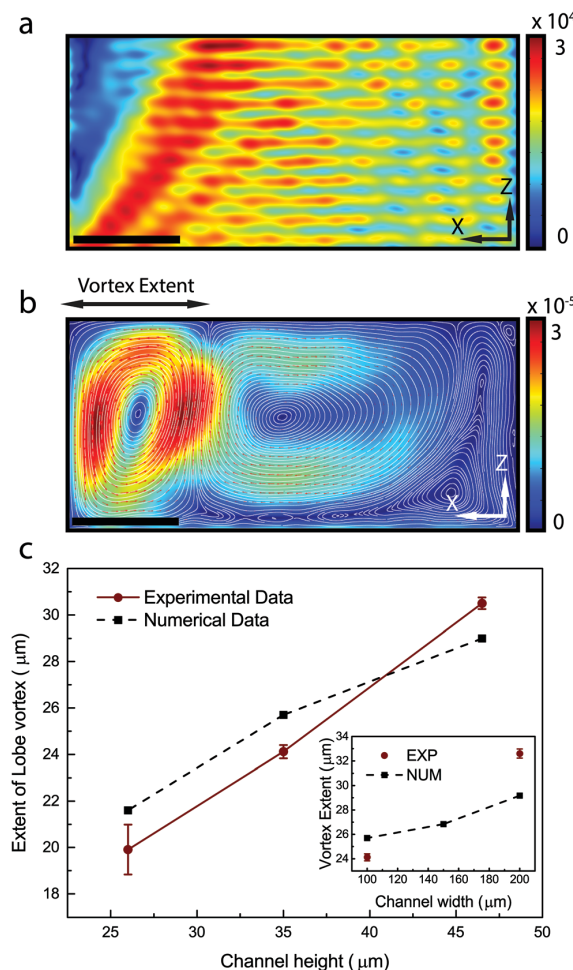


Fig. 6 Surface plot for a $100 \mu\text{m}$ wide, $46.5 \mu\text{m}$ high channel of the (a) time-averaged absolute pressure field $\langle |P_1| \rangle$ and (b) streamlines illustrating the simulated streaming field ($\lambda_{SAW} = 21 \mu\text{m}$) along the channels' width. (c) Extent of the lobe streaming as a function of channel height H and width W . Numerical results (dashed lines) are compared with experimental results (solid lines). The error bars indicate standard error. Pressure and velocity surface plots have units of Pa and m s^{-1} respectively. Scale bars are $20 \mu\text{m}$.

been performed (scan resolution = $10.5 \mu\text{m}$) to characterise the width of the beam emerging from a $750 \mu\text{m}$ wide IDT operated at 180 MHz frequency and 18 dBm generator power level with no channel attached. The resultant displacement field arises from diffraction effects within the substrate which occur because of the finite IDT aperture. Across the T-SAW beam, the area of maximum amplitude is in front of the IDT, though its width varies with propagation distance. Within the beam there are regions of higher and lower displacement amplitudes. Fig. 4 shows line scan data at three distinct distances (D) from the IDT. The distance between the peak displacements in the beam decreases with propagation distance.

Fig. 5a shows the experimental data taken for four different aperture widths and 3 distinct channel locations along

the SAW beam. In every case the distance between the centre of each peripheral vortex is measured. By defining vortical spacing as a function of IDT aperture with the slope of 0.9, (vortical spacing = 0.9 aperture), it can be seen that in each case the separation distance is smaller than the IDT width (x -axis), in line with the LDV data. However, the downside is that this measure combines information about where the edge of the vortex is with the size of the vortex. To better compare how the vortex location changes with channel location, in Fig. 5b, the images from the $750 \mu\text{m}$ IDT are presented and the distance between the inner edge of the vortices (extremity of the swirling flow) is measured, something which is more easily seen in the experimental videos. For larger propagation distances the vortex edges are closer together, measuring $573 \mu\text{m}$, $468 \mu\text{m}$ and $428 \mu\text{m}$ at propagation distances of $680 \mu\text{m}$, $1400 \mu\text{m}$ and $2050 \mu\text{m}$, respectively. This is expected as observed from the narrowing beam seen in the LDV scan (Fig. 4), in which the separation between the two locations of maximum displacement on either side of the beam is $580 \mu\text{m}$, $537 \mu\text{m}$ and $494 \mu\text{m}$. The relationship between the separation between peaks in the displacement field and the edges of the resulting vortices is complicated by the complex link between body force generation, the resulting fluid motion and by the omission of a channel in the LDV scan. However, it is clear that the vortex separation is somewhat smaller than the peak to peak beam width, as expected.

4.3. Lobe streaming

Within the area between the two lateral vortices, some particles are influenced predominately by ARF and others by acoustic streaming induced drag forces, this spatial variation in which mechanism is dominant was shown by Devendran *et al.*⁴⁵ for a SAW system, and is similarly observed here. Within this region we observe a vortex near the channel edge that occurs in the x - z plane.

The result of our numerical model, Fig. 6a, considers the absolute pressure field in a plane across the channel width (x - z plane with reference to Fig. 1a). As such it captures the diffraction which occurs in the fluid. The “anechoic corner”^{55,56} an area of low pressure at the channel edge closest to the IDT, can be seen. The diffraction lobes which are formed, are present as areas of high pressure, the first of which occurs at approximately the Rayleigh angle and marks the boundary of the anechoic corner. In this region, the $1 \mu\text{m}$ particles follow the fluid streamlines. Fig. 6b shows the predicted flow field in this plane, and shows a streaming vortex within the anechoic corner. As the lobe streaming vortex is driven by the first diffraction lobe, emerging from the substrate at an angle close to the Rayleigh angle, a change in channel height can be expected to change the extent of the vortex in an approximately linear manner. Fig. 6c, which compares simulation and experimental data, shows that this is indeed the case. In addition, the data (Fig. 6c inset) demonstrates that an increase in channel width also increases the extent of the vertical vortex. From Fig. 6b, it can be seen

4. Diffraction Driven Mechanisms

[View Article Online](#)

that the lobe vortex drives a weaker vortex across the rest of the channel width, where an increase in channel width results in a weakened secondary vortex. This, in turn, allows the lobe vortex to grow in size. This increase in size is, however, small compared to the increase in channel width, indicating that at larger widths there is considerably more channel area, in which streaming is not dominant.

4.4. Orthogonal trapping

It is only in areas which are less influenced by streaming that particle patterning can be observed. This occurs between the two peripheral streaming vortices and beyond the extent of the lobe vortex, it is in this region that ARF dominates. These patterns can be seen in Fig. 2, for the two wider IDT widths ($750\text{ }\mu\text{m}$ and $1500\text{ }\mu\text{m}$). The particles' location is dictated by radiation forces acting in both the x and y -directions. Such patterns occur due to diffraction of the TSW in both the substrate and the fluid. We examine the formation of these patterns in two stages, firstly dealing with the periodic clustering along the length of the channel (orthogonal trapping), and then subsequently examining the periodicity across the channel width (parallel trapping). Whilst the spacing between the peripheral streaming vortices is related to the width of the SAW beam as it diffracts in the substrate, orthogonal trapping is caused by finer details within the diffraction pattern. It can be seen from the LDV data in Fig. 4a that there are ripples in the displacement amplitudes across the width of the beam. This data is captured from a bare chip, thus, the diffraction causing these ripples is entirely on the substrate. Generally, in ultrasonic beamforming, the nearfield

pressure amplitude (in a fluid bound wave) has a complex distribution of peaks and troughs arranged laterally across the beam width. For increasing distances from the IDT, these features remain present but diminish in quantity and the spacing tends to increase. Consider the width of the IDT to be a series of point sources, in line with Huygens-Fresnel principle; at a point in front of the aperture the distance to each of these point sources will differ, hence the phase of each wavelet is different. This governs the resulting amplitude at that location. If the point is further from the aperture, this difference in phase from each point source is smaller. The resulting features in the displacement field are therefore larger in size. These features can be seen more clearly in the line scans across the width of the beam (Fig. 4b-d). It can be seen that for the line scan closer to the IDT that the features are indeed finer and more numerous. In addition, it can be seen that the inter-trough spacing is wider at each edge of the beam than in the middle.

In order to demonstrate that orthogonal trapping is due to substrate diffraction, we have examined the patterns formed using channels located at different distances from the IDT. Fig. 7 shows this data, with the spacing between clusters plotted against cluster location for three different channel locations and two IDT widths (the curves are fitted and intended simply to visually tie the relevant data points together). When comparing with the LDV measurement (Fig. 4), we must bear in mind that these measurements are made in the absence of the channel, and that the measurement plane is on the substrate surface and not in the fluid. Nonetheless, the trends match well. The experimental data shows that the spacing (ΔY) between the particle clusters are larger at the edges of

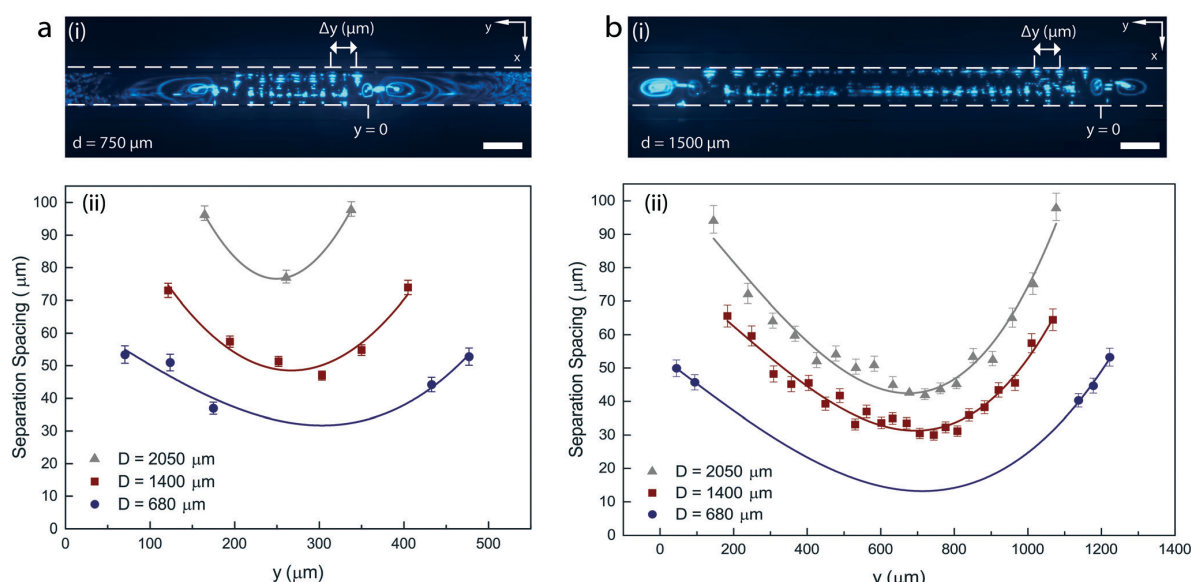


Fig. 7 Spacing of particle aggregation as a function of y locations with $y = 0$ corresponding to the rightmost approximated edge of the SAW-beam. Experimental results for three distinct channel/IDT distances (D) shown for devices, each consisting of an IDT with (a) $d = 750\text{ }\mu\text{m}$ and (b) $d = 1500\text{ }\mu\text{m}$. The error bars indicate standard error. Scale bar is $100\text{ }\mu\text{m}$.

4. Diffraction Driven Mechanisms

[View Article Online](#)

Paper

Lab on a Chip

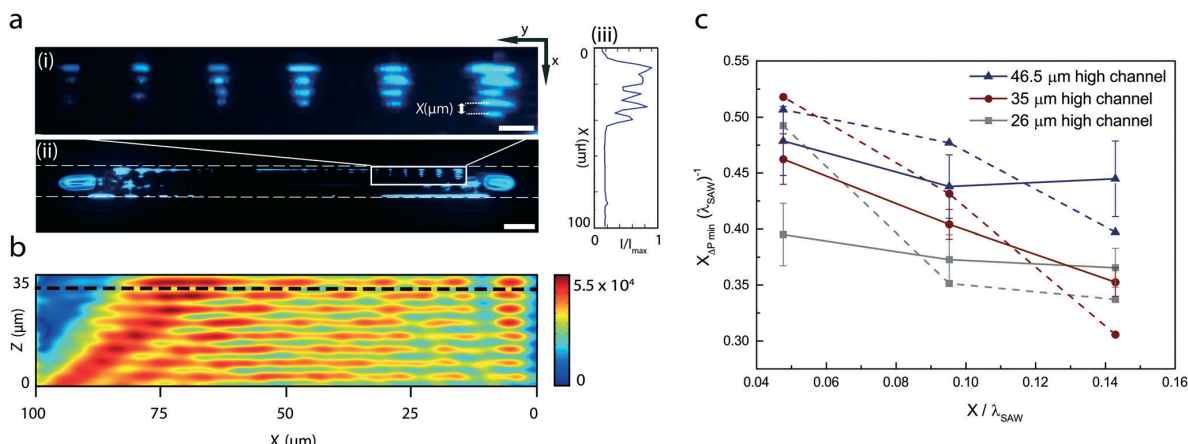


Fig. 8 (a) Experimental results demonstrating the observed parallel trapping along channel width ($W = 100 \mu\text{m}$, $H = 35 \mu\text{m}$) driven by IDT ($\lambda_{SAW} = 21 \mu\text{m}$, $d = 1500 \mu\text{m}$). The image (i) is an inset of a particular section in (ii) bounded by the white rectangle. (iii) Peaks in y -averaged image intensity indicates particle alignment locations. (b) Numerical model depicting the first-order time-averaged absolute pressure field ($|P_1|$) established within the channel. (c) The spacing between parallel trapping locations (in experimental observations represented with solid lines) as well as minimum pressure locations (numerical results for a $W = 100 \mu\text{m}$, $H = 35 \mu\text{m}$ channel shown in dashed lines) as a function of x locations, normalized by λ_{SAW} . The error bars indicate standard error. Pressure surface plot has unit of Pa. Scale bars are 30 μm and 100 μm in (a)(i) and (a)(ii) respectively.

the beam, and that the feature spacings are larger when the channel is positioned further from the IDT. The variation in separation across the width of the IDT is clearly indicative that this is not simply a case of reflections causing a wave to be established along the length of the channel, as this would have yielded regularly spaced clustering.

4.5. Parallel trapping

Particle clustering also takes place across the width of the channel. This is due to diffraction which occurs in the cross-sectional plane of the channel (x - z plane in Fig. 1a). As the SAW couples into the microfluidic channel, its finite width acts as an aperture and diffraction ensues. As with the diffraction in the substrate, the geometry of the system dictates that the particles are within the near-field of the sound field, in this region lobes of maximum pressure occur. Devendran *et al.*⁵⁸ showed that the diffraction in this plane can cause particle trapping across the width of the channel, though in their paper, this trapping was located at the edge of the channel closest to the IDT. In the systems studied here, the width of the channels are considerably smaller, so the effect stretches across the full width of the channel. However at the edge nearest the IDT these patterns are disturbed by the lobe vortex.

Fig. 8 highlights the patterns and shows a model of the pressure field in this plane. The first pressure lobe is easily seen and occurs at approximately the Rayleigh angle. More careful inspection also reveals other lobes at lower angles which result in variation in the amplitude of the absolute pressure across the width of the channel. Upon actuation, the particles are pushed along these structures in the sound field to the top of the channel where they are held in the lo-

cal pressure minima. Due to the angled nature of these lobes, a higher channel will result in wider separation between the clusters, and likewise the structures nearest to the far wall should be separated by the greatest distances. Both these trends are seen in the experimental and simulation data shown in Fig. 8c, in which image intensities are analysed to precisely identify particle alignment positions across the channel's width. The spacing of the particles is plotted against the location of each set of particles in the x (opposite to propagation) direction with both distances normalized by the SAW wavelength. It should be noted that these features are not due to reflection of the fluid bound wave from the channel wall, firstly, this reflection is highly inefficient, an analysis of the acoustic impedance mismatch shows that only approximately 4% of the acoustic energy is reflected.⁷⁰ Secondly, if this were the case, the separation between the lines should be consistently $0.5\lambda_{SAW}$ regardless of channel width or height, not the case here.

The experimental images of particle behaviour have been used to identify five mechanisms. Of these, propagation migration is well understood and widely described in the literature. The analysis performed has allowed the other four mechanisms to be related to diffraction in the substrate (yielding peripheral streaming and orthogonal patterning) and in the fluid (yielding lobe streaming and parallel patterning).

5. Conclusion

In this study, we have experimentally investigated various phenomena arising from the incidence of a propagating finite-width SAW beam into an enclosed quiescent fluid. The Huygens-Fresnel principle, wherein superposition of edge

4. Diffraction Driven Mechanisms

[View Article Online](#)

Lab on a Chip

Paper

waves with planar waves yield rather complex diffraction patterns in the propagating TSAW is utilized to describe experimental findings, aided by numerical simulations. Acoustic radiation force arises from pressure field distributions in the fluid, with configurations significantly affected by diffraction effects in the propagating TSAW within the fluid and along fluid/LN interface. The resultant radiation force translates particles to the stabilised pressure minima locations despite the TSAW's continuous propagation. As such, distinct particle patterning along channel width and length parallel and orthogonal to the propagation direction are achieved respectively. In addition, streaming is observed in the form of large lateral vortices at the periphery regions of the ultrasonic beam, and a vertical vortex between the channel edge and first diffraction lobe. The cross over from streaming-dominated to radiation-dominated behaviour of particles depend on the geometries of IDT as well as that of the microfluidic channel. These findings and observations give rise to a better understanding of the underlying physics in SAW-driven technologies that can be achieved, which is essential in unlocking the full potential of such systems and introducing a broader range of applications.

Conflicts of interest

There are no conflicts to declare.

Acknowledgements

We gratefully acknowledge support received from the Australian Research Council, Grant No. DP160101263. All devices used in this work were fabricated at the Melbourne Centre for Nanofabrication (MCN). This research was undertaken with the assistance of resources from the National Computational Infrastructure (NCI), which is supported by the Australian Government.

References

- M. Fouet, M. A. Mader, S. Irain, Z. Yanha, A. Naillon, S. Cargou, A. M. Gue and P. Joseph, *Lab Chip*, 2016, **16**, 720–733.
- K. He, S. T. Retterer, B. R. Srijanto, J. C. Conrad and R. Krishnamoorti, *ACS Nano*, 2014, **8**, 4221–4227.
- J. McGrath, M. Jimenez and H. Bridle, *Lab Chip*, 2014, **14**, 4139–4158.
- M. Yamada, M. Nakashima and M. Seki, *Anal. Chem.*, 2004, **76**, 5465–5471.
- Y. Wang, Y. Zhao and S. K. Cho, *J. Micromech. Microeng.*, 2007, **17**, 2148–2156.
- N. Xia, T. P. Hunt, B. T. Mayers, E. Alsborg, G. M. Whitesides, R. M. Westervelt and D. E. Ingber, *Biomed. Microdevices*, 2006, **8**, 299–308.
- P. R. Gascoyne and J. Vykoukal, *Electrophoresis*, 2002, **23**, 1973.
- H. Shafiee, M. B. Sano, E. A. Henslee, J. L. Caldwell and R. V. Davalos, *Lab Chip*, 2010, **10**, 438–445.
- B. Landenberger, H. Hofemann, S. Wadle and A. Rohrbach, *Lab Chip*, 2012, **12**, 3177–3183.
- H. F. Levison and A. Morbidelli, *Nature*, 2003, **426**, 419–421.
- X. Ding, S.-C. S. Lin, B. Kiraly, H. Yue, S. Li, I.-K. Chiang, J. Shi, S. J. Benkovic and T. J. Huang, *Proc. Natl. Acad. Sci. U. S. A.*, 2012, **109**, 11105–11109.
- M. Wiklund, *Lab Chip*, 2012, **12**, 2018–2028.
- D. Bazou, R. Kearney, F. Mansergh, C. Bourdon, J. Farrar and M. Wrude, *Ultrasound Med. Biol.*, 2011, **37**, 321–330.
- J. Hultstrom, O. Manneberg, K. Dopf, H. M. Hertz, H. Brismar and M. Wiklund, *Ultrasound Med. Biol.*, 2007, **33**, 145–151.
- N. Sivanantha, C. Ma, D. J. Collins, M. Sesen, J. Brenker, R. L. Coppel, A. Neild and T. Alan, *Appl. Phys. Lett.*, 2014, **105**, 103704.
- A. Haake, A. Neild, G. Radziwill and J. Dual, *Biotechnol. Bioeng.*, 2005, **92**, 8–14.
- M. Hill, Y. Shen and J. J. Hawkes, *Ultrasonics*, 2002, **40**, 385–392.
- M. Hill and R. J. Wood, *Ultrasonics*, 2000, **38**, 662–665.
- X. Ding, P. Li, S.-C. S. Lin, Z. S. Stratton, N. Nama, F. Guo, D. Slotcavage, X. Mao, J. Shi and F. Costanzo, *Lab Chip*, 2013, **13**, 3626–3649.
- V. Skowronek, R. W. Rambach, L. Schmid, K. Haase and T. Franke, *Anal. Chem.*, 2013, **85**, 9955–9959.
- L. Y. Yeo and J. R. Friend, *Biomicrofluidics*, 2009, **3**, 012002.
- S.-C. S. Lin, X. Mao and T. J. Huang, *Lab Chip*, 2012, **12**, 2766–2770.
- T. Laurell, F. Petersson and A. Nilsson, *Chem. Soc. Rev.*, 2007, **36**, 492–506.
- I. Leibacher, P. Reichert and J. Dual, *Lab Chip*, 2015, **15**, 2896–2905.
- I. Leibacher, S. Schatzer and J. Dual, *Lab Chip*, 2014, **14**, 463–470.
- G. Vuillermet, P.-Y. Gires, F. Casset and C. Poulain, *Phys. Rev. Lett.*, 2016, **116**, 184501.
- G. Destgeer, K. H. Lee, J. H. Jung, A. Alazzam and H. J. Sung, *Lab Chip*, 2013, **13**, 4210–4216.
- F. Guo, Z. Mao, Y. Chen, Z. Xie, J. P. Lata, P. Li, L. Ren, J. Liu, J. Yang and M. Dao, *et al.*, *Proc. Natl. Acad. Sci. U. S. A.*, 2016, **113**, 1522–1527.
- M. Wu, Y. Ouyang, Z. Wang, R. Zhang, P.-H. Huang, C. Chen, H. Li, P. Li, D. Quinn and M. Dao, *et al.*, *Proc. Natl. Acad. Sci. U. S. A.*, 2017, **114**, 10584–10589.
- J. C. Brenker, D. J. Collins, H. Van Phan, T. Alan and A. Neild, *Lab Chip*, 2016, **16**, 1675–1683.
- M. Sesen, T. Alan and A. Neild, *Lab Chip*, 2014, **14**, 3325–3333.
- L. Schmid and T. Franke, *Appl. Phys. Lett.*, 2014, **104**, 133501.
- M. Sesen, C. Devendran, S. Malikides, T. Alan and A. Neild, *Lab Chip*, 2017, **17**, 438–447.
- S. R. Heron, R. Wilson, S. A. Shaffer, D. R. Goodlett and J. M. Cooper, *Anal. Chem.*, 2010, **82**, 3985–3989.
- A. Qi, L. Y. Yeo and J. R. Friend, *Phys. Fluids*, 2008, **20**, 074103.

4. Diffraction Driven Mechanisms

[View Article Online](#)

Paper

Lab on a Chip

- 36 D. J. Collins, B. Morahan, J. Garcia-Bustos, C. Doerig, M. Plebanski and A. Neild, *Nat. Commun.*, 2015, **6**, 8686.
- 37 J. Shi, D. Ahmed, X. Mao, S.-C. S. Lin, A. Lawit and T. J. Huang, *Lab Chip*, 2009, **9**, 2890–2895.
- 38 D. J. Collins, T. Alan and A. Neild, *Lab Chip*, 2014, **14**, 1595–1603.
- 39 J. Shi, H. Huang, Z. Stratton, Y. Huang and T. J. Huang, *Lab Chip*, 2009, **9**, 3354–3359.
- 40 C. Devendran, N. R. Gunasekara, D. J. Collins and A. Neild, *RSC Adv.*, 2016, **6**, 5856–5864.
- 41 A. Fakhfouri, C. Devendran, D. J. Collins, Y. Ai and A. Neild, *Lab Chip*, 2016, **16**, 3515–3523.
- 42 D. J. Collins, Z. Ma and Y. Ai, *Anal. Chem.*, 2016, **88**, 5513–5522.
- 43 H. Bruus, *J. Fluid Mech.*, 2017, **826**, 1–4.
- 44 P. B. Muller, R. Barnkob, M. J. H. Jensen and H. Bruus, *Lab Chip*, 2012, **12**, 4617–4627.
- 45 C. Devendran, T. Albrecht, J. Brenker, T. Alan and A. Neild, *Lab Chip*, 2016, **16**, 3756–3766.
- 46 C. Devendran, I. Gralinski and A. Neild, *Microfluid. Nanofluid.*, 2014, **17**, 879–890.
- 47 H. Bruus, *Lab Chip*, 2012, **12**, 1014–1021.
- 48 G. Destgeer, B. H. Ha, J. Park, J. H. Jung, A. Alazzam and H. J. Sung, *Phys. Procedia*, 2015, **70**, 34–37.
- 49 J. Shi, X. Mao, D. Ahmed, A. Colletti and T. J. Huang, *Lab Chip*, 2008, **8**, 221–223.
- 50 C. Grenvall, P. Augustsson, J. R. Folkenberg and T. Laurell, *Anal. Chem.*, 2009, **81**, 6195–6200.
- 51 J. Dual, P. Hahn, I. Leibacher, D. Möller, T. Schwarz and J. Wang, *Lab Chip*, 2012, **12**, 4010–4021.
- 52 J. Lei, P. Glynne-Jones and M. Hill, *Lab Chip*, 2013, **13**, 2133–2143.
- 53 P. B. Muller, M. Rossi, Á. Marín, R. Barnkob, P. Augustsson, T. Laurell, C. J. Kaehler and H. Bruus, *Phys. Rev. E: Stat., Nonlinear, Soft Matter Phys.*, 2013, **88**, 023006.
- 54 A. Neild, S. Oberti, A. Haake and J. Dual, *Ultrasonics*, 2006, **44**, e455–e460.
- 55 G. Destgeer, B. H. Ha, J. Park, J. H. Jung, A. Alazzam and H. J. Sung, *Anal. Chem.*, 2015, **87**, 4627–4632.
- 56 F. Kiebert, S. Wege, J. Massing, J. König, C. Cierpka, R. Weser and H. Schmidt, *Lab Chip*, 2017, **17**, 2104–2114.
- 57 G. Destgeer, A. Alam, H. Ahmed, J. Park, J. H. Jung, K. Park and H. J. Sung, *Appl. Phys. Lett.*, 2018, **112**, 083501.
- 58 C. Devendran, D. J. Collins, Y. Ai and A. Neild, *Phys. Rev. Lett.*, 2017, **118**, 154501.
- 59 D. J. Collins, R. O'Rorke, C. Devendran, Z. Ma, J. Han, A. Neild and Y. Ai, *Phys. Rev. Lett.*, 2018, **120**, 074502.
- 60 J. W. Ng, C. Devendran and A. Neild, *Lab Chip*, 2017, **17**, 3489–3497.
- 61 J. W. Ng, D. J. Collins, C. Devendran, Y. Ai and A. Neild, *Microfluid. Nanofluid.*, 2016, **20**, 151.
- 62 S.-C. Wooh and Y. Shi, *J. Nondestruct. Eval.*, 1999, **18**, 39–57.
- 63 H. G. Kraus, *J. Opt. Soc. Am. A*, 1989, **6**, 1196–1205.
- 64 M. Settnes and H. Bruus, *Phys. Rev. E: Stat., Nonlinear, Soft Matter Phys.*, 2012, **85**, 016327.
- 65 W. L. M. Nyborg, *Physical Acoustics*, Elsevier, 1965, vol. 2, pp. 265–331.
- 66 D. J. Collins, C. Devendran, Z. Ma, J. W. Ng, A. Neild and Y. Ai, *Sci. Adv.*, 2016, **2**, e1600089.
- 67 Z. Zhu and C. J. Yang, *Acc. Chem. Res.*, 2016, **50**, 22–31.
- 68 G. Destgeer, B. H. Ha, J. H. Jung and H. J. Sung, *Lab Chip*, 2014, **14**, 4665–4672.
- 69 T. Franke, A. R. Abate, D. A. Weitz and A. Wixforth, *Lab Chip*, 2009, **9**, 2625–2627.
- 70 D. J. Collins, A. Neild and Y. Ai, *Lab Chip*, 2016, **16**, 471–479.
- 71 X. Ding, S.-C. S. Lin, M. I. Lapsley, S. Li, X. Guo, C. Y. Chan, I.-K. Chiang, L. Wang, J. P. McCoy and T. J. Huang, *Lab Chip*, 2012, **12**, 4228–4231.
- 72 W. Ung, K. Mutafopoulos, P. Spink, R. W. Rambach, T. Franke and D. A. Weitz, *Lab Chip*, 2017, **17**, 4059–4069.
- 73 D. J. Collins, Z. Ma, J. Han and Y. Ai, *Lab Chip*, 2017, **17**, 91–103.
- 74 D. J. Collins, B. L. Khoo, Z. Ma, A. Winkler, R. Weser, H. Schmidt, J. Han and Y. Ai, *Lab Chip*, 2017, **17**, 1769–1777.

This chapter explores the role of particle size, as a function of frequency and power, in travelling surface acoustic wave (TSAW) systems. The transition between distinct behaviour of particles is characterised, and in contrary to the present literature, here the periodic patterning arise from diffractive effects are taken into account.

5

Size-dependant Behaviour of Particles

5.1 Overview

The present literature on travelling SAW broadly discuss two physical phenomena; particles drifting along TSAW propagation direction (driven by acoustic radiation force) and particle swirling in continuous vortices (driven by acoustic streaming). As a result, discussions on the transitions in particles behaviour typically focus on the transition between these two behaviours. In an experimental study, Skowronek *et al* [230] introduce a dimensionless parameter, κ , that determines the cross-over from streaming dominated to radiation dominated behaviour. However, this parameter is an oversimplification and as discussed in chapter 4, there are other force regimes that are previously overlooked.

In chapter 4 various mechanisms coexisting in an individual travelling SAW system were discussed, where a scenario was introduced in TSAW systems in which patterning of particles in a spatial manner takes place. This effect is arisen by the complex amplitude in diffractive patterns. Here we further delve into this effect by exploring the influence of size on the behaviour of particles contained in a TSAW-driven system. Through an experimental and numerical study of the system, three distinct outcome behaviour along with two transitional regions have been observed, representing the dominance of various forcing mechanisms; firstly, migration of particles along propagation direction, here termed drifting; secondly spatial periodic patterning of particles driven by diffractive patterns; finally, continuous swirling

5. Size-dependant Behaviour of Particles

of particles driven by acoustic streaming. We have found that the transition between these regions depends on particle size as a function of frequency and power. At a constant frequency, below a certain size particles are dominated by acoustic streaming that induces drag force to the particles and entrains them in continuous vortices. Increasing particle size transfer their behaviour to the next regions where initially patterning, then drifting takes place. Apart from this, there are two regions where the combination of streaming-patterning and patterning-drifting occurs. We also found that the applied power plays a role such that at a constant frequency and size, increasing power result in transition in behaviour.

5.2 Publication

The following publication was reproduced from [1] with kind permission from the Royal Society of Chemistry.



Lab on a Chip

PAPER

[View Article Online](#)

[View Journal](#) | [View Issue](#)



Cite this: *Lab Chip*, 2018, **18**, 3926

The size dependant behaviour of particles driven by a travelling surface acoustic wave (TSAW)†

Armaghan Fakhfouri, ^a Citsabehsan Devendran, ^a Asif Ahmed, ^b Julio Soria^b and Adrian Neild ^{*a}

The use of travelling surface acoustic waves (TSAW) in a microfluidic system provides a powerful tool for the manipulation of particles and cells. In a TSAW driven system, acoustophoretic effects can cause suspended micro-objects to display three distinct responses: (1) swirling, driven by acoustic streaming forces, (2) migration, driven by acoustic radiation forces and (3) patterning in a spatially periodic manner, resulting from diffraction effects. Whilst the first two phenomena have been widely discussed in the literature, the periodic patterning induced by TSAW has only recently been reported and is yet to be fully elucidated. In particular, more in-depth understanding of the size-dependant nature of this effect and the factors involved are required. Herein, we present an experimental and numerical study of the transition in acoustophoretic behaviour of particles influenced by relative dominance of these three mechanisms and characterise it based on particle diameter, channel height, frequency and intensity of the TSAW driven microfluidic system. This study will enable better understanding of the performance of TSAW sorters and allow the development of TSAW systems for particle collection and patterning.

Received 26th October 2018,
Accepted 15th November 2018

DOI: 10.1039/c8lc01155a

rsc.li/loc

1 Introduction

The manipulation of particles and cells is essential to a number of applications within microfluidic technologies, particularly in the development of systems for cell patterning, concentration or sorting. A wide range of methods for particle manipulation have been developed using hydrodynamic,^{1–3} magnetic,^{4,5} dielectrophoretic (DEP),^{6,7} optical,^{8,9} and acoustic force fields.¹⁰ Acoustic fields provide a powerful tool for precise, non-contact and biocompatible^{11,12} manipulation of particles and cells, thus, have received considerable attention recently.

Acoustophoresis, defined as the movement of particles by acoustic forces, is key for acoustic manipulation. In a typical acoustically driven system, suspended objects are subjected to steady state acoustic forces that are generated through two main mechanisms. Firstly, the presence of particles in a sound field leads to scattering and this in turn results in acoustic radiation forces¹³ (ARF) which act to move particles

in a certain direction. Secondly, gradients in the resultant acoustic field give rise to a steady state flow, termed acoustic streaming.^{14,15} This flow field in turn induces drag forces that act on the suspended particles. The particle behaviour depends on the relative significance of these distinct acoustophoretic mechanisms. In order to control the intended manipulation and achieve a desired outcome, we seek to present an understanding of the origin of each effect, and establish the critical factors that influence the relative dominance of these forces.

Acoustically driven microfluidic systems are mainly actuated using either bulk acoustic waves^{16–21} (BAW) or surface acoustic waves^{22–25} (SAW). The former are excited within volumes of fluid using a piezoelectric transducer affixed to the microfluidic channel, typically operated at frequencies corresponding to resonant modes in the fluid volume. As such, the sound fields that are established, consist of standing waves. Within standing waves, the ARFs act to hold particles at certain locations, usually corresponding to the nodes or antinodes of the field, hence patterns of particles are formed as they cluster at these stable locations. In addition, acoustic streaming flows exist within these systems, which act to drag particles along a swirling trajectory. Thorough theoretical and numerical studies^{21,26,27} have determined the nature of both the radiation force and streaming fields, establishing an understanding of the relative dominance of these two effects as a function of particle diameter. Below a frequency dependant critical particle size, streaming induced drag forces act

^a Laboratory for Micro Systems, Department of Mechanical and Aerospace Engineering, Monash University, Clayton, Victoria 3800, Australia.

E-mail: Adrian.neild@monash.edu

^b Laboratory for Turbulence Research in Aerospace and Combustion (LTRAC), Department of Mechanical and Aerospace Engineering, Monash University, Clayton, Victoria 3800, Australia

† Electronic supplementary information (ESI) available. See DOI: [10.1039/c8lc01155a](https://doi.org/10.1039/c8lc01155a)

5. Size-dependant Behaviour of Particles

[View Article Online](#)

to keep the particles in constant motion driven by the fluid flow, whilst above this cut-off size ARF dominates and particles are held in fixed locations.¹⁴

Contrary to BAW systems, SAWs are generated on the surface of a piezoelectric substrate by a set of interdigitated electrodes. Upon application of an alternating voltage, each electrode finger displaces, creating a wave. By designing the spacing between each electrode in accordance to the SAW wavelength at an intended operational frequency, constructive interference will occur, improving the efficiency of the system.^{22,28} In contrast to BAW, fluid resonances are not excited, and hence, there is a greater flexibility in the sound fields that can be generated within fluid volumes confined on the substrate. SAW systems are suitable for diverse applications including droplet generation,^{29,30} merging³¹ and steering,^{32,33} atomization,^{34,35} size-based sorting,³⁶ particle filtration³⁷ and patterning.³⁸

In SAW-driven devices, acoustic fields are generally classified as being either travelling³⁹ (TSAW) or standing^{40,41} (SSAW) in nature. SSAWs are generated when two counter propagating SAWs interfere, resulting in the formation of time-averaged nodal and anti-nodal positions in the sound field. In SSAW field radiation forces collect suspended particles to either the nodal⁴² or antinodal⁴³ positions based on their acoustic contrast with the host fluid. Whilst, fields have been established with counter propagating SAW of differing frequencies for adjustable locations,⁴⁴ and pulsed actuation for spatially selective patterning,⁴⁵ typically the standing field is established across the entire channel area using frequency-matched counter propagating waves, resulting in periodic patterning.^{46–48} As with BAW, the dominant mechanism (patterning or streaming) has a size dependency, however, in SSAW systems, the critical particle size varies locally across the width of the channel due to inherent SAW attenuation.⁴⁶

In a TSAW system, the SAW propagates in one direction, as does the wave which is coupled from the TSAW into the fluid. As such, it is broadly assumed that the resultant radiation forces act to continuously push particles away from the acoustic source. Whilst this mono-directional mechanism has been used successfully for particle sorting,⁴⁹ it is not the only form of behaviour resulting from TSAW. Indeed, Skowronek *et al.*⁵⁰ demonstrate that there is a dimensionless parameter (defined by Kappa, κ) that determines the cross-over from streaming dominated to radiation dominated behaviour of particles. However, a series of recent studies have observed some rather complex features within a TSAW system which significantly affect the particle outcome behaviour. Destgeer *et al.*^{51,52} have demonstrated the existence of an “anechoic corner” within the channel. This is located along the edge of the channel nearest to the source; in this region, the sound field is weak and strong streaming flows exist. Additionally, through numerical and experimental studies, periodic patterning has been demonstrated, formerly only linked to SSAW. The patterning of particles into stable locations results from diffraction effects as the TSAW couples into the fluid volume and is affected by the channel edge, which acts as a discontinuity.^{53,54}

The literature on TSAW widely discusses the physical phenomena of streaming driven particle behaviour and the drifting of particles due to acoustic radiation force. As a result, discussions of the transition in behaviour type, as a function of particle size, focus on the transition between these two behaviours. In our previous work,⁵⁴ we detailed the occurrence of another phenomenon in TSAW systems, that of particle patterning. As a result, in this work, we revisit the idea of characterising particle outcomes based on size, but using this new complete framework of behaviour types including that of particle patterning. Consequently, we analyse the transitions between streaming based behaviour, patterning and drifting of particles as a function of size. Furthermore, we characterise the dominant effect based on TSAW wavelength (frequency), power intensity and channel height. In doing so, IDTs with a range of wavelengths (15, 21, 25 and 36 μm) and channels heights (15 and 26 μm) are used.

2 System mechanics

Surface acoustic waves are actuated by a set of conducting interdigitated transducers (IDT) structured on a piezoelectric substrate. The IDTs are actuated at a frequency such that the surface displacements originating from each electrode constructively interfere with waves emanating from adjacent electrode. As such, the spacing of the electrodes dictate the optimum frequency of operation and wavelength of the propagating SAW, with $\lambda_{\text{SAW}} = C_s/f$, where C_s and f represent the speed of sound and frequency, respectively.

Upon arrival at the edge of the microfluidic channel, the SAW couples energy into the fluid at the Rayleigh angle $\theta_R = \sin^{-1}(C_l/C_s)$ with C_l and C_s representing the speed of sound in a given liquid and substrate, respectively. The acoustic wave is coupled into the fluid in the form of a plane wave, albeit with spatial variations in the amplitude of the plane wave across its wavefront due to inherent diffractive effects, based on Huygens-Fresnel principle.⁵³ As a result, a field with complex amplitude patterns is created within the fluid. Two main mechanisms arise, that of acoustic streaming and acoustic radiation forces and, as we will show, the latter gives rise to mono-directional motion and particle patterning. These two mechanisms lead to three distinct outcomes in terms of the particle behaviour; drifting in the direction of propagation (Fig. 1a), patterning in stable locations (Fig. 1b) and continuous motion in circular trajectories (Fig. 1c).

The two mechanisms of acoustic streaming and ARF are well known, so we describe their origin, briefly. Firstly, acoustic streaming, arises from gradients in a sound field as it propagates through a viscous fluid, which give rise to time-averaged body forces acting on the fluid.⁵⁵ As a result, a steady swirling flow is generated (Fig. 1c), inducing a drag force on the suspended particles, with $F_{\text{drag}} \propto a$, where a is the particle radius.

Additionally, particles are directly subjected to primary acoustic radiation forces, where, in a pure standing wave this force is proportional to the radius cubed,^{13,56} whilst in a pure

5. Size-dependant Behaviour of Particles

[View Article Online](#)

Paper

Lab on a Chip

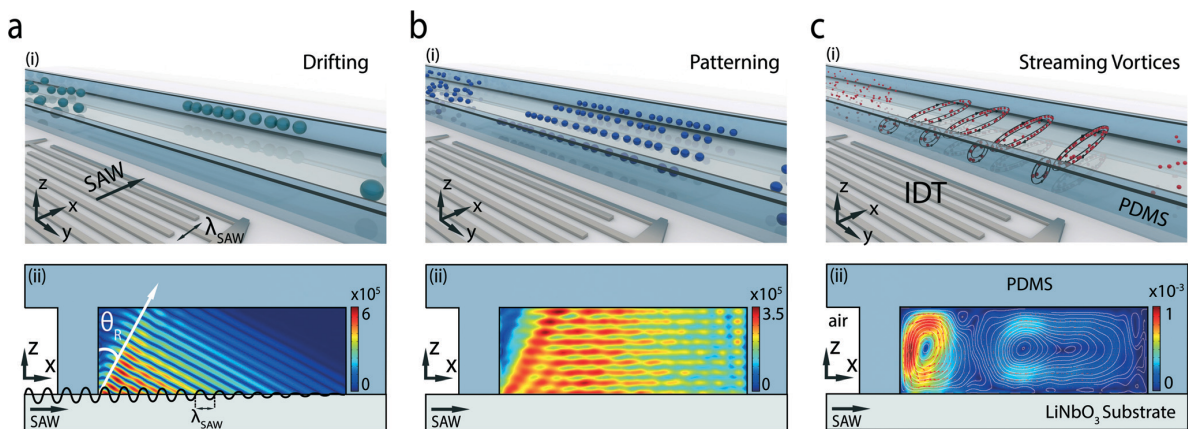


Fig. 1 Conceptual illustration of three distinct behaviour of particles resulted from acoustophoretic mechanisms within a TSAW driven system. 3-dimensional rendered drawing of the system exhibiting (a-i) particle drifting in the direction of TSAW propagation (b-i) particle patterning resulted from diffraction effects (c-i) acoustic streaming flow field. (a-ii) illustration of the instant transmission of TSAW into the fluid, where a simulated instantaneous absolute pressure field after initial excitation is shown. This effect is classically understood to drift particles away from TSAW source. (b-ii) a simulated time-averaged absolute pressure field $\langle |P_1| \rangle$ with lobe patterns which serve to pattern particles into stable locations. (c-ii) The simulated streaming field indicated by white streamlines across the channel width. Red arrows show streaming velocity. Streaming vortices induce drag force on the small particles. It should be noted that airpockets are situated on both side of the channel to minimise the energy loss into the PDMS that exists in between the IDT and the channel as illustrated in ESI† Fig. S1. Pressure and velocity surface plots have units of Pa and m s^{-1} , respectively.

travelling wave, the relationship is to the sixth power⁵⁷ (with the wavelength assumed to be significantly larger than the particle size in both cases ($a \ll \lambda_{\text{SAW}}$)). As such, the ARF can be expected to dominate over streaming induced drag as particle sizes increase.⁵⁸ Here, we have neither a pure travelling nor standing wave, rather a complex field arising from the amplitude patterns caused by diffraction.⁵⁴ Nonetheless, we can expect that, streaming will be the dominant mechanism for the small particles. Whilst, for a certain range of particle sizes which this study will determine, the ARF will act to pattern particles within stable locations dictated by diffraction lobes as shown in Fig. 1b. Beyond a second critical size, the particles will move mono-directionally in the TSAW propagation direction, akin to particles drifting away from the source (Fig. 1a).

3 Methods

In this work, one set of straight interdigital transducers (IDTs) with 15, 21, 25 or 36 μm pitch (operating at 260, 185, 155 or 110 MHz, respectively) was used in each experiment to generate the TSAW. The IDT, with aperture (overlapping width) of 750 μm , is made of a 10 nm chromium (adhesive layer) and 200 nm aluminium (conductive layer) deposited on a piezoelectric 128° rotated Y-cut X propagating lithium niobate (LN, LiNbO_3) wafer by an e-beam evaporator. The 200 μm wide microfluidic channels (with 9.5 μm , 26 μm or 35 μm height) were cast in polydimethylsiloxane (PDMS; 1:10 ratio of curing agent/base) and subsequently bonded to the LN substrate aided by plasma treatment (Harrick Plasma, PDC-32G). The devices used here contain sufficiently long channels (13.5 mm $\sim 60 \times$ channel's width) to ensure that

any boundary effect arisen by the channel's length is negligible. The PDMS between the IDT and the channel act as a resistance to the propagating wave resulting in partial attenuation of the incident SAW into the PDMS prior to coupling into the fluid. To minimise the energy loss into the PDMS, there are airpockets on both sides of the channel to retain the PDMS thickness at 50 μm as illustrated in ESI† Fig. S1. To prevent corrosion of the electrodes and to enhance bonding of the PDMS, a 270 nm thick layer of SiO_2 was deposited on the LN wafer. Fluorescent polystyrene particles (Magsphere, Pasadena, CA, USA) with a range of diameters including 0.1 μm (green), 0.3 μm (blue), 0.5 μm (yellow-green), 1 μm (blue), 2 μm (green), 3 μm (blue), 5 μm (blue) and 6 μm (green), were suspended in a homogenous solution of 1:10 particles/water, diluted with 0.2% polyethylene glycol (PEG). A signal generator (Anapico, APGEN3000) was used to apply an AC signal to the IDT at the intended frequency. For visualisation, two set-ups were used. The first used a fluorescence microscope (Olympus BX43) coupled with a compatible light source (Olympus URF-T) and a PixeLink (PL-B782U usb2) CCD colour camera to capture particle behaviour. The experimental images are produced by time-averaging the intensities of 200 experimental video frames to visualise particle trajectories/trapping over the period of the experiment. Image intensity analysis was conducted on the captured images using MATLAB, yielding data on the spatial distribution of the particles. Prior to the analysis, all figures are converted to grey scale for consistency. Total of 5 lines (in x-direction) along which clear patterning of particles are observed are chosen across the channel length (y-direction). The image intensity is measured across each individual line, then averaged over 5 lines.

5. Size-dependant Behaviour of Particles

[View Article Online](#)

In the second set up, the experiments were conducted on the stage of an inverted microscope (Olympus IX51), where particle behaviour was captured using a high speed camera (MEMRECAM HX). Particle image velocimetry (PIV) was then utilized to obtain a more precise temporal and spatial observation of particles behaviour. The single exposed image pairs were analysed using multi-grid/multi-pass cross-correlation digital particle image velocimetry (MCCDPIV) implemented in the in-house developed parallel program 2C-2D-CCDPIV +PTV which uses MPI. The algorithm is described by Soria *et al.*⁵⁹ with its origin explained by Soria.^{60,61} It uses an iterative and adaptive cross-correlation algorithm to increase the velocity dynamic range and reduce the uncertainty, yielding 2-component – 2-dimensional (2C-2D) instantaneous velocity fields. The performance, accuracy, and uncertainty of the algorithm with applications to the analysis of a single exposed 2C-2D PIV and holographic 3C-3D PIV (HPIV) images have been reported by Soria⁶² and von Ellenrieder *et al.*⁶³ The 2C-2D MCCDPIV algorithm also incorporates a local cross-correlation function multiplication method⁶⁴ to improve the search for the location of the maximum value of the cross-correlation function. For the subpixel peak calculation, a two-dimensional Gaussian function model is used to find the location of the maximum of the cross-correlation function using the least mean square value.^{60,61}

Prior to PIV analysis, the raw image data were cropped to remove the unwanted peripheral region. The size of the interrogation window used for the MCCDPIV analysis was 32×32 pixels² with a spacing of 16 pixels between the velocity vectors. A local chi-squared χ^2 fit, utilizing 13 points to the velocity field, is used to filter the velocity field and remove noise.⁶¹ The velocity in physical units is determined by multiplying the velocity displacement by the imaging scale factor and dividing by the time separation between the two single-exposed images.

To better investigate the transition mechanisms, a simplified 2-dimensional fully coupled LN substrate and fluid domain is modelled using COMSOL Multiphysics v5.1. To generate the intended surface acoustic waves, a voltage potential is applied along equipotential lines mimicking the IDT design used experimentally. The LN crystal matrices were rotated to represent the crystal cut used in the experiments (*i.e.* 128° Y-cut X-propagating).

The fluid domain is modelled using two different approaches, probing the distinct transition regimes independently. Firstly, to probe the streaming to patterning transition characteristics, the fluid domain is fully coupled to the LN substrate, and solved using the thermoviscous set of equations (*i.e.* thermoacoustic module in COMSOL Multiphysics) to accurately obtain the pressure and velocity fluctuations. To obtain the streaming fields (*i.e.* v_2), the first order solutions were used to calculate the body force (*i.e.* Reynolds stress), which in turn is utilised to drive the fluid flow in a laminar flow stationary study. A similar approach is used in previous publications.^{14,54,65} The transition characteristics were probed by increasing the particle size and observing the re-

sultant particle trajectory. The acoustic force exerted on a particle considerably smaller than the wavelength is given by eqn (1a).^{14,65,66}

$$\mathbf{F}_{\text{ARF}} = -\pi a^3 \left[\frac{2\kappa_0}{3} \mathbb{R}[f_1^* P_1^* \nabla P_1] - \rho_0 \mathbb{R}[f_2^* v_1^* \cdot \nabla v_1] \right] \quad (1a)$$

The asterisk indicates complex conjugates and $\mathbb{R}[\cdot]$ the real part. P_1 and v_1 are the first order pressure and velocity field and factors f_1 and f_2 are given by,

$$f_1 = 1 - \frac{\kappa_p}{\kappa_0} \quad (1b)$$

and

$$f_2 = \frac{2(1-\gamma)(\rho_p - \rho_0)}{2\rho_p + \rho_0(1-3\gamma)} \quad (1c)$$

where,

$$\gamma = -\frac{3}{2} [1 + i(1 + \tilde{\delta}_v)] \tilde{\delta}_v \quad (1d)$$

$$\tilde{\delta}_v = \frac{\sqrt{2\eta}}{\sqrt{\omega\rho_0}} \quad (1e)$$

$\kappa_0 = 1/(\rho_0 c_0^2)$ and κ_p denote the compressibility of the liquid and particle respectively, ρ_0 and ρ_p represent density of liquid and particles respectively, ω is the angular frequency of excitation and η is the shear viscosity coefficient of the fluid.

$$F_{\text{drag}} = 6\pi\eta a(v_2 - v_p) \quad (2)$$

where v_2 and v_p are the streaming (steady state) velocity and particle velocity respectively.

Secondly, to investigate the second transition regime, in which the particles are no longer small in comparison to the wavelength, a different approach must be used. Here, a fully coupled fluid domain is modelled using the Pressure Acoustics module in COMSOL Multiphysics. The resultant acoustic forces must be calculated by integrating over the particle's surface due to the particle's size, the numerical complexity and requirements placed on element size means that only a 2-dimensional model can be constructed (hence, the particle is represented as a cylinder, rather than a sphere). The force equation is given by,^{26,46,67}

$$\mathbf{F}_{\text{ARF}} = \frac{1}{2} \rho_0 \int_{S_0} \left[\langle v_1^2 \rangle - \frac{1}{\rho_0^2 c_0^2} \langle P_1^2 \rangle \right] \mathbf{n} dS - \rho_0 \int_{S_0} \langle (\mathbf{n} \cdot \mathbf{v}_1) \mathbf{v}_1 \rangle dS \quad (3)$$

A study was carried out to investigate the relative difference between the resultant acoustic forces obtained when solving the Helmholtz set of equations (*i.e.* pressure acoustics

5. Size-dependant Behaviour of Particles

[View Article Online](#)

Paper

Lab on a Chip

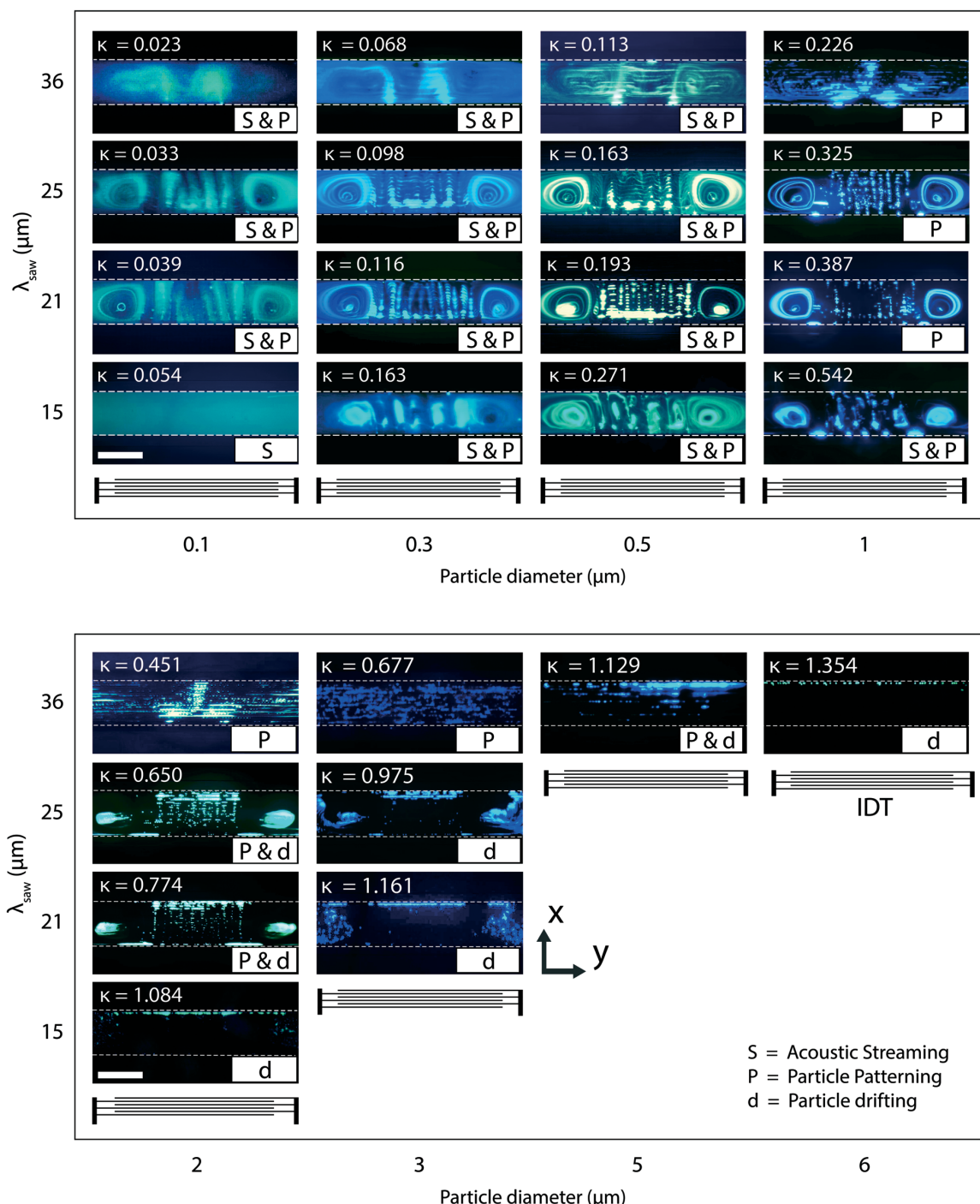


Fig. 2 Experimental observations representing the transition in particle behaviour influenced by the TSAW wavelength (frequency) as a function of particle diameter. The applied power is constant at 25 dBm. The microchannel is 26 μm -high and 200 μm -wide. The study focuses on particles behaviour in the central region, between the peripheral streaming vortices.⁵⁴ The (κ) value predict the cross-over from streaming dominated to radiation dominated behaviour as explained by Skowronek *et al.*⁵⁰ to calculate the (κ) value, the sound speeds of 3880 m s^{-1} in LN and 1500 m s^{-1} in water are used. The relative location of the IDT compared to the channel is indicated only in the y-direction. It should be noted that the distance between the IDT and the channel location (x-direction) is 1400 μm and is not reflected in the figure. Scale bar is 200 μm .

module) as opposed to the significantly more computationally expensive thermoviscous set of equations (thermoacoustic module). No significant difference in calculated forces were observed for the particle sizes considered. This is consistent with the findings detailed in Habibi *et al.*⁶⁷ Thus, the computationally more efficient pressure acoustic module was used in the data presented here.

4 Results and discussion

To determine the effect of TSAW frequency and particle diameter on the transition in the acoustophoretic behaviour, a series of experiments were conducted under stationary condition (no external flow) and the particles response were observed, as shown in Fig. 2 and ESI† Video 1 (the acoustofluidic effects in correspondence to an external flow can be observed in ESI† Video 2). Here, the experimental data is obtained for a range of particle diameters and four distinct TSAW wavelengths, whilst TSAW power intensity (25 dBm) and channel dimensions ($h = 26 \mu\text{m}$ and $W = 200 \mu\text{m}$) are held constant. It should be noted that this study only focuses on the transition in behaviour of particles at the regions between the “Peripheral streaming” and beyond the extent of the “Lobe streaming”⁵⁴ vortices. In the series of images shown in Fig. 2, the experimental results inform the mechanism at play by observation of key features in the image.

Areas of higher and lower intensity corresponding to local concentration and rarefaction of particles is a result of patterning, ARF being the dominant mechanism, as in Fig. 2 (denoted P). In images demonstrating a different effect, a line of particles are formed at the wall of the channel furthest from the IDT, this is a result of the particles having been pushed across the channel width due to the dominance of mono-directional motion as a result of ARF, we term this effect (most commonly associated with TSAW) drifting, (denoted d). There is a transitional region present, between distinct patterning and drifting (denoted P & d) characteristics, in which both of these features occur.

In contrast to ARF, the streaming dominated motion of particles causes them to be carried continuously through the fluid volume, thus images of such motion in Fig. 2 appear uniform in colour and somewhat blurred (denoted S). In some images, patterning is seen in the form of bands of high and low intensity superimposed on a uniform background, this is the, rather large, transition region in which both streaming and patterning occur (denoted S & P). Observations through the microscope, clearly depict a continuous motion, whilst resulting in a structure to the image, indicating simultaneous trapping of some particles.

Skowronek *et al.*⁵⁰ examined streaming and drifting in a TSAW system actuated with a different configuration than the conventional systems (coupling *via* pillars). They identified a dimensionless constant, (κ), to describe the transition between the two regimes, wherein the frequency and particle diameter play the key roles, $\kappa = ka$, where k and a denote wave number and particle radius, respectively. Several studies

have identified the critical value of κ beyond which radiation force dominates as ~ 1 in a sessile droplet leading to particle concentration,^{68–71} and ~ 1.2 in a microfluidic channel leading to drifting.^{39,50} As illustrated in Fig. 2, in this work drifting takes place even for the case of $\kappa = 0.97$, though at a relatively slower rate compared to the case of $\kappa = 1.35$. In Fig. 3, which summarises the observed behaviour in Fig. 2, the κ relationship has been plotted. It is observed to lie between the streaming and drifting regions identified in our data which was a conventionally actuated system. It is also evident, however, that a linear relationship between diameter and wavelength cannot be used to describe the transitions we observe.

The regimes of particle behaviour are clearly identified in Fig. 3, we now examine them further by way of numerical analysis, probing the key features and examining the transitions between the regimes. In doing this, we consider the forces which occur and dominate, starting with large particles before decreasing the size.

4.1 Transition from drifting to patterning

Examining the behaviour shown by Fig. 2 for a $25 \mu\text{m}$ wavelength, it can be seen that $3 \mu\text{m}$ particles drift, whilst $1 \mu\text{m}$ particles form patterns. This transition is shown in Fig. 4, in which the intensity is plotted as measured across the width of the channel at two excitation power levels. For both powers

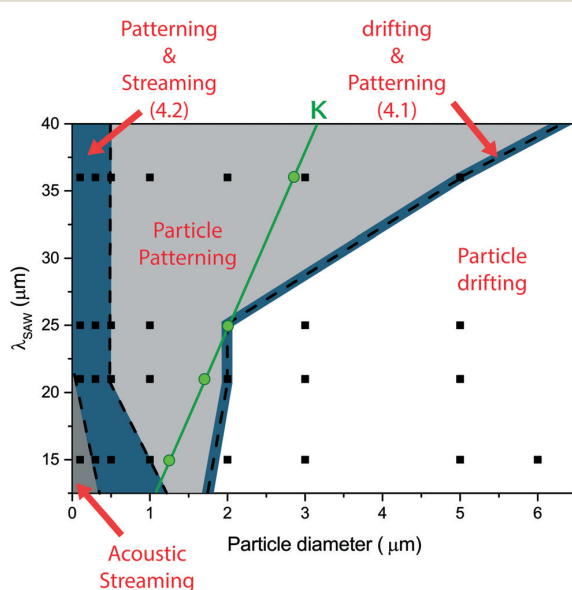


Fig. 3 The plot of transition behaviour where each region (indicated by different colour) shows the dominant mechanism governing particle behaviour. The black squares indicate the position of experiments illustrated in Fig. 2. Dotted lines are the predicted locations for the cross-over behaviour. The red circles represent the cross-over from streaming dominated to radiation dominated behaviour predicted based on κ value (the dimensionless constant) as explained by Skowronek *et al.*⁵⁰

5. Size-dependant Behaviour of Particles

[View Article Online](#)

Paper

Lab on a Chip

examined the highest intensity is clearly at the edge of the channel away from the IDT for $3\text{ }\mu\text{m}$ particles (Fig. 4c), whilst a patterned intensity is seen for the $1\text{ }\mu\text{m}$ particles (Fig. 4a). However, for the $2\text{ }\mu\text{m}$ particles, a clear transition in behaviour is observed with an increase in drifting as a result of increasing power (Fig. 4b). At 15 and 25 dBm (the powers used in Fig. 4a and c) both patterning and drifting traits are seen, thus, this size sits in the transition region between the two distinct outcomes.

To probe the underlying physics associated with this transition in behaviour, a numerical model is used, this consists of a microfluidic channel (width $100\text{ }\mu\text{m}$; height $26\text{ }\mu\text{m}$) excited by TSAW with a wavelength of $15\text{ }\mu\text{m}$ (propagating in the positive x -direction). It should be noted that the channels width is $200\text{ }\mu\text{m}$ in experiments and $100\text{ }\mu\text{m}$ in the numerical models. The diffraction effects in the near field (*i.e.* close to the wave source; IDTs) do not differ, as such the $100\text{ }\mu\text{m}$ channel is used in simulations to minimise computational expense. In Fig. 5a the resultant instantaneous absolute pressure field generated after initial excitation is shown. At this moment in time the TSAW can be seen to couple into the fluid at an angle (the Rayleigh angle, θ_R). As a result a region, in the upper left of the channel, which remains largely unaffected by the propagating wave is present, this has been termed the anechoic corner.^{51,52} However, this field is only transient in nature, the relative slowness of the particle motion compared to the speed of sound, means that they respond rather to the steady state sound field (albeit distorted locally by their own presence). In Fig. 5b the time-averaged

absolute pressure field generated by the TSAW when coupled into fluid contained in a $100\text{ }\mu\text{m}$ -wide PDMS channel is shown. Several features are present in this sound field, firstly, there is a decay in amplitude with increasing distance across the channel width (x -direction) as energy in the surface wave decays due to coupling of energy into the fluid (this is also seen in Fig. 5a). Secondly, in the z -direction, bands of higher and lower pressures (one such band of lower pressures has been labelled alpha-line) are present, this arises due to waves being reflected by the upper boundary of the fluid volume (despite this PDMS boundary being relatively low reflecting). This feature has the potential to trap particles in bands along the z -direction. Thirdly, there are bands of lower pressure at angles across the fluid chamber, one such band is labelled beta-line (Fig. 5b). These bands, or lobes, are caused due to the diffraction of the wave as it couples into the fluid and is due to the finite nature of the fluid volume.^{53,54}

Fig. 5c and d show the forces experienced by particles of different sizes placed in the sound field. The model integrates the forces around the circumference of the particles (eqn (3)) in a 2D plane. By placing the particle in the field the wave scattering is accurately captured, coupling this with calculation of the force by integration allows accurate assessment of forces for particles of sizes which approach the wavelength, albeit in 2D. The forces in the z -direction are shown for particles placed along beta-line in Fig. 5d. It can be seen that at low values of x (which also indicates low values of z), the large particles are pushed upwards, however, there are stable trapping locations at $x = 20$ and $23\text{ }\mu\text{m}$ (where the x

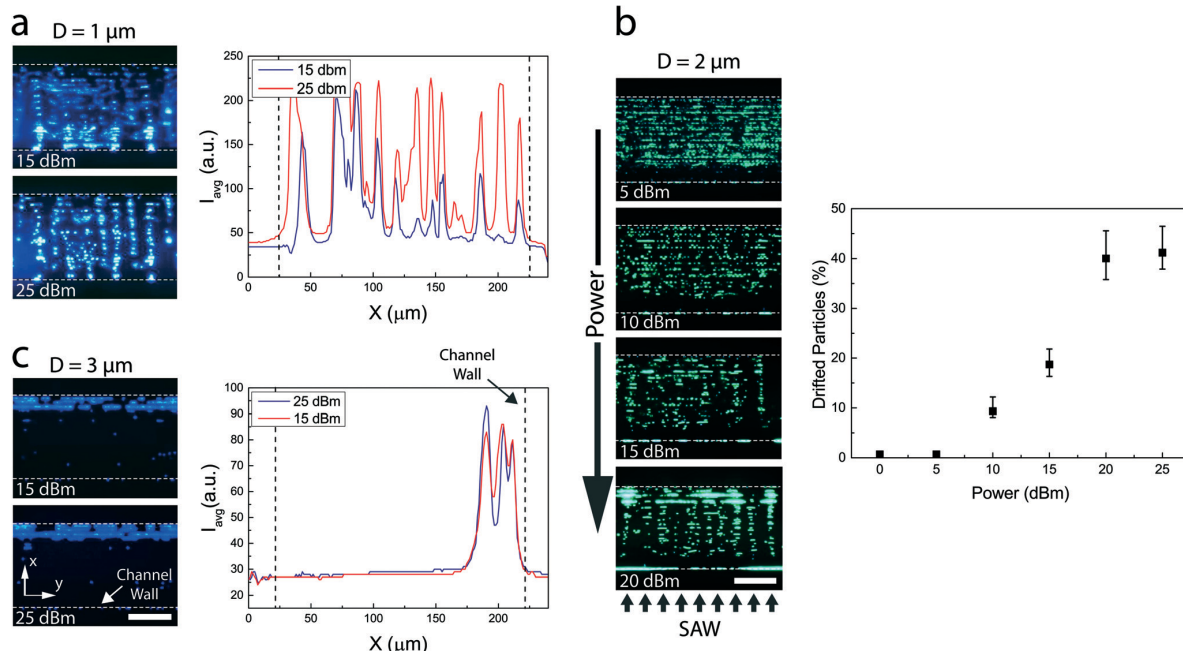


Fig. 4 Influence of applied TSAW power on transition in behaviour of $1\text{ }\mu\text{m}$, $2\text{ }\mu\text{m}$ and $3\text{ }\mu\text{m}$ particles, where at 155 MHz (a) $1\text{ }\mu\text{m}$ particles only experience patterning, (b) $2\text{ }\mu\text{m}$ particle behaviour changes from pure patterning to an intermediate state where mixture of patterning and drifting take place and (c) $3\text{ }\mu\text{m}$ particles only experience drifting. Scale bars are $100\text{ }\mu\text{m}$.

5. Size-dependant Behaviour of Particles

[View Article Online](#)

Lab on a Chip

Paper

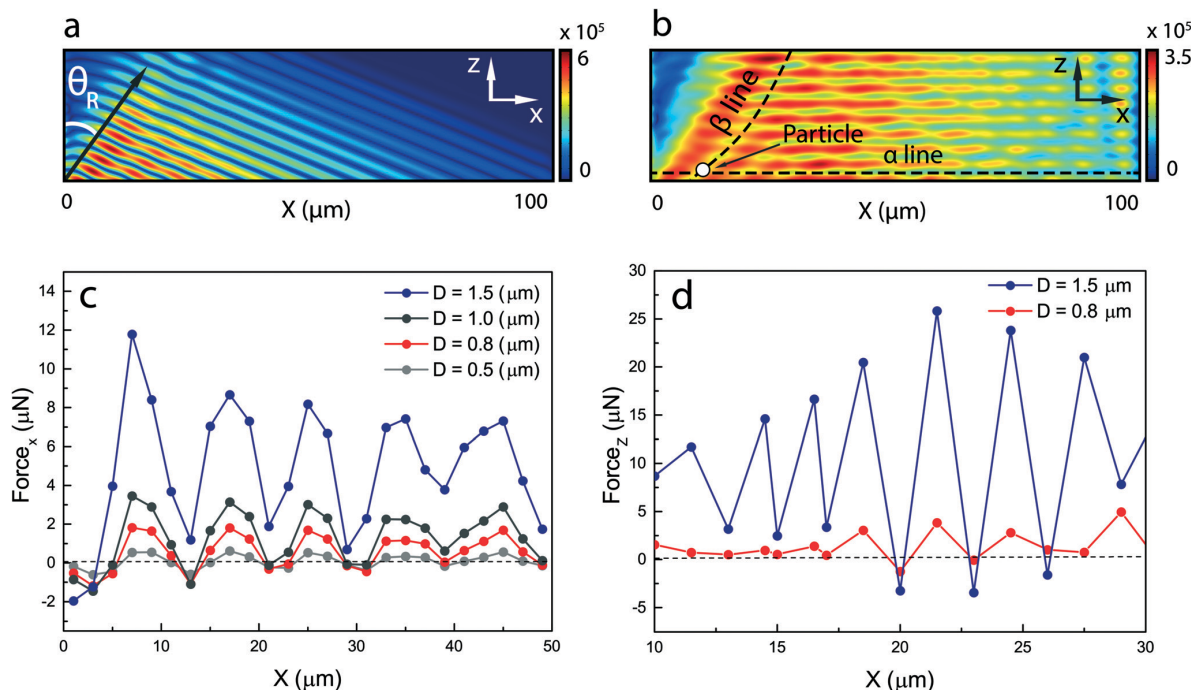


Fig. 5 (a) Instantaneous absolute pressure field once TSAW is coupled to the fluid along θ_R angle. (b) The FEA model of the time-averaged absolute pressure fields $\langle |P_1| \rangle$. Spatial radiation forces where (c) indicates the titx-component along the α line and (d) the z-component along the β line as represented by the dashed lines within (b). The unit of pressure surface plot is Pa. The forces affecting particles with different diameter (D) are compared.

component of the force is zero). This potential for trapping at different heights is also present for the smaller particles, albeit the trapping forces are weaker.

In Fig. 5c, the forces in the x -direction are shown along alpha-line. It can be seen that there are strong variations in force amplitude at different x -locations as expected from the pressure field. For the smaller particles the forces change in sign as x is increased, including stable trapping locations, and the particles can be expected to be held at multiple stable locations; patterning occurs. Whilst for the larger particles, the force varies in amplitude but is always positive, hence, the particles will move in a monodirectional manner; drifting occurs. The particle size at which this transition between behaviours cannot be directly compared to the experimental data due to the 2D nature of the simulation, however, the trends are consistent.

The nature of the force field indicates that, as a result of ARF, the particles will migrate away from the IDT source. In some cases (smaller particles), this migration in the positive x -direction is expected to occur until the next stable location (*i.e.* $F_{a_{ac},x} = 0$) is reached, whilst for larger particles the migration will continue to the far edge of the channel.

To confirm the unidirectional migration which occurs prior to patterns being formed, the particle trajectories have been measured using PIV as shown in Fig. 6. In contrast to usual flow visualisation methods, here the particles are migrating from an initial location to an end loca-

tion (as seen in the experimental images and ESI† Video 3), being driven by acoustic radiation forces rather than drag. As such, there are rapid changes in the particle motions on a spatial scale dictated by the spacing between the patterned lines. As the spatial pitch of the velocity arrows is rather large compared to this spacing, capturing a full idea of the trajectory of the particles is challenging. Instead, what we wish to draw attention to is the nature of the velocities shown. For the following parameters, 1 μm particles at 25 μm wavelength, contained within a 35 μm high and 200 μm wide channel, we observe particle patterning. The data shows that for the initial 6 s of particle migration, the velocity arrows have a component across the width of the channel in one direction as particles migrate to the stable patterning locations (Fig. 6b-d). Whilst later (Fig. 6f-h), the velocities are predominately along the channel length, and represent migration along the patterned lines. Whilst the patterning behaviour appears visually to have similarities to that of a SAW system, in that it is periodic (albeit with different spacing⁵³) and stable, the migration pattern which causes the patterning is dissimilar. In a standing wave system, homogeneously suspended particles are free to move in either direction to reach the nearest pressure minima location, whereas, the initial translation of particles in a TSAW system takes place unidirectionally along beta-lines (in Fig. 5b) and the other pressure minima between the pressure lobes.

5. Size-dependant Behaviour of Particles

[View Article Online](#)

Paper

Lab on a Chip

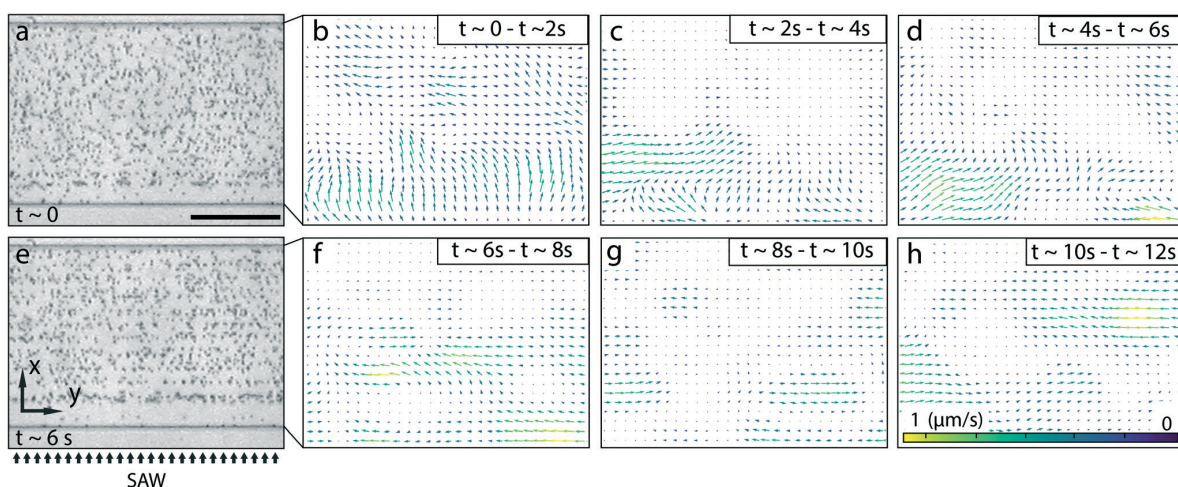


Fig. 6 Transient study of particle trajectories from initially quiescent at the instant of TSAW application towards steady state. Particle image velocimetry (PIV) method is used, where the arrows indicate the direction of particles displacement. The arrow's length is proportional to the relative magnitude of the particle's velocity (the actual magnitude of velocity ($\mu\text{m s}^{-1}$) is represented by the arrow's colour). (a) Homogeneously suspended $1\ \mu\text{m}$ particles in a quiescent fluid (contained in a $35\ \mu\text{m}$ -high $200\ \mu\text{m}$ -wide channel) at the initial state. (b)-(d) Migrate in the direction of TSAW to arrive to the pressure minima lobes within which they are trapped. (e) Particles form spatial periodic patterns after 6 s of TSAW application. After this state (f)-(h) further migration of particles in the x -direction is prohibited by forces resulted from diffraction lobes, however particles are free to move in the y -direction. Scale bar is $100\ \mu\text{m}$.

4.2 Transition from patterning to streaming

As shown in Fig. 3, at a $25\ \mu\text{m}$ SAW wavelength, the $0.1\ \mu\text{m}$ particles are strongly influenced by streaming despite some structure present due to patterning. However, as the particle size increases to $0.3\ \mu\text{m}$ and $0.5\ \mu\text{m}$ the prevalence of this structure increases; though streaming is still observed, patterning becomes increasingly significant. This blended streaming and patterning regime occurs over a range of particle sizes examined and hence has been denoted as a separate regime in Fig. 3. We note, that the transition between streaming and patterning in a SAW system is also observed to be broad due to spatial variations in which effect was dominant.⁶⁵

To confirm the presence of patterning and streaming, in Fig. 7 we show the light intensity distribution as measured across the width of the channel. This data is presented for two channel heights and powers. It is observed, that the $100\ \text{nm}$ particles in the deeper channel (comparable to Fig. 2) show a large baseline intensity with a weak periodic fluctuation, indicating behaviour dominated by streaming with relatively weak patterning occurring.

We now examine and seek to explain trends in this data. Two trends, in the relative size of the baseline level and periodic peaks, are evident. The first is that as the particle size increases, the periodicity increases and the baseline level decreases. This is due to the patterning forces of small particles being related to the particle size cubed, whilst the drag forces are related to the size linearly. The second trend is that the baseline is higher for the channels of larger height, especially for the 100 and $300\ \text{nm}$ particles. This means that there is an increase in streaming effects for the deeper channels. This is

consistent with an expectation that a larger separation between the non-slip boundary condition on the base and roof of the channel allows larger streaming velocities.⁶⁵

A third trend is that, especially for the deeper channels, there is a large feature at the edge of the channel nearest to the IDT. This is observed in Fig. 7d and f, but less clearly observed in the shallower channel (Fig. 7c and e). This particle response is a result of the nature of the streaming flow field in the (x - z) plane, which is shown in Fig. 1. There are two main flows, a strong swirl which is (largely) contained within the anechoic corner, and that a secondary swirl occurs which stretches across the rest of the channel. It is the swirl within the anechoic corner which causes this feature. It is more prominent for the larger channel heights as anechoic corner is bound by a line at the Rayleigh angle, hence a larger height channel will correspond to this swirl stretching further across the channel width.

A fourth observation from this dataset is that the number of lines of particles formed due to the patterning is larger for the shallow channels. We know that a reduction of the channel height; firstly, minimises the effects of streaming enabling more patterning of particles, and secondly, reduces the number of stable locations, along the z -direction, present for patterning. We believe, the spacing between lines of collected particles is more easily distinguishable in shallower channels (Fig. 7a, c and e). Whereas in deeper channels, particles appear to form clusters as there are multiple patterning locations (along the z -direction) possible. This is a direct result of the existence of periodicity, along the z -direction, in the lobed pressure fields which permits patterning of particles at distinct heights (Fig. 7b, d and f).

5. Size-dependant Behaviour of Particles

[View Article Online](#)

Lab on a Chip

Paper

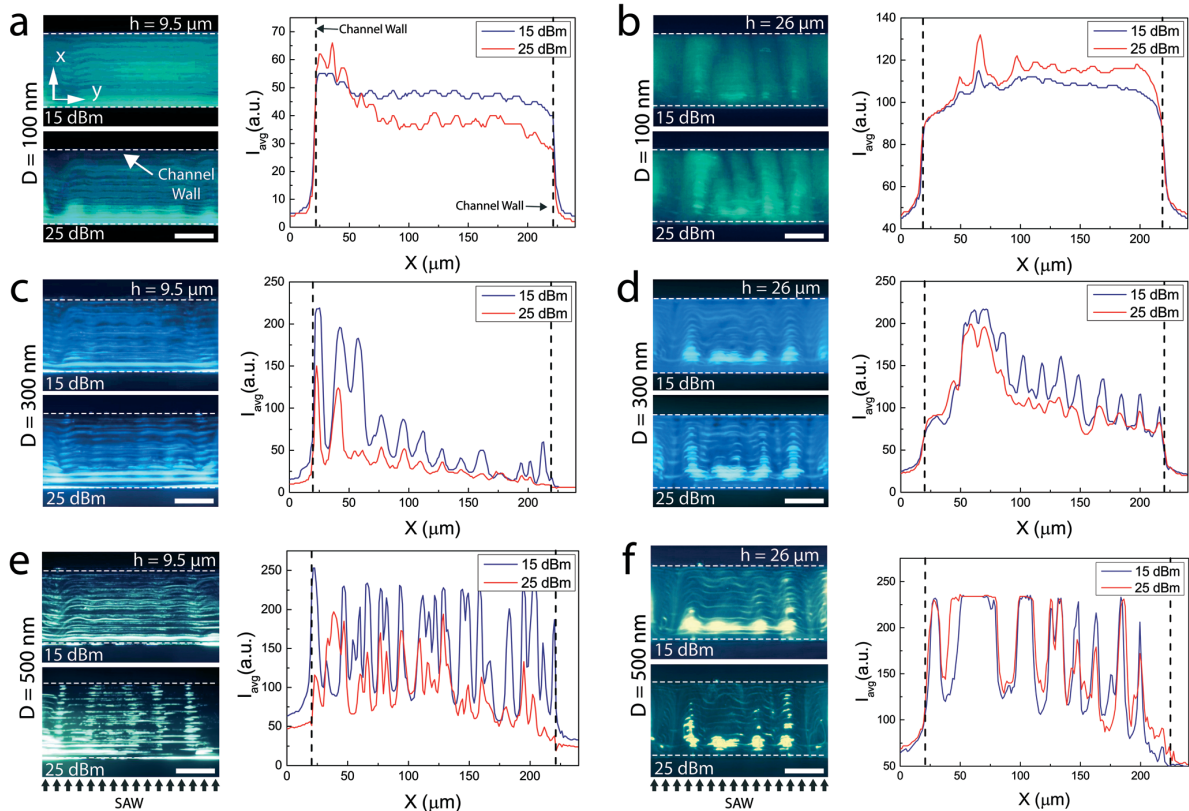


Fig. 7 Experimental observations of two simultaneous particle behaviour; patterning and swirling for submicron particles with diameters of 100, 300 and 500 nm. The frequency of operation is 155 MHz ($\lambda_{SAW} = 25 \mu\text{m}$). The channel width is 200 μm . The effect of TSWA power intensity and channel height are recognized by using plots of image mean intensity against x positions across channel width. The diffraction effects result in particle patterning across width of the channel. The absorption of this effect within the system increases with reducing channel height and increasing applied power. Scale bars are 100 μm .

Finally, we examine the cause of the broad transition region which occurs between streaming and patterning dominated behaviour (seen in Fig. 3). As discussed and shown in Fig. 5c, smaller particles are subjected to smaller upward forces, yet can be trapped at different heights. Particles trapped at different heights will experience different drag forces from the streaming flow; hence, there will be a local variation in the critical diameter, which globally will be seen as a broad transition region. This is explored further in the numerical models.

Whilst the force fields shown in Fig. 5 assist with understanding the transition from patterning to drifting, and they indicate that particles are held at different heights, which assists with understanding the broad transition seen between streaming dominated and patterning dominated behaviour, they do not directly consider the streaming flows. In Fig. 1c, a numerical model has been used to predict the streaming field and thus, the drag forces experienced by particles suspended within it. These drag forces are added to the acoustic radiation force arising from the force field (calculated using eqn (1a), and assuming the particle size is signifi-

cantly smaller than the wavelength). The resultant particle trajectories are shown in Fig. 8 (see ESI† Video 4; 0.2 μm and 0.5 μm particles) the smaller particles swirl around the channel and the larger particles begin to exhibit patterning behaviour, as observed from the intensity data. In addition, it is observed that for the larger particles, some will be patterned at certain heights in the fluid, but those closer to the top and bottom of the channel will be exposed to stronger fluid flows and as such are entrained within them.

4.3 Effect of power on transition

In Fig. 4, distinct regions of behaviour have been identified for a wavelength of 25 μm , over a range of particle sizes and powers. This is examined further in Fig. 7, in which the degree of patterning and streaming is observed to differ with respect to the power used. The features used to distinguish between regions are the same as those used in Fig. 2. The power applied to the IDT is linearly related to the amplitude of the ARF and strength of the acoustic streaming. Consequently, the two forcing mechanisms discussed, so far,

5. Size-dependant Behaviour of Particles

[View Article Online](#)

Paper

Lab on a Chip

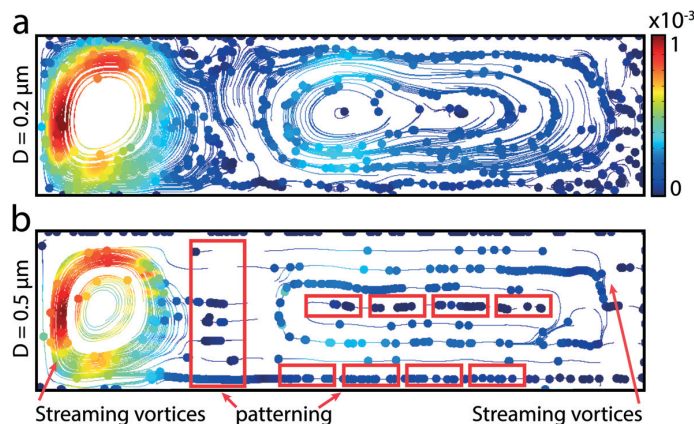


Fig. 8 Particle trajectories driven by TSAW with a wavelength of 15 μm in a 26 μm high, 100 μm wide channel of (a) 0.2 μm particles, where two main streaming vortices are observed; one within the anechoic corner and the other that stretches across the rest of channel width and of (b) 0.5 μm particles exhibiting streaming-dominated and patterning behaviour (see ESI† Video 4; 0.2 μm and 0.5 μm particles).

should increase linearly as a result of power increase. The behaviour of the particles is dictated by the relative dominance of the forcing mechanisms, and an equal increase in both, will not alter this dominance. However, an increase in the velocity of the suspended particles will be observed. As such, the transition between regions, observed with increasing power in Fig. 4, is unexpected.

For a given power and wavelength, as the particle size is increased, the regimes move from streaming dominated, to streaming and patterning, patterning, patterning and drifting

and drifting. Considering this, and in reference to Fig. 9, an increase in power can shift the particles behaviour from that expected at lower powers to that expected for slightly larger particles. That is, upon increase from 10 dBm to 20 dBm, 0.5 μm particles behaviour shifts from streaming to streaming and patterning. As such, we believe this results from particle-particle interactions. That as the power increases the coagulation of particles as a result of Bjerknes forces,^{67,72} from the interaction of scattered waves from one particle on a neighbouring particle, causes particles to cluster and as such assume the behaviour of relatively larger particles.

5 Conclusion

Travelling surface acoustic waves have found applications in particle sorting and droplet manipulation, however, it is only recently that a wider range of forcing mechanisms has been identified, with the additional understanding regarding the occurrence of particle patterning. This work has delved into better understanding the effect of particle size on particle behaviour as a function of both acoustic wavelength and power. Three main regimes along with transitional regions have been identified representing the dominance of different forcing mechanisms: namely, streaming, patterning and drifting. To probe the underlying physics associated with these distinct particle migration behaviours and its transitional characteristics, numerical models of the acoustic radiation force and streaming flows are implemented. It is important to note that an increase in power can alter the behaviour of smaller particles to that of a larger particle size, most likely due to the coagulation of particles at these higher powers.

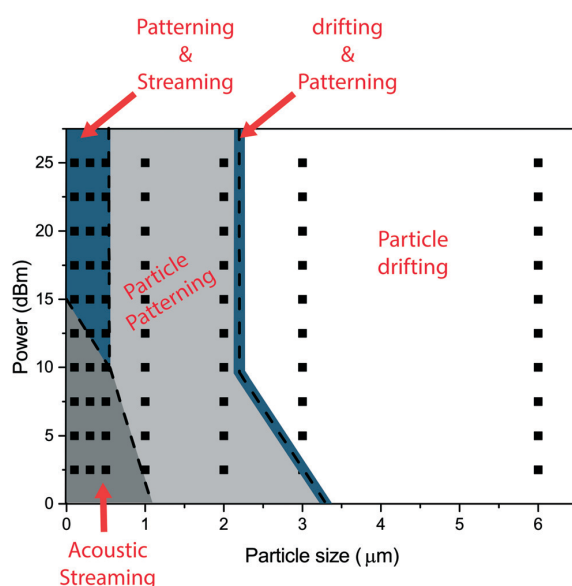


Fig. 9 The plot representing transition in behaviour of particles affected by TSAW power intensity as a function of particle diameter. Regions within the plot that are dominated by various behaviours are distinctively indicated with different colours. The black squares represent the position of experiments conducted. The border lines of each region are shown in dashed.

Conflicts of interest

There are no conflicts to declare.

5. Size-dependant Behaviour of Particles

[View Article Online](#)

Lab on a Chip

Paper

Acknowledgements

We gratefully acknowledge support received from the Australian Research Council, Grant No. DP160101263. This work was performed in part at the Melbourne Centre for Nanofabrication (MCN) in the Victorian Node of the Australian National Fabrication Facility (ANFF). This research was undertaken with the assistance of resources from the National Computational Infrastructure (NCI), which is supported by the Australian Government. Special thanks to Mr Mohammad ali Forouzandeh and A/Prof. Nemai Chandra Karmakar from Monash Antenna and RFID Lab for their contribution.

References

- 1 M. E. Warkiani, G. Guan, K. B. Luan, W. C. Lee, A. A. S. Bhagat, P. K. Chaudhuri, D. S.-W. Tan, W. T. Lim, S. C. Lee and P. C. Chen, *Lab Chip*, 2014, **14**, 128–137.
- 2 J. Zhang, S. Yan, D. Yuan, G. Alici, N.-T. Nguyen, M. E. Warkiani and W. Li, *Lab Chip*, 2016, **16**, 10–34.
- 3 Y. Zhou, Z. Ma and Y. Ai, *Microsyst. Nanoeng.*, 2018, **4**, 5.
- 4 I. De Vlaminek and C. Dekker, *Annu. Rev. Biophys.*, 2012, **41**, 453–472.
- 5 F. Martinez-Pedrero and P. Tierno, *Phys. Rev. Appl.*, 2015, **3**, 051003.
- 6 P. R. Gascoyne and J. Vykovkal, *Electrophoresis*, 2002, **23**, 1973.
- 7 W. Liu, J. Zhang, L. Wan, K. Jiang, B. Tao, H. Li, W. Gong and X. Tang, *Sens. Actuators, B*, 2008, **133**, 664–670.
- 8 J. R. Moffitt, Y. R. Chemla, S. B. Smith and C. Bustamante, *Annu. Rev. Biochem.*, 2008, **77**, 205–228.
- 9 J. van Mameren, G. J. Wuite and I. Heller, in *Introduction to Optical Tweezers: Background, System Designs, and Commercial Solutions*, Springer, 2018, pp. 3–23.
- 10 X. Ding, S.-C. S. Lin, B. Kiraly, H. Yue, S. Li, I.-K. Chiang, J. Shi, S. J. Benkovic and T. J. Huang, *Proc. Natl. Acad. Sci. U. S. A.*, 2012, **109**, 11105–11109.
- 11 T. Gupta, R. Ghosh and R. Ganguly, *Int. J. Numer Method Biomed. Eng.*, 2018, **34**, e2943.
- 12 M. Wiklund, *Lab Chip*, 2012, **12**, 2018–2028.
- 13 H. Bruus, *Lab Chip*, 2012, **12**, 1014–1021.
- 14 P. B. Muller, R. Barnkob, M. J. H. Jensen and H. Bruus, *Lab Chip*, 2012, **12**, 4617–4627.
- 15 H. Bruus, *J. Fluid Mech.*, 2017, **826**, 1–4.
- 16 A. Haake, A. Neild, G. Radziwill and J. Dual, *Biotechnol. Bioeng.*, 2005, **92**, 8–14.
- 17 M. Hill, Y. Shen and J. J. Hawkes, *Ultrasonics*, 2002, **40**, 385–392.
- 18 M. Hill and R. J. Wood, *Ultrasonics*, 2000, **38**, 662–665.
- 19 A. Neild, S. Oberti, F. Beyeler, J. Dual and B. J. Nelson, *J. Micromech. Microeng.*, 2006, **16**, 1562–1570.
- 20 A. Neild, S. Oberti and J. Dual, *Sens. Actuators, B*, 2007, **121**, 452–461.
- 21 A. Neild, S. Oberti, A. Haake and J. Dual, *Ultrasonics*, 2006, **44**, e455–e460.
- 22 X. Ding, P. Li, S.-C. S. Lin, Z. S. Stratton, N. Nama, F. Guo, D. Slotcavage, X. Mao, J. Shi and F. Costanzo, *Lab Chip*, 2013, **13**, 3626–3649.
- 23 S.-C. S. Lin, X. Mao and T. J. Huang, *Lab Chip*, 2012, **12**, 2766–2770.
- 24 L. Y. Yeo and J. R. Friend, *Biomicrofluidics*, 2009, **3**, 012002.
- 25 L. Y. Yeo and J. R. Friend, *Annu. Rev. Fluid Mech.*, 2014, **46**, 379–406.
- 26 J. Dual, P. Hahn, I. Leibacher, D. Möller, T. Schwarz and J. Wang, *Lab Chip*, 2012, **12**, 4010–4021.
- 27 J. Lei, P. Glynn-Jones and M. Hill, *Lab Chip*, 2013, **13**, 2133–2143.
- 28 W. Connacher, N. Zhang, A. Huang, J. Mei, S. Zhang, T. Gopesh and J. Friend, *Lab Chip*, 2018, 1952–1996.
- 29 D. J. Collins, T. Alan, K. Helmerson and A. Neild, *Lab Chip*, 2013, **13**, 3225–3231.
- 30 J. C. Brenker, D. J. Collins, H. Van Phan, T. Alan and A. Neild, *Lab Chip*, 2016, **16**, 1675–1683.
- 31 M. Sesen, T. Alan and A. Neild, *Lab Chip*, 2014, **14**, 3325–3333.
- 32 L. Schmid and T. Franke, *Appl. Phys. Lett.*, 2014, **104**, 133501.
- 33 M. Sesen, T. Alan and A. Neild, *Lab Chip*, 2015, **15**, 3030–3038.
- 34 D. Ashtiani, H. Venugopal, M. Belousoff, B. Spicer, J. Mak, A. Neild and A. de Marco, *J. Struct. Biol.*, 2018, 94–101.
- 35 A. Qi, L. Y. Yeo and J. R. Friend, *Phys. Fluids*, 2008, **20**, 074103.
- 36 D. J. Collins, T. Alan and A. Neild, *Lab Chip*, 2014, **14**, 1595–1603.
- 37 A. Fakhfouri, C. Devendran, D. J. Collins, Y. Ai and A. Neild, *Lab Chip*, 2016, **16**, 3515–3523.
- 38 D. J. Collins, B. Morahan, J. Garcia-Bustos, C. Doerig, M. Plebanski and A. Neild, *Nat. Commun.*, 2015, **6**, 8686.
- 39 G. Destgeer, B. H. Ha, J. Park, J. H. Jung, A. Alazzam and H. J. Sung, *Phys. Procedia*, 2015, **70**, 34–37.
- 40 X. Ding, J. Shi, S. C. Lin, S. Yazdi, B. Kiraly and T. J. Huang, *Lab Chip*, 2012, **12**, 2491–2497.
- 41 J. Nam, Y. Lee and S. Shin, *Microfluid. Nanofluid.*, 2011, **11**, 317–326.
- 42 J. Shi, X. Mao, D. Ahmed, A. Colletti and T. J. Huang, *Lab Chip*, 2008, **8**, 221–223.
- 43 C. Grenvall, P. Augustsson, J. R. Folkenberg and T. Laurell, *Anal. Chem.*, 2009, **81**, 6195–6200.
- 44 J. W. Ng, C. Devendran and A. Neild, *Lab Chip*, 2017, **17**, 3489–3497.
- 45 D. J. Collins, C. Devendran, Z. Ma, J. W. Ng, A. Neild and Y. Ai, *Sci. Adv.*, 2016, **2**, e1600089.
- 46 C. Devendran, N. R. Gunasekara, D. J. Collins and A. Neild, *RSC Adv.*, 2016, **6**, 5856–5864.
- 47 F. Guo, P. Li, J. B. French, Z. Mao, H. Zhao, S. Li, N. Nama, J. R. Fick, S. J. Benkovic and T. J. Huang, *Proc. Natl. Acad. Sci. U. S. A.*, 2015, **112**, 43–48.
- 48 Y. Chen, S. Li, Y. Gu, P. Li, X. Ding, L. Wang, J. P. McCoy, S. J. Levine and T. J. Huang, *Lab Chip*, 2014, **14**, 924–930.
- 49 G. Destgeer, B. H. Ha, J. H. Jung and H. J. Sung, *Lab Chip*, 2014, **14**, 4665–4672.

5. Size-dependant Behaviour of Particles

[View Article Online](#)

Paper

Lab on a Chip

- 50 V. Skowronek, R. W. Rambach, L. Schmid, K. Haase and T. Franke, *Anal. Chem.*, 2013, **85**, 9955–9959.
- 51 G. Destgeer, A. Alam, H. Ahmed, J. Park, J. H. Jung, K. Park and H. J. Sung, *Appl. Phys. Lett.*, 2018, **112**, 083501.
- 52 G. Destgeer, B. H. Ha, J. Park, J. H. Jung, A. Alazzam and H. J. Sung, *Anal. Chem.*, 2015, **87**, 4627–4632.
- 53 C. Devendran, D. J. Collins, Y. Ai and A. Neild, *Phys. Rev. Lett.*, 2017, **118**, 154501.
- 54 A. Fakhfouri, C. Devendran, T. Albrecht, D. J. Collins, A. Winkler, H. Schmidt and A. Neild, *Lab Chip*, 2018, **18**, 2214–2224.
- 55 W. L. M. Nyborg, in *Acoustic streaming*, Elsevier, 1965, vol. 2, pp. 265–331.
- 56 L. Gor'Kov, *Phys.-Dokl.*, 1962, 773–775.
- 57 L. V. King, *et al.*, *Proc. R. Soc. London, Ser. A*, 1934, **147**, 212–240.
- 58 R. Barnkob, N. Nama, L. Ren, T. J. Huang, F. Costanzo and C. J. Kähler, *Phys. Rev. Appl.*, 2018, **9**, 014027.
- 59 J. Soria, J. Cater and J. Kostas, *Opt. Laser Technol.*, 1999, **31**, 3–12.
- 60 J. Soria, *International Colloquium on Jets, Wakes and Shear Layers*, 1994, pp. 25.1–25.8.
- 61 J. Soria, *Exp. Therm. Fluid Sci.*, 1996, **12**, 221–233.
- 62 J. Soria, *13th Australasian Fluid Mechanics Conference*, 1998, pp. 381–384.
- 63 K. von Ellenrieder, J. Kostas and J. Soria, *Journal of Turbulence*, 2001, **2**, 1–15.
- 64 D. P. Hart, *Exp. Fluids*, 2000, **29**, 13–22.
- 65 C. Devendran, T. Albrecht, J. Brenker, T. Alan and A. Neild, *Lab Chip*, 2016, **16**, 3756–3766.
- 66 M. Settnes and H. Bruus, *Phys. Rev. E: Stat., Nonlinear, Soft Matter Phys.*, 2012, **85**, 016327.
- 67 R. Habibi, C. Devendran and A. Neild, *Lab Chip*, 2017, **17**, 3279–3290.
- 68 I. De Vlaminck and C. Dekker, *Annu. Rev. Biophys.*, 2012, **41**, 453–472.
- 69 G. Destgeer, H. Cho, B. H. Ha, J. H. Jung, J. Park and H. J. Sung, *Lab Chip*, 2016, **16**, 660–667.
- 70 G. Destgeer, B. Ha, J. Park and H. J. Sung, *Anal. Chem.*, 2016, **88**, 3976–3981.
- 71 G. Destgeer, J. H. Jung, J. Park, H. Ahmed and H. J. Sung, *Anal. Chem.*, 2016, **89**, 736–744.
- 72 S. Sepehrirahnama, K.-M. Lim and F. S. Chau, *J. Acoust. Soc. Am.*, 2015, **137**, 2614–2622.

The final chapter summarizes the key findings and contributions made by the research in this thesis. Following this a discussion on possible future work is presented.

6

Conclusions & Future Work

6.1 Conclusions

With an increasing interest in the SAW-driven microfluidics, the need for proper exploration of the physical phenomena underlying these systems increases. SAW actuation allows for certain key capabilities that are not accessible to BAW actuated systems. These include the ability to operate (i) at very high frequencies and (ii) in the travelling wave excitation mode. That being the case, these are fertile grounds to find new effects and new potential, what has been studied for longer with BAW. By challenging the common assumptions typically made in the present literature, through experimental characterisation and numerical modelling, here we seek a more in-depth understanding of the SAW key capabilities and their influential factors. The following sections provide a summary of the contributions of this thesis.

Chapter 3 reports on the development of a highly sensitive particle sorting system which has been termed the virtual membrane. As opposed to typical SAW-driven devices, this system operates at an elevated frequency enabling the development of an acoustic field with a wavelength on the order of the particle dimension. By identifying a critical diameter, 0.3 times the acoustic half-wavelength, the system filters particles of distinct sizes based on two phenomena: firstly, particles larger than the critical size experience a repulsive force inhibiting their entrance to the acoustic field, thus filtered. Particles smaller than the critical diameter are able to pass through the force field along the pressure minima nodes (akin to

6. Conclusions & Future Work

a filter's pores). The system benefit from a highly localized standing SAW field by using a pair of focused interdigitated transducers (IDT) at an angle relative to the fluid.

Chapter 4 investigates various mechanisms arising from transmission of a travelling SAW to an enclosed quiescent fluid. As opposed to the literature, here we emphasise on the influence of complex diffractive patterns in the outcome behaviour of particles. A scenario causing trapping of particles into spatially periodic locations, orthogonal and parallel to the propagation direction was reported, whereas the periodic nature of this trapping is often observed in standing SAW systems.

In **Chapter 5**, the particle patterning phenomena in TSAW systems was further explored. Here, the behaviour of particles in these systems was numerically and experimentally characterised based on the particle size as a function of frequency and power. Contrary to the literature that reports on two distinct behaviours, here we have identified three, namely, drifting, patterning and swirling. The transition between these regions and the influential factors were presented.

6.2 Future Work

The research into the physical phenomena underlying SAW actuated devices presented in this thesis provides many opportunities for further investigation. A few potential avenues for further research along with their possible applications are provided in this section.

In chapter 4, it is demonstrated that particles suspended in an acoustic field are subjected to acoustic radiation forces (ARF) and acoustic streaming induced drag forces and is shown that their dominance depends on the spatial location in the channel. Furthermore, the size-dependent nature of these two forces has been investigated in chapter 5 showing that reduction of the particle dimensions increases the dominance of acoustic streaming forces which can be disruptive to the manipulation of submicron/nano particles based on ARF. However, theoretical and numerical literature report that acoustic field is established much faster than the acoustic streaming field. [243] By realising this, several approaches based on either suppression or enhancement of acoustic streaming can be developed to meet the

6. Conclusions & Future Work

rapidly increasing demand for manipulation of nanoparticles. These approaches, however, require a more detailed characterisation of the acoustic streaming field.

In a possible future work, a thorough study of acoustic streaming, particularly the transient nature of the streaming field is made possible using particle image velocimetry (PIV) analysis. As explained in chapter 4, the acoustic streaming that arises by the incidence of a finite SAW in a quiescent fluid results in the formation of fluid swirling in two orthogonal planes. These include lateral vortices at the periphery (here termed peripheral streaming) and vertical vortices within the extent of the SAW beam (here termed lobe streaming). Understanding the transient nature of streaming requires a thorough analysis of the temporal build-up of the streaming field from an initially quiescent state towards a steady state. The amplitude analysis of the streaming field is made possible by using a 2-dimensional PIV for the peripheral streaming [244] and a 3-dimensional holographic PIV for the lobe streaming. [245]

Bibliography

- [1] Armaghan Fakhfouri, Citsabehsan Devendran, Asif Ahmed, Julio Soria, and Adrian Neild. The size dependant behaviour of particles driven by a travelling surface acoustic wave (tsaw). *Lab Chip*, 18:3926–3938, 2018.
- [2] Nam-Trung Nguyen, Steven T Wereley, and Steven T Wereley. *Fundamentals and applications of microfluidics*. Artech House, 2002.
- [3] Howard A Stone, Abraham D Stroock, and Armand Ajdari. Engineering flows in small devices: microfluidics toward a lab-on-a-chip. *Annu. Rev. Fluid Mech.*, 36:381–411, 2004.
- [4] Todd M Squires and Stephen R Quake. Microfluidics: Fluid physics at the nanoliter scale. *Reviews of Modern Physics*, 77(3):977, 2005.
- [5] Javier Atencia and David J Beebe. Controlled microfluidic interfaces. *Nature*, 437(7059):648, 2004.
- [6] George M Whitesides. The origins and the future of microfluidics. *Nature*, 442(7101):368, 2006.
- [7] J Heikenfeld, K Zhou, E Kreit, B Raj, S Yang, B Sun, A Milarcik, L Clapp, and R Schwartz. Electrofluidic displays using young–laplace transposition of brilliant pigment dispersions. *Nature Photonics*, 3(5):292, 2009.
- [8] Carl D Meinhart and Hongsheng Zhang. The flow structure inside a microfabricated inkjet printhead. *Journal of Microelectromechanical Systems*, 9(1):67–75, 2000.
- [9] Charles Q Choi. “memjet” momentum. *Scientific American*, 296(6):24–26, 2007.
- [10] Joseph Wang. Microchip devices for detecting terrorist weapons. *Analytica Chimica Acta*, 507(1):3–10, 2004.
- [11] Chee Meng Benjamin Ho, Sum Huan Ng, King Ho Holden Li, and Yong-Jin Yoon. 3d printed microfluidics for biological applications. *Lab Chip*, 15(18):3627–3637, 2015.
- [12] Ali Khademhosseini, Robert Langer, Jeffrey Borenstein, and Joseph P Vacanti. Microscale technologies for tissue engineering and biology. *Proceedings of the National Academy of Sciences*, 103(8):2480–2487, 2006.
- [13] Daniel Figeys and Devanand Pinto. Lab-on-a-chip: a revolution in biological and medical sciences. *ACS Publications*, 2000.
- [14] Curtis D Chin, Vincent Linder, and Samuel K Sia. Lab-on-a-chip devices for global health: Past studies and future opportunities. *Lab Chip*, 7(1):41–57, 2007.
- [15] Iwijn De Vlaminck and Cees Dekker. Recent advances in magnetic tweezers. *Annual Review of Biophysics*, 41:453–472, 2012.
- [16] Fernando Martinez-Pedrero and Pietro Tierno. Magnetic propulsion of self-assembled colloidal carpets: efficient cargo transport via a conveyor-belt effect. *Physical Review Applied*, 3(5):051003, 2015.
- [17] Peter RC Gascoyne and Jody Vykhoukal. Particle separation by dielectrophoresis. *Electrophoresis*, 23(13):1973–1983, 2002.

Bibliography

- [18] WJ Liu, J Zhang, LJ Wan, KW Jiang, BR Tao, HL Li, WL Gong, and XD Tang. Dielectrophoretic manipulation of nano-materials and its application to micro/nano-sensors. *Sensors and Actuators B: Chemical*, 133(2):664–670, 2008.
- [19] Joost van Mameren, Gijs JL Wuite, and Iddo Heller. Introduction to optical tweezers: background, system designs, and commercial solutions. In *Single Molecule Analysis*, pages 1–20. Springer, 2011.
- [20] Jeffrey R Moffitt, Yann R Chemla, Steven B Smith, and Carlos Bustamante. Recent advances in optical tweezers. *Annu. Rev. Biochem.*, 77:205–228, 2008.
- [21] Albrecht Haake, Adrian Neild, Gerald Radziwill, and Jurg Dual. Positioning, displacement, and localization of cells using ultrasonic forces. *Biotechnology and Bioengineering*, 92(1):8–14, 2005.
- [22] Xiaoyun Ding, Peng Li, Sz-Chin Steven Lin, Zackary S Stratton, Nitesh Nama, Feng Guo, Daniel Slotcavage, Xiaole Mao, Jinjie Shi, Francesco Costanzo, et al. Surface acoustic wave microfluidics. *Lab Chip*, 13(18):3626–3649, 2013.
- [23] Xiaoyun Ding, Sz-Chin Steven Lin, Brian Kiraly, Hongjun Yue, Sixing Li, I-Kao Chiang, Jinjie Shi, Stephen J Benkovic, and Tony Jun Huang. On-chip manipulation of single microparticles, cells, and organisms using surface acoustic waves. *Proceedings of the National Academy of Sciences*, 109(28):11105–11109, 2012.
- [24] Christoph J Strobl, Zeno von Guttenberg, and Achim Wixforth. Nano-and pico-dispensing of fluids on planar substrates using saw. *IEEE Transactions on Ultrasonics, Ferroelectrics, and Frequency Control*, 51(11):1432–1436, 2004.
- [25] Leslie Y Yeo and James R Friend. Ultrafast microfluidics using surface acoustic waves. *Biomicrofluidics*, 3(1):012002, 2009.
- [26] Jonathan Knight. Microfluidics: Honey, i shrunk the lab, 2002.
- [27] Andréas Manz, N Gruber, and H áM Widmer. Miniaturized total chemical analysis systems: a novel concept for chemical sensing. *Sensors and Actuators B: Chemical*, 1(1-6):244–248, 1990.
- [28] Felix Gattiker, F Umbrech, J Neuenschwander, U Sennhauser, and C Hierold. Novel ultrasound read-out for a wireless implantable passive strain sensor (wipss). *Sensors and Actuators A: Physical*, 145:291–298, 2008.
- [29] JC Rife, MI Bell, JS Horwitz, MN Kabler, RCY Auyeung, and WJ Kim. Miniature valveless ultrasonic pumps and mixers. *Sensors and Actuators A: Physical*, 86(1-2):135–140, 2000.
- [30] Stefano Oberti, Adrian Neild, and Tuck Wah Ng. Microfluidic mixing under low frequency vibration. *Lab Chip*, 9(10):1435–1438, 2009.
- [31] Jue Nee Tan and Adrian Neild. Microfluidic mixing in a y-junction open channel. *Aip Advances*, 2(3):032160, 2012.
- [32] Priscilla Rogers and Adrian Neild. Selective particle trapping using an oscillating microbubble. *Lab Chip*, 11(21):3710–3715, 2011.
- [33] Peter Woias. Micropumps—past, progress and future prospects. *Sensors and Actuators B: Chemical*, 105(1):28–38, 2005.
- [34] Rosamund Daw and Joshua Finkelstein. Lab on a chip. *Nature*, 442(7101):367, 2006.
- [35] Ivan K Dimov, Lourdes Basabe-Desmonts, Jose L Garcia-Cordero, Benjamin M Ross, Antonio J Ricco, and Luke P Lee. Stand-alone self-powered integrated microfluidic blood analysis system (simbas). *Lab on a Chip*, 11(5):845–850, 2011.

Bibliography

- [36] Karin Jacobs. Introduction to microfluidics. by patrick tabeling. *Angewandte Chemie International Edition*, 45(47):7875–7875, 2006.
- [37] Steve CC Shih, Hao Yang, Mais J Jebrail, Ryan Fobel, Nathan McIntosh, Osama Y Al-Dirbashi, Pranesh Chakraborty, and Aaron R Wheeler. Dried blood spot analysis by digital microfluidics coupled to nanoelectrospray ionization mass spectrometry. *Analytical Chemistry*, 84(8):3731–3738, 2012.
- [38] Mehdi Ghodbane, Elizabeth C Stucky, Tim J Maguire, Rene S Schloss, David I Shreiber, Jeffrey D Zahn, and Martin L Yarmush. Development and validation of a microfluidic immunoassay capable of multiplexing parallel samples in microliter volumes. *Lab Chip*, 15(15):3211–3221, 2015.
- [39] Alphonsus HC Ng, M Dean Chamberlain, Haozhong Situ, Victor Lee, and Aaron R Wheeler. Digital microfluidic immunocytochemistry in single cells. *Nature Communications*, 6:7513, 2015.
- [40] Mohtashim H Shamsi, Kihwan Choi, Alphonsus HC Ng, and Aaron R Wheeler. A digital microfluidic electrochemical immunoassay. *Lab Chip*, 14(3):547–554, 2014.
- [41] Tao Wu, Ying Mei, Joao T Cabral, Chang Xu, and Kathryn L Beers. A new synthetic method for controlled polymerization using a microfluidic system. *Journal of the American Chemical Society*, 126(32):9880–9881, 2004.
- [42] Irena Barbulovic-Nad, Sam H Au, and Aaron R Wheeler. A microfluidic platform for complete mammalian cell culture. *Lab Chip*, 10(12):1536–1542, 2010.
- [43] BL Karger, YH Chu, and F Foret. Capillary electrophoresis of proteins and nucleic acids. *Annual Review of Biophysics and Biomolecular Structure*, 24(1):579–610, 1995.
- [44] Adam T Woolley and Richard A Mathies. Ultra-high-speed dna fragment separations using microfabricated capillary array electrophoresis chips. *Proceedings of the National Academy of Sciences*, 91(24):11348–11352, 1994.
- [45] Dieter Schmalzing, Aram Adourian, Lance Koutny, Liuda Ziaugra, Paul Matsudaira, and Daniel Ehrlich. Dna sequencing on microfabricated electrophoretic devices. *Analytical Chemistry*, 70(11):2303–2310, 1998.
- [46] David J Collins, Tuncay Alan, Kristian Helmerson, and Adrian Neild. Surface acoustic waves for on-demand production of picoliter droplets and particle encapsulation. *Lab Chip*, 13(16):3225–3231, 2013.
- [47] Petra S Dittrich and Andreas Manz. Lab-on-a-chip: microfluidics in drug discovery. *Nature Reviews Drug Discovery*, 5(3):210, 2006.
- [48] Amir M Ghaemmaghami, Matthew J Hancock, Helen Harrington, Hirokazu Kaji, and Ali Khademhosseini. Biomimetic tissues on a chip for drug discovery. *Drug Discovery Today*, 17(3-4):173–181, 2012.
- [49] Andres W Martinez, Scott T Phillips, and George M Whitesides. Three-dimensional microfluidic devices fabricated in layered paper and tape. *Proceedings of the National Academy of Sciences*, 105(50):19606–19611, 2008.
- [50] Johannes GE Gardeniers and Albert van den Berg. Lab-on-a-chip systems for biomedical and environmental monitoring. *Analytical and Bioanalytical Chemistry*, 378(7):1700–1703, 2004.
- [51] J Wiest, T Stadthagen, M Schmidhuber, M Brischwein, J Ressler, U Raeder, H Grothe, A Melzer, and B Wolf. Intelligent mobile lab for metabolics in environmental monitoring. *Analytical Letters*, 39(8):1759–1771, 2006.
- [52] Leanne Marle and Gillian M Greenway. Microfluidic devices for environmental monitoring. *TrAC Trends in Analytical Chemistry*, 24(9):795–802, 2005.

Bibliography

- [53] Patrick Tabeling. *Introduction to microfluidics*. Oxford University Press on Demand, 2005.
- [54] David J Beebe, Glennys A Mensing, and Glenn M Walker. Physics and applications of microfluidics in biology. *Annual Review of Biomedical Engineering*, 4(1):261–286, 2002.
- [55] Eric K Sackmann, Anna L Fulton, and David J Beebe. The present and future role of microfluidics in biomedical research. *Nature*, 507(7491):181, 2014.
- [56] Daniel Mark, Stefan Haeberle, Günter Roth, Felix Von Stetten, and Roland Zengerle. Microfluidic lab-on-a-chip platforms: requirements, characteristics and applications. In *Microfluidics Based Microsystems*, pages 305–376. Springer, 2010.
- [57] Michael Kirschbaum, Christian R Guernth-Marschner, Solène Cherré, Albora de Pablo Peña, Magnus S Jaeger, Richard A Kroczeck, Thomas Schnelle, Torsten Mueller, and Claus Duschl. Highly controlled electrofusion of individually selected cells in dielectrophoretic field cages. *Lab Chip*, 12(3):443–450, 2012.
- [58] Emma Eriksson, Kristin Sott, Fredrik Lundqvist, Martin Svenningsson, Jan Scrimgeour, Dag Hanstorp, Mattias Goksör, and Annette Granéli. A microfluidic device for reversible environmental changes around single cells using optical tweezers for cell selection and positioning. *Lab Chip*, 10(5):617–625, 2010.
- [59] Galileo Galilei. *Dialogues Concerning Two New Sciences: Galileo Galilei*. Dover, 1954.
- [60] Darcy Wentworth Thompson et al. On growth and form. *On Growth and Form.*, 1942.
- [61] P Sajeesh and Ashis Kumar Sen. Particle separation and sorting in microfluidic devices: a review. *Microfluidics and Nanofluidics*, 17(1):1–52, 2014.
- [62] AS Utada, L-Y Chu, A Fernandez-Nieves, DR Link, C Holtze, and DA Weitz. Dripping, jetting, drops, and wetting: The magic of microfluidics. *Mrs Bulletin*, 32(9):702–708, 2007.
- [63] Song Chen, Huijie Zhang, Xuetao Shi, Hongkai Wu, and Nobutaka Hanagata. Microfluidic generation of chitosan/cpg oligodeoxynucleotide nanoparticles with enhanced cellular uptake and immunostimulatory properties. *Lab on a Chip*, 14(11):1842–1849, 2014.
- [64] Arnold Chen and Tingrui Pan. Fit-to-flow (f2f) interconnects: Universal reversible adhesive-free microfluidic adaptors for lab-on-a-chip systems. *Lab on a Chip*, 11(4):727–732, 2011.
- [65] Haishui Huang, Yin Yu, Yong Hu, Xiaoming He, O Berk Usta, and Martin L Yarmush. Generation and manipulation of hydrogel microcapsules by droplet-based microfluidics for mammalian cell culture. *Lab on a Chip*, 17(11):1913–1932, 2017.
- [66] Liang-Yin Chu, Andrew S Utada, Rhutesh K Shah, Jin-Woong Kim, and David A Weitz. Controllable monodisperse multiple emulsions. *Angewandte Chemie*, 119(47):9128–9132, 2007.
- [67] Wei Wang, Rui Xie, Xiao-Jie Ju, Tao Luo, Li Liu, David A Weitz, and Liang-Yin Chu. Controllable microfluidic production of multicomponent multiple emulsions. *Lab on a Chip*, 11(9):1587–1592, 2011.
- [68] Helen Song, Michelle R Bringer, Joshua D Tice, Cory J Gerdts, and Rustem F Ismagilov. Experimental test of scaling of mixing by chaotic advection in droplets moving through microfluidic channels. *Applied Physics Letters*, 83(22):4664–4666, 2003.
- [69] Masumi Yamada, Megumi Nakashima, and Minoru Seki. Pinched flow fractionation: continuous size separation of particles utilizing a laminar flow profile in a pinched microchannel. *Analytical Chemistry*, 76(18):5465–5471, 2004.

Bibliography

- [70] Arjun P Sudarsan and Victor M Ugaz. Fluid mixing in planar spiral microchannels. *Lab Chip*, 6(1):74–82, 2006.
- [71] Vibhu Vivek and Eun Sok Kim. Novel acoustic-wave micromixer. In *Micro Electro Mechanical Systems, 2000. MEMS 2000. The Thirteenth Annual International Conference on*, pages 668–673. IEEE, 2000.
- [72] Wei-Kuo Tseng, Jr-Lung Lin, Wang-Chou Sung, Shu-Hui Chen, and Gwo-Bin Lee. Active micro-mixers using surface acoustic waves on y-cut 128 linbo3. *Journal of Micromechanics and Microengineering*, 16(3):539, 2006.
- [73] Takashi Yasuda, Shouhei Harada, and Katsuya Daimon. Microfluidic dispensing device using wettability gradient and electrowetting. *IEEJ Transactions on Sensors and Micromachines*, 128(3):75–79, 2008.
- [74] Masumi Yamada and Minoru Seki. Nanoliter-sized liquid dispenser array for multiple biochemical analysis in microfluidic devices. *Analytical Chemistry*, 76(4):895–899, 2004.
- [75] P Ferraro, S Coppola, S Grilli, M Paturzo, and V Vespi. Dispensing nano–pico droplets and liquid patterning by pyroelectrodynamic shooting. *Nature Nanotechnology*, 5(6):429, 2010.
- [76] Richard W Light, M Isabelle Macgregor, Peter C Luchsinger, and Wilmot C Ball. Pleural effusions: the diagnostic separation of transudates and exudates. *Annals of Internal Medicine*, 77(4):507–513, 1972.
- [77] R Huang, TA Barber, MA Schmidt, RG Tompkins, M Toner, DW Bianchi, R Kapur, and WL Flejter. A microfluidics approach for the isolation of nucleated red blood cells (nrbc) from the peripheral blood of pregnant women. *Prenatal Diagnosis*, 28(10):892–899, 2008.
- [78] Chen Qian, Shan Wu, Hongmei Chen, Xiaofen Zhang, Rongrong Jing, Lei Shen, Xudong Wang, Shaoqing Ju, Chunping Jia, and Hui Cong. Clinical significance of circulating tumor cells from lung cancer patients using microfluidic chip. *Clinical and Experimental Medicine*, 18(2):191–202, 2018.
- [79] Jian Zhou, Chunlong Tu, Yitao Liang, Bobo Huang, Yifeng Fang, Xiao Liang, Ian Papautsky, and Xuesong Ye. Isolation of cells from whole blood using shear-induced diffusion. *Scientific Reports*, 8(1):9411, 2018.
- [80] David K Wood, David M Weingeist, Sangeeta N Bhatia, and Bevin P Engelward. Single cell trapping and dna damage analysis using microwell arrays. *Proceedings of the National Academy of Sciences*, 2010.
- [81] Johan Nilsson, Mikael Evander, Björn Hammarström, and Thomas Laurell. Review of cell and particle trapping in microfluidic systems. *Analytica Chimica Acta*, 649(2):141–157, 2009.
- [82] Lifeng Kang, Bong Geun Chung, Robert Langer, and Ali Khademhosseini. Microfluidics for drug discovery and development: from target selection to product lifecycle management. *Drug Discovery Today*, 13(1-2):1–13, 2008.
- [83] Bertrand Guillotin and Fabien Guillemot. Cell patterning technologies for organotypic tissue fabrication. *Trends in Biotechnology*, 29(4):183–190, 2011.
- [84] Ishwari Poudel, Daniel E Menter, and Jung Yul Lim. Directing cell function and fate via micropatterning: role of cell patterning size, shape, and interconnectivity. *Biomedical Engineering Letters*, 2(1):38–45, 2012.
- [85] Jingyun Ma, Yachen Wang, and Jing Liu. Bioprinting of 3d tissues/organs combined with microfluidics. *RSC Advances*, 8(39):21712–21727, 2018.

Bibliography

- [86] David J Collins, Belinda Morahan, Jose Garcia-Bustos, Christian Doerig, Magdalena Plebanski, and Adrian Neild. Two-dimensional single-cell patterning with one cell per well driven by surface acoustic waves. *Nature Communications*, 6:8686, 2015.
- [87] Jun Miao and Liwang Cui. Rapid isolation of single malaria parasite–infected red blood cells by cell sorting. *Nature Protocols*, 6(2):140, 2011.
- [88] EH Zhou, CT Lim, KSW Tan, and Ser Tong Quek. Finite element modeling of the micropipette aspiration of malaria-infected red blood cells. In *Third International Conference on Experimental Mechanics and Third Conference of the Asian Committee on Experimental Mechanics*, volume 5852, pages 763–768. International Society for Optics and Photonics, 2005.
- [89] Won Gu Lee, Yun-Gon Kim, Bong Geun Chung, Utkan Demirci, and Ali Khademhosseini. Nano/microfluidics for diagnosis of infectious diseases in developing countries. *Advanced Drug Delivery Reviews*, 62(4-5):449–457, 2010.
- [90] D Gobby, P Angeli, and Asterios Gavriilidis. Mixing characteristics of t-type microfluidic mixers. *Journal of Micromechanics and Microengineering*, 11(2):126, 2001.
- [91] Yu-Cheng Lin, Yung-Chiang Chung, and Chung-Yi Wu. Mixing enhancement of the passive microfluidic mixer with j-shaped baffles in the tee channel. *Biomedical Microdevices*, 9(2):215–221, 2007.
- [92] Yung-Chiang Chung, Yuh-Lih Hsu, Chun-Ping Jen, Ming-Chang Lu, and Yu-Cheng Lin. Design of passive mixers utilizing microfluidic self-circulation in the mixing chamber. *Lab Chip*, 4(1):70–77, 2004.
- [93] John Oakey, Robert W Applegate Jr, Erik Arellano, Dino Di Carlo, Steven W Graves, and Mehmet Toner. Particle focusing in staged inertial microfluidic devices for flow cytometry. *Analytical Chemistry*, 82(9):3862–3867, 2010.
- [94] Han Wei Hou, Ali Asgar S Bhagat, Alvin Guo Lin Chong, Pan Mao, Kevin Shyong Wei Tan, Jongyoon Han, and Chwee Teck Lim. Deformability based cell margination—a simple microfluidic design for malaria-infected erythrocyte separation. *Lab Chip*, 10(19):2605–2613, 2010.
- [95] John A Davis, David W Inglis, Keith J Morton, David A Lawrence, Lotien R Huang, Stephen Y Chou, James C Sturm, and Robert H Austin. Deterministic hydrodynamics: taking blood apart. *Proceedings of the National Academy of Sciences*, 103(40):14779–14784, 2006.
- [96] Brenda S Cho, Timothy G Schuster, Xiaoyue Zhu, David Chang, Gary D Smith, and Shuichi Takayama. Passively driven integrated microfluidic system for separation of motile sperm. *Analytical Chemistry*, 75(7):1671–1675, 2003.
- [97] Junya Takagi, Masumi Yamada, Masahiro Yasuda, and Minoru Seki. Continuous particle separation in a microchannel having asymmetrically arranged multiple branches. *Lab Chip*, 5(7):778–784, 2005.
- [98] Tomoki Morijiri, Satoshi Sunahiro, Masashi Senaha, Masumi Yamada, and Minoru Seki. Sedimentation pinched-flow fractionation for size-and density-based particle sorting in microchannels. *Microfluidics and Nanofluidics*, 11(1):105–110, 2011.
- [99] Jae-Sung Park and Hyo-Il Jung. Multiorifice flow fractionation: continuous size-based separation of microspheres using a series of contraction/expansion microchannels. *Analytical Chemistry*, 81(20):8280–8288, 2009.
- [100] Dino Di Carlo, Jon F Edd, Daniel Irimia, Ronald G Tompkins, and Mehmet Toner. Equilibrium separation and filtration of particles using differential inertial focusing. *Analytical Chemistry*, 80(6):2204–2211, 2008.

Bibliography

- [101] Asger Laurberg Vig, Rodolphe Marie, Eric Jensen, and Anders Kristensen. Optofluidic microscope with 3d spatial resolution. *Optics express*, 18(5):4158–4169, 2010.
- [102] Eric Lin, Lianette Rivera-Báez, Shamileh Fouladdel, Hyeun Joong Yoon, Stephanie Guthrie, Jacob Wieger, Yadwinder Deol, Evan Keller, Vaibhav Sahai, Diane M Simeone, et al. High-throughput microfluidic labyrinth for the label-free isolation of circulating tumor cells. *Cell systems*, 5(3):295–304, 2017.
- [103] Xing Chen, Chang Chun Liu, Hui Li, et al. Microfluidic chip for blood cell separation and collection based on crossflow filtration. *Sensors and Actuators B: Chemical*, 130(1):216–221, 2008.
- [104] Dongeun Huh, Joong Hwan Bahng, Yibo Ling, Hsien-Hung Wei, Oliver D Kripfgans, J Brian Fowlkes, James B Grotberg, and Shuichi Takayama. Gravity-driven microfluidic particle sorting device with hydrodynamic separation amplification. *Analytical Chemistry*, 79(4):1369–1376, 2007.
- [105] Tohid Fatanat Didar and Maryam Tabrizian. Adhesion based detection, sorting and enrichment of cells in microfluidic lab-on-chip devices. *Lab Chip*, 10(22):3043–3053, 2010.
- [106] Masumi Yamada and Minoru Seki. Hydrodynamic filtration for on-chip particle concentration and classification utilizing microfluidics. *Lab Chip*, 5(11):1233–1239, 2005.
- [107] Masumi Yamada, Kyoko Kano, Yukiko Tsuda, Jun Kobayashi, Masayuki Yamato, Minoru Seki, and Teruo Okano. Microfluidic devices for size-dependent separation of liver cells. *Biomedical Microdevices*, 9(5):637–645, 2007.
- [108] Lidan Wu, Guofeng Guan, Han Wei Hou, Ali Asgar S Bhagat, and Jongyoon Han. Separation of leukocytes from blood using spiral channel with trapezoid cross-section. *Analytical Chemistry*, 84(21):9324–9331, 2012.
- [109] Majid Ebrahimi Warkiani, Guofeng Guan, Khoo Bee Luan, Wong Cheng Lee, Ali Asgar S Bhagat, Parthiv Kant Chaudhuri, Daniel Shao-Weng Tan, Wan Teck Lim, Soo Chin Lee, Peter CY Chen, et al. Slanted spiral microfluidics for the ultra-fast, label-free isolation of circulating tumor cells. *Lab Chip*, 14(1):128–137, 2014.
- [110] Hansen Bow, Igor V Pivkin, Monica Diez-Silva, Stephen J Goldfless, Ming Dao, Jacquin C Niles, Subra Suresh, and Jongyoon Han. A microfabricated deformability-based flow cytometer with application to malaria. *Lab Chip*, 11(6):1065–1073, 2011.
- [111] Pascal Preira, Véronique Grandne, J-M Forel, Sylvain Gabriele, M Camara, and Olivier Theodoly. Passive circulating cell sorting by deformability using a microfluidic gradual filter. *Lab Chip*, 13(1):161–170, 2013.
- [112] Timm Krüger, David Holmes, and Peter V Coveney. Deformability-based red blood cell separation in deterministic lateral displacement devices—a simulation study. *Biomicrofluidics*, 8(5):054114, 2014.
- [113] S Cerbelli. Separation of polydisperse particle mixtures by deterministic lateral displacement. the impact of particle diffusivity on separation efficiency. *Asia-Pacific Journal of Chemical Engineering*, 7:S356–S371, 2012.
- [114] S Winoto-Morbach, V Tchikov, and W Mueller-Ruchholtz. Magnetophoresis: I. detection of magnetically labeled cells. *Journal of Clinical Laboratory Analysis*, 8(6):400–406, 1994.
- [115] Maciej Zborowski and Jeffrey J Chalmers. Magnetophoresis: fundamentals and applications. *Wiley Encyclopedia of Electrical and Electronics Engineering*, pages 1–23, 1999.

Bibliography

- [116] Akira Ito, Masashige Shinkai, Hiroyuki Honda, and Takeshi Kobayashi. Medical application of functionalized magnetic nanoparticles. *Journal of Bioscience and Bioengineering*, 100(1):1–11, 2005.
- [117] C Wilhelm, F Gazeau, J Roger, JN Pons, and J-C Bacri. Interaction of anionic superparamagnetic nanoparticles with cells: kinetic analyses of membrane adsorption and subsequent internalization. *Langmuir*, 18(21):8148–8155, 2002.
- [118] Ki-Ho Han, Arum Han, and A Bruno Frazier. Microsystems for isolation and electrophysiological analysis of breast cancer cells from blood. *Biosensors and bioelectronics*, 21(10):1907–1914, 2006.
- [119] Ki-Ho Han and A Bruno Frazier. A microfluidic system for continuous magnetophoretic separation of suspended cells using their native magnetic properties. *Proc. Nanotech*, 1:187–190, 2005.
- [120] P Dunnill and MD Lilly. Purification of enzymes using magnetic bio-affinity materials. *Biotechnology and Bioengineering*, 16(7):987–990, 1974.
- [121] K Mosbach and L Andersson. Magnetic ferrofluids for preparation of magnetic polymers and their application in affinity chromatography. *Nature*, 270(5634):259, 1977.
- [122] Akihiko Kondo, Hiroko Kamura, and Ko Higashitani. Development and application of thermo-sensitive magnetic immunomicrospheres for antibody purification. *Applied Microbiology and Biotechnology*, 41(1):99–105, 1994.
- [123] Ulrike Lehmann, Caroline Vandevyver, Virendra K Parashar, and Martin AM Gijs. Droplet-based dna purification in a magnetic lab-on-a-chip. *Angewandte Chemie International Edition*, 45(19):3062–3067, 2006.
- [124] Sylvia Kwakye and Antje Baeumner. A microfluidic biosensor based on nucleic acid sequence recognition. *Analytical and Bioanalytical Chemistry*, 376(7):1062–1068, 2003.
- [125] William H Grover and Richard A Mathies. An integrated microfluidic processor for single nucleotide polymorphism-based dna computing. *Lab Chip*, 5(10):1033–1040, 2005.
- [126] Mark A Hayes, Nolan A Polson, and Antonio A Garcia. Active control of dynamic supraparticle structures in microchannels. *Langmuir*, 17(9):2866–2871, 2001.
- [127] Antonio A Garcia, Ana Egatz-Gómez, Solitaire A Lindsay, P Dominguez-Garcia, Sonia Melle, Manuel Marquez, Miguel A Rubio, ST Picraux, Dongqing Yang, P Aella, et al. Magnetic movement of biological fluid droplets. *Journal of Magnetism and Magnetic Materials*, 311(1):238–243, 2007.
- [128] Ronald Pethig. Dielectrophoresis: Status of the theory, technology, and applications. *Biomicrofluidics*, 4(2):022811, 2010.
- [129] DW Pimbley, PD Patel, and CJ Robertson. Dielectrophoresis. In *Environmental Monitoring of Bacteria*, pages 35–53. Springer, 1999.
- [130] Günter Fuhr, Torsten Müller, Vera Baukloh, and Kurt Lucas. High-frequency electric field trapping of individual human spermatozoa. *Human Reproduction (Oxford, England)*, 13(1):136–141, 1998.
- [131] Tjitske Heida, Wim LC Rutten, and Enrico Marani. Dielectrophoretic trapping of dissociated fetal cortical rat neurons. *IEEE Transactions on Biomedical Engineering*, 48(8):921–930, 2001.
- [132] M Mischel, F Rouge, I Lamprecht, C Aubert, and G Prota. Dielectrophoresis of malignant human melanocytes. *Archives of Dermatological Research*, 275(3):141–143, 1983.

Bibliography

- [133] GP Archer, WB Betts, and T Haigh. Rapid differentiation of untreated, autoclaved and ozone-treated cryptosporidium parvum oocysts using dielectrophoresis. *Microbios*, 73(296):165–172, 1993.
- [134] Herbert A Pohl. Dielectrophoresis: Applications to the characterization and separation of cells. In *Methods of Cell Separation*, pages 67–169. Springer, 1977.
- [135] Lukas Novotny, Randy X Bian, and X Sunney Xie. Theory of nanometric optical tweezers. *Physical Review Letters*, 79(4):645, 1997.
- [136] Jungwoo Lee, Kangyeol Ha, and K Kirk Shung. A theoretical study of the feasibility of acoustical tweezers: Ray acoustics approach. *The Journal of the Acoustical Society of America*, 117(5):3273–3280, 2005.
- [137] Takayuki Nishizaka, Hidetake Miyata, Hiroshi Yoshikawa, Shin’ichi Ishiwata, and Kazuhiko Kinoshita Jr. Unbinding force of a single motor molecule of muscle measured using optical tweezers. *Nature*, 377(6546):251, 1995.
- [138] Amit D Mehta, Katherine A Pullen, and James A Spudich. Single molecule biochemistry using optical tweezers. *FEBS Letters*, 430(1-2):23–27, 1998.
- [139] Michelle D Wang, Hong Yin, Robert Landick, Jeff Gelles, and Steven M Block. Stretching dna with optical tweezers. *Biophysical Journal*, 72(3):1335–1346, 1997.
- [140] Benjamin B Yellen, Ondrej Hovorka, and Gary Friedman. Arranging matter by magnetic nanoparticle assemblers. *Proceedings of the National Academy of Sciences*, 102(25):8860–8864, 2005.
- [141] David G Grier. A revolution in optical manipulation. *nature*, 424(6950):810, 2003.
- [142] Tayloria NG Adams, Alan YL Jiang, Prema D Vyas, and Lisa A Flanagan. Separation of neural stem cells by whole cell membrane capacitance using dielectrophoresis. *Methods*, 2017.
- [143] Ana Valero, Thomas Braschler, Alex Rauch, Nicolas Demierre, Yves Barral, and Philippe Renaud. Tracking and synchronization of the yeast cell cycle using dielectrophoretic opacity. *Lab on a Chip*, 11(10):1754–1760, 2011.
- [144] Wong Cheng Lee, Ali Asgar S Bhagat, Sha Huang, Krystyn J Van Vliet, Jongyoon Han, and Chwee Teck Lim. High-throughput cell cycle synchronization using inertial forces in spiral microchannels. *Lab Chip*, 11(7):1359–1367, 2011.
- [145] Mark Tondra, Mike Granger, Rachel Fuerst, Marc Porter, Catherine Nordman, John Taylor, and Seraphin Akou. Design of integrated microfluidic device for sorting magnetic beads in biological assays. *IEEE Transactions on Magnetics*, 37(4):2621–2623, 2001.
- [146] LP Gor’Kov. On the forces acting on a small particle in an acoustical field in an ideal fluid. In *Sov. Phys. Dokl.*, volume 6, pages 773–775, 1962.
- [147] Arthur Ashkin, James M Dziedzic, JE Bjorkholm, and Steven Chu. Observation of a single-beam gradient force optical trap for dielectric particles. *Optics Letters*, 11(5):288–290, 1986.
- [148] Louis Vessot King et al. On the acoustic radiation pressure on spheres. *Proc. R. Soc. Lond. A*, 147(861):212–240, 1934.
- [149] Despina Bazou, Roisin Kearney, Fiona Mansergh, Celine Bourdon, Jane Farrar, and Michael Wride. Gene expression analysis of mouse embryonic stem cells following levitation in an ultrasound standing wave trap. *Ultrasound in medicine & biology*, 37(2):321–330, 2011.

Bibliography

- [150] Jessica Hultström, Otto Manneberg, Katja Dopf, Hans M Hertz, Hjalmar Brismar, and Martin Wiklund. Proliferation and viability of adherent cells manipulated by standing-wave ultrasound in a microfluidic chip. *Ultrasound in medicine & biology*, 33(1):145–151, 2007.
- [151] Velimir M Ristic. *Principles of acoustic devices*. Krieger Publishing Company, 1983.
- [152] Constantin Chilovsky and Paul Langevin. Procédés et appareils pour la production de signaux sous-marins dirigés et pour la localisation à distance d'obstacles sous-marins. *French Patent*, 502913, 1916.
- [153] Caroline Holmes, Bruce W Drinkwater, and Paul D Wilcox. Post-processing of the full matrix of ultrasonic transmit-receive array data for non-destructive evaluation. *NDT & e International*, 38(8):701–711, 2005.
- [154] Shobha Muthukumaran, Katerina Yang, Annette Seuren, Sandra Kentish, Muthupandian Ashokkumar, Geoffrey W Stevens, and Franz Grieser. The use of ultrasonic cleaning for ultrafiltration membranes in the dairy industry. *Separation and Purification Technology*, 39(1-2):99–107, 2004.
- [155] Peter R Hoskins, Kevin Martin, and Abigail Thrush. *Diagnostic ultrasound: physics and equipment*. Cambridge University Press, 2010.
- [156] A Bauer, G Becker, A Krone, T Fröhlich, and U Bogdahn. Transcranial duplex sonography using ultrasound contrast enhancers. *Clinical Radiology*, 51:19–23, 1996.
- [157] Lord Rayleigh. On the circulation of air observed in kundt's tubes, and on some allied acoustical problem. *Phil. Trans. Roy. Soc.*, 175:1–21, 1884.
- [158] Michael Faraday. Xvii. on a peculiar class of acoustical figures; and on certain forms assumed by groups of particles upon vibrating elastic surfaces. *Philosophical Transactions of the Royal Society of London*, 121:299–340, 1831.
- [159] John Miles. On rayleigh's investigation of crispations of fluid resting on a vibrating support. *Journal of Fluid Mechanics*, 244:645–648, 1992.
- [160] James Friend and Leslie Y Yeo. Microscale acoustofluidics: Microfluidics driven via acoustics and ultrasonics. *Reviews of Modern Physics*, 83(2):647, 2011.
- [161] RM White and FW Voltmer. Direct piezoelectric coupling to surface elastic waves. *Applied Physics Letters*, 7(12):314–316, 1965.
- [162] William Connacher, Naiqing Zhang, An Huang, Jiyang Mei, Shuai Zhang, Tilwawala Gopesh, and James Friend. Micro/nano acoustofluidics: materials, phenomena, design, devices, and applications. *Lab Chip*, 2018.
- [163] Lord Rayleigh. On waves propagated along the plane surface of an elastic solid. *Proceedings of the London Mathematical Society*, 1(1):4–11, 1885.
- [164] Wesley Le Mars Nyborg. Acoustic streaming. In *Physical Acoustics*, volume 2, pages 265–331. Elsevier, 1965.
- [165] Lawrence A Crum. Bjerknes forces on bubbles in a stationary sound field. *The Journal of the Acoustical Society of America*, 57(6):1363–1370, 1975.
- [166] TG Leighton, AJ Walton, and MJW Pickworth. Primary bjerknes forces. *European Journal of Physics*, 11(1):47, 1990.
- [167] Henrik Bruus. Acoustofluidics 2: Perturbation theory and ultrasound resonance modes. *Lab Chip*, 12(1):20–28, 2012.
- [168] Alexander A Doinikov. Acoustic radiation pressure on a compressible sphere in a viscous fluid. *Journal of Fluid Mechanics*, 267:1–22, 1994.

Bibliography

- [169] Peter Barkholt Muller, Rune Barnkob, Mads Jakob Herring Jensen, and Henrik Bruus. A numerical study of microparticle acoustophoresis driven by acoustic radiation forces and streaming-induced drag forces. *Lab Chip*, 12(22):4617–4627, 2012.
- [170] Thomas Laurell and Andreas Lenshof. *Microscale Acoustofluidics*. Royal Society of Chemistry, 2014.
- [171] Citsabehsan Devendran, Thomas Albrecht, Jason Brenker, Tuncay Alan, and Adrian Neild. The importance of travelling wave components in standing surface acoustic wave (ssaw) systems. *Lab Chip*, 16(19):3756–3766, 2016.
- [172] SS Sadhal. Acoustofluidics 13: Analysis of acoustic streaming by perturbation methods. *Lab on a Chip*, 12(13):2292–2300, 2012.
- [173] Martin Wiklund, Roy Green, and Mathias Ohlin. Acoustofluidics 14: Applications of acoustic streaming in microfluidic devices. *Lab on a Chip*, 12(14):2438–2451, 2012.
- [174] David J Collins, Bee Luan Khoo, Zhichao Ma, Andreas Winkler, Robert Weser, Hagen Schmidt, Jongyoon Han, and Ye Ai. Selective particle and cell capture in a continuous flow using micro-vortex acoustic streaming. *Lab on a Chip*, 17(10):1769–1777, 2017.
- [175] Jeffrey S Marshall and Junru Wu. Acoustic streaming, fluid mixing, and particle transport by a gaussian ultrasound beam in a cylindrical container. *Physics of Fluids*, 27(10):103601, 2015.
- [176] Richard Shilton, Ming K Tan, Leslie Y Yeo, and James R Friend. Particle concentration and mixing in microdrops driven by focused surface acoustic waves. *Journal of Applied Physics*, 104(1):014910, 2008.
- [177] Michael B Dentry, James R Friend, and Leslie Y Yeo. Continuous flow actuation between external reservoirs in small-scale devices driven by surface acoustic waves. *Lab Chip*, 14(4):750–758, 2014.
- [178] Po-Hsun Huang, Nitesh Nama, Zhangming Mao, Peng Li, Joseph Rufo, Yuchao Chen, Yuliang Xie, Cheng-Hsin Wei, Lin Wang, and Tony Jun Huang. A reliable and programmable acoustofluidic pump powered by oscillating sharp-edge structures. *Lab Chip*, 14(22):4319–4323, 2014.
- [179] Ghulam Destgeer, Hyunjun Cho, Byung Hang Ha, Jin Ho Jung, Jinsoo Park, and Hyung Jin Sung. Acoustofluidic particle manipulation inside a sessile droplet: four distinct regimes of particle concentration. *Lab Chip*, 16(4):660–667, 2016.
- [180] Julien Reboud, Yannyk Bourquin, Rab Wilson, Gurman S Pall, Meesbah Jiwaji, Andrew R Pitt, Anne Graham, Andrew P Waters, and Jonathan M Cooper. Shaping acoustic fields as a toolset for microfluidic manipulations in diagnostic technologies. *Proceedings of the National Academy of Sciences*, 109(38):15162–15167, 2012.
- [181] Chengxun Liu, Liesbet Lagae, and Gustaaf Borghs. Manipulation of magnetic particles on chip by magnetophoretic actuation and dielectrophoretic levitation. *Applied Physics Letters*, 90(18):184109, 2007.
- [182] Jonas T Karlsen, Wei Qiu, Per Augustsson, and Henrik Bruus. Acoustic streaming and its suppression in inhomogeneous fluids. *Physical Review Letters*, 120(5):054501, 2018.
- [183] Ruhollah Habibi, Citsabehsan Devendran, and Adrian Neild. Trapping and patterning of large particles and cells in a 1d ultrasonic standing wave. *Lab Chip*, 17(19):3279–3290, 2017.
- [184] Ivo Leibacher, Peter Reichert, and Jürg Dual. Microfluidic droplet handling by bulk acoustic wave (baw) acoustophoresis. *Lab Chip*, 15(13):2896–2905, 2015.

Bibliography

- [185] Adrian Neild, Stefano Oberti, and Jürg Dual. Design, modeling and characterization of microfluidic devices for ultrasonic manipulation. *Sensors and Actuators B: Chemical*, 121(2):452–461, 2007.
- [186] Adrian Neild, Stefano Oberti, Gerald Radziwill, and Jürg Dual. Simultaneous positioning of cells into two-dimensional arrays using ultrasound. *Biotechnology and Bioengineering*, 97(5):1335–1339, 2007.
- [187] Stefano Oberti, Adrian Neild, and Jürg Dual. Manipulation of micrometer sized particles within a micromachined fluidic device to form two-dimensional patterns using ultrasound. *The Journal of the Acoustical Society of America*, 121(2):778–785, 2007.
- [188] K Yosioka and Y Kawasima. Acoustic radiation pressure on a compressible sphere. *Acta Acustica united with Acustica*, 5(3):167–173, 1955.
- [189] Andreas Lenshof, Asilah Ahmad-Tajudin, Kerstin Järås, Ann-Margret Swärd-Nilsson, Lena Åberg, György Marko-Varga, Johan Malm, Hans Lilja, and Thomas Laurell. Acoustic whole blood plasmapheresis chip for prostate specific antigen microarray diagnostics. *Analytical chemistry*, 81(15):6030–6037, 2009.
- [190] Martin Wiklund and Hans M Hertz. Ultrasonic enhancement of bead-based bioaffinity assays. *Lab Chip*, 6(10):1279–1292, 2006.
- [191] Filip Petersson, Lena Åberg, Ann-Margret Swärd-Nilsson, and Thomas Laurell. Free flow acoustophoresis: microfluidic-based mode of particle and cell separation. *Analytical Chemistry*, 79(14):5117–5123, 2007.
- [192] Andreas Nilsson, Filip Petersson, Henrik Jönsson, and Thomas Laurell. Acoustic control of suspended particles in micro fluidic chips. *Lab Chip*, 4(2):131–135, 2004.
- [193] Stefano Oberti, Adrian Neild, Raymond Quach, and Jürg Dual. The use of acoustic radiation forces to position particles within fluid droplets. *Ultrasonics*, 49(1):47–52, 2009.
- [194] CS Hartmann. Systems impact of modern rayleigh wave technology. In *Rayleigh-Wave Theory and Application*, pages 238–253. Springer, 1985.
- [195] Cheng-kai Luo, Prasad S Gudem, and James F Buckwalter. A 0.4–6-ghz 17-dbm b1db 36-dbm iip3 channel-selecting low-noise amplifier for saw-less 3g/4g fdd diversity receivers. *IEEE Transactions on Microwave Theory and Techniques*, 64(4):1110–1121, 2016.
- [196] Colin Campbell. *Surface Acoustic Wave Devices for Mobil and Wireless Communications*. Academic Press, Inc., 1998.
- [197] Henry Wohltjen and Raymond Dessim. Surface acoustic wave probe for chemical analysis. i. introduction and instrument description. *Analytical Chemistry*, 51(9):1458–1464, 1979.
- [198] Amnon Yariv and Pochi Yeh. Optical waves in crystal propagation and control of laser radiation. *John Wiley and Sons, Inc., New York, NY*, 1983.
- [199] Donald B Armstrong, Jeffrey W Asher, Susan P Benitez, Richard A Jones, Joel C Kent, Michael L Lewis, and Robert C Phares. Surface acoustic wave touchscreen with housing seal, July 21 1998. US Patent 5,784,054.
- [200] Jason C Brenker, David J Collins, Hoang Van Phan, Tuncay Alan, and Adrian Neild. On-chip droplet production regimes using surface acoustic waves. *Lab Chip*, 16(9):1675–1683, 2016.
- [201] Muhsincan Sesen, Tuncay Alan, and Adrian Neild. Microfluidic on-demand droplet merging using surface acoustic waves. *Lab Chip*, 14(17):3325–3333, 2014.

Bibliography

- [202] Lothar Schmid and Thomas Franke. Acoustic modulation of droplet size in a t-junction. *Applied Physics Letters*, 104(13):133501, 2014.
- [203] Muhsincan Sesen, Tuncay Alan, and Adrian Neild. Microfluidic plug steering using surface acoustic waves. *Lab Chip*, 15(14):3030–3038, 2015.
- [204] Dariush Ashtiani, Hari Venugopal, Matthew Belousoff, Bradley Spicer, Johnson Mak, Adrian Neild, and Alex de Marco. Delivery of femtolitre droplets using surface acoustic wave based atomisation for cryo-em grid preparation. *Journal of Structural Biology*, 2018.
- [205] Scott R Heron, Rab Wilson, Scott A Shaffer, David R Goodlett, and Jonathan M Cooper. Surface acoustic wave nebulization of peptides as a microfluidic interface for mass spectrometry. *Analytical Chemistry*, 82(10):3985–3989, 2010.
- [206] Aisha Qi, Leslie Y Yeo, and James R Friend. Interfacial destabilization and atomization driven by surface acoustic waves. *Physics of Fluids*, 20(7):074103, 2008.
- [207] David J Collins, Tuncay Alan, and Adrian Neild. Particle separation using virtual deterministic lateral displacement (vdld). *Lab Chip*, 14(9):1595–1603, 2014.
- [208] Bojan Vukasinovic, Marc K Smith, and Ari Glezer. Dynamics of a sessile drop in forced vibration. *Journal of Fluid Mechanics*, 587:395–423, 2007.
- [209] Xiaoyun Ding, Zhangli Peng, Sz-Chin Steven Lin, Michela Geri, Sixing Li, Peng Li, Yuchao Chen, Ming Dao, Subra Suresh, and Tony Jun Huang. Cell separation using tilted-angle standing surface acoustic waves. *Proceedings of the National Academy of Sciences*, 111(36):12992–12997, 2014.
- [210] Kentaro Nakamura. *Ultrasonic transducers: Materials and design for sensors, actuators and medical applications*. Elsevier, 2012.
- [211] RT Smith and FS Welsh. Temperature dependence of the elastic, piezoelectric, and dielectric constants of lithium tantalate and lithium niobate. *Journal of Applied Physics*, 42(6):2219–2230, 1971.
- [212] James F Tressler, Sedat Alkoy, and Robert E Newnham. Piezoelectric sensors and sensor materials. *Journal of Electroceramics*, 2(4):257–272, 1998.
- [213] Don A Berlincourt, Daniel R Curran, and Hans Jaffe. Piezoelectric and piezomagnetic materials and their function in transducers. *Physical Acoustics: Principles and Methods*, 1(Part A):247, 1964.
- [214] IS Zheludev. Theory of spontaneous polarization. In *Physics of Crystalline Dielectrics*, pages 251–336. Springer, 1971.
- [215] Thomas L Szabo and AJ Slobodnik. The effect of diffraction on the design of acoustic surface wave devices. *IEEE Transactions on Sonics and Ultrasonics*, 20(3):240–251, 1973.
- [216] Jinjie Shi, Xiaole Mao, Daniel Ahmed, Ashley Colletti, and Tony Jun Huang. Focusing microparticles in a microfluidic channel with standing surface acoustic waves (ssaw). *Lab Chip*, 8(2):221–223, 2008.
- [217] Tsung-Tsong Wu, He-Tai Tang, Yung-Yu Chen, and Pei-Ling Liu. Analysis and design of focused interdigital transducers. *IEEE Transactions on Ultrasonics, Ferroelectrics, and Frequency Control*, 52(8):1384–1392, 2005.
- [218] Hiromi Yatsuda. Design techniques for saw filters using slanted finger interdigital transducers. *IEEE Transactions on Ultrasonics, Ferroelectrics, and Frequency Control*, 44(2):453–459, 1997.

Bibliography

- [219] Andreas Winkler, Paul Bergelt, Lars Hillemann, and Siegfried Menzel. Influence of viscosity in fluid atomization with surface acoustic waves. *Open Journal of Acoustics*, 6(03):23, 2016.
- [220] RM Arzt, E Salzmann, and K Dransfeld. Elastic surface waves in quartz at 316 mhz. *Applied Physics Letters*, 10(5):165–167, 1967.
- [221] Michael B Dentry, Leslie Y Yeo, and James R Friend. Frequency effects on the scale and behavior of acoustic streaming. *Physical Review E*, 89(1):013203, 2014.
- [222] Ghulam Destgeer, Byung Hang Ha, Jin Ho Jung, and Hyung Jin Sung. Submicron separation of microspheres via travelling surface acoustic waves. *Lab on a Chip*, 14(24):4665–4672, 2014.
- [223] Thomas Franke, Adam R Abate, David A Weitz, and Achim Wixforth. Surface acoustic wave (saw) directed droplet flow in microfluidics for pdms devices. *Lab on a Chip*, 9(18):2625–2627, 2009.
- [224] Ghulam Destgeer, Byung Hang Ha, Jinsoo Park, Jin Ho Jung, Anas Alazzam, and Hyung Jin Sung. Travelling surface acoustic waves microfluidics. *Physics Procedia*, 70:34–37, 2015.
- [225] Zhi Zhu and Chaoyong James Yang. Hydrogel droplet microfluidics for high-throughput single molecule/cell analysis. *Accounts of chemical research*, 50(1):22–31, 2016.
- [226] David J Collins, Adrian Neild, and Ye Ai. Highly focused high-frequency travelling surface acoustic waves (saw) for rapid single-particle sorting. *Lab on a Chip*, 16(3):471–479, 2016.
- [227] Ghulam Destgeer, Byung Hang Ha, Jinsoo Park, Jin Ho Jung, Anas Alazzam, and Hyung Jin Sung. Microchannel anechoic corner for size-selective separation and medium exchange via traveling surface acoustic waves. *Analytical Chemistry*, 87(9):4627–4632, 2015.
- [228] Ghulam Destgeer, Ashar Alam, Husnain Ahmed, Jinsoo Park, Jin Ho Jung, Kwangseok Park, and Hyung Jin Sung. Characterization of microchannel anechoic corners formed by surface acoustic waves. *Applied Physics Letters*, 112(8):083501, 2018.
- [229] Citsabehsan Devendran, David J Collins, Ye Ai, and Adrian Neild. Huygens-fresnel acoustic interference and the development of robust time-averaged patterns from traveling surface acoustic waves. *Physical Review Letters*, 118(15):154501, 2017.
- [230] Viktor Skowronek, Richard W Rambach, Lothar Schmid, Katharina Haase, and Thomas Franke. Particle deflection in a poly (dimethylsiloxane) microchannel using a propagating surface acoustic wave: size and frequency dependence. *Analytical Chemistry*, 85(20):9955–9959, 2013.
- [231] Citsabehsan Devendran, Nipuna R Gunasekara, David J Collins, and Adrian Neild. Batch process particle separation using surface acoustic waves (saw): integration of travelling and standing saw. *RSC Advances*, 6(7):5856–5864, 2016.
- [232] David J Collins, Citsabehsan Devendran, Zhichao Ma, Jia Wei Ng, Adrian Neild, and Ye Ai. Acoustic tweezers via sub-time-of-flight regime surface acoustic waves. *Science Advances*, 2(7):e1600089, 2016.
- [233] Jia Wei Ng, Citsabehsan Devendran, and Adrian Neild. Acoustic tweezing of particles using decaying opposing travelling surface acoustic waves (dotsaw). *Lab Chip*, 17(20):3489–3497, 2017.
- [234] Amr Arisha, Paul Young, and Mohie El Baradie. A simulation model to characterize the photolithography process of a semiconductor wafer fabrication. *Journal of Materials Processing Technology*, 155:2071–2079, 2004.

Bibliography

- [235] D Ciplys and R Rimeika. Measurements of electromechanical coupling coefficient for surface acoustic waves in proton-exchanged lithium niobate. *Ultragarsas" Ultrasound"*, 33(3):14–20, 1999.
- [236] B-H Jo, Linda M Van Lerberghe, Kathleen M Motsegood, and David J Beebe. Three-dimensional micro-channel fabrication in polydimethylsiloxane (pdms) elastomer. *Journal of Microelectromechanical Systems*, 9(1):76–81, 2000.
- [237] James Friend and Leslie Yeo. Fabrication of microfluidic devices using polydimethylsiloxane. *Biomicrofluidics*, 4(2):026502, 2010.
- [238] Athanasios T Giannitsis. Microfabrication of biomedical lab-on-chip devices. a review. *Estonian Journal of Engineering*, 17(2):109, 2011.
- [239] Mark A Eddings, Michael A Johnson, and Bruce K Gale. Determining the optimal pdms–pdms bonding technique for microfluidic devices. *Journal of Micromechanics and Microengineering*, 18(6):067001, 2008.
- [240] Shantanu Bhattacharya, Arindom Datta, Jordan M Berg, and Shubhra Gangopadhyay. Studies on surface wettability of poly (dimethyl) siloxane (pdms) and glass under oxygen-plasma treatment and correlation with bond strength. *Journal of Microelectromechanical Systems*, 14(3):590–597, 2005.
- [241] Armaghan Fakhfouri, Citsabehsan Devendran, David J Collins, Ye Ai, and Adrian Neild. Virtual membrane for filtration of particles using surface acoustic waves (saw). *Lab on a Chip*, 16(18):3515–3523, 2016.
- [242] Armaghan Fakhfouri, Citsabehsan Devendran, Thomas Albrecht, David J. Collins, Andreas Winkler, Hagen Schmidt, and Adrian Neild. Surface acoustic wave diffraction driven mechanisms in microfluidic systems. *Lab Chip*, 18:2214–2224, 2018.
- [243] Peter Barkholt Muller and Henrik Bruus. Theoretical study of time-dependent, ultrasound-induced acoustic streaming in microchannels. *Physical Review E*, 92(6):063018, 2015.
- [244] Julio Soria. An investigation of the near wake of a circular cylinder using a video-based digital cross-correlation particle image velocimetry technique. *Experimental Thermal and Fluid Science*, 12(2):221–233, 1996.
- [245] Klaus D Hinsch. Holographic particle image velocimetry. *Measurement Science and Technology*, 13(7):R61, 2002.